

On the Use of Bagging for Local Intrinsic Dimensionality Estimation

Kristóf Péter¹

University of Southern Denmark
Odense, Denmark

krp@imada.sdu.dk
ORCID: 0009-0008-1552-3361

Ricardo J. G. B. Campello¹

University of Southern Denmark
Odense, Denmark

campello@imada.sdu.dk
ORCID: 0000-0003-0266-3492

James Bailey¹

Monash University
Melbourne, Australia

james.a.bailey@monash.edu
ORCID: 0000-0002-3769-3811

Michael E. Houle¹

New Jersey Institute of Technology
Newark, New Jersey, United States

michael.houle@njit.edu
ORCID: 0000-0001-8486-8015

Abstract

The theory of Local Intrinsic Dimensionality (LID) has become a valuable tool for characterizing local complexity within and across data manifolds, supporting a range of data mining and machine learning tasks. Accurate LID estimation requires samples drawn from small neighborhoods around each query to avoid biases from nonlocal effects and potential manifold mixing, yet limited data within such neighborhoods tends to cause high estimation variance. As a variance reduction strategy, we propose an ensemble approach that uses subbagging to preserve the local distribution of nearest neighbor (NN) distances. The main challenge is that the uniform reduction in total sample size within each subsample increases the proximity threshold for finding a fixed number k of NNs around the query. As a result, in the specific context of LID estimation, the sampling rate has an additional, complex interplay with the neighborhood size, where both combined determine the sample size as well as the locality and resolution considered for estimation. We analyze both theoretically and experimentally how the choice of the sampling rate and the k -NN size used for LID estimation, alongside the ensemble size, affects performance, enabling informed prior selection of these hyper-parameters depending on application-based preferences. Our results indicate that within broad and well-characterized regions of the hyper-parameters space, using a bagged estimator will most often significantly reduce variance as well as the mean squared error when compared to the corresponding non-bagged baseline, with controllable impact on bias. We additionally propose and evaluate different ways of combining bagging with neighborhood smoothing for substantial further improvements on LID estimation performance.

Keywords: Local Intrinsic Dimensionality · Bagging · Smoothing

1 Introduction

Local Intrinsic Dimensionality (LID) is part of a broader notion of Intrinsic Dimension (ID), which has been conceptualized in different ways aiming to characterize the true complexity of a data space beyond its full representation dimension, under the assumption that one or more data submanifolds may exist within that space [23, 13, 25, 41, 36, 42, 28]. One can think of LID as the minimum number of variables or *effective dimensions* required to explain the underlying distribution at a particular location of the data space, or the smallest dimension surface on which a sample from that distribution would locally lie on. It has found a growing number of applications, including outlier detection [7], similarity search [8, 16], IoT intrusion detection [22], adversarial example analysis [38, 3], self-supervised learning regularization [30], graph embedding design [43], data segmentation [1], and granular deformation analysis [49], just to mention a few.

A wide range of LID estimators has been proposed, among which a major class is based on the extreme value theoretic (EVT) limiting distribution of distances as a neighborhood radius around a query location shrinks to zero — e.g., MLE, MoM, PWM, TLE [4, 6]. Other well-known approaches include MADA [20], ESS [32], and originally global ID estimators, such as TWO-NN [19], which can be generalized to locally estimate LID [9]. The above techniques employ k -NN search for sampling around the query location, however, there are model-based alternatives — such

as LIDL (using approximate likelihood) [44] and FLIPD (employing diffusion models) [34] — with different ways of quantifying locality.

Despite their differences, most estimators evaluate LID at a query location using only nearby observations to capture local properties of the data space. Using faraway data points risks introducing nonlocal biases, e.g., by mixing nearby manifolds with different dimensionalities, or violating local isotropy on an anisotropic surface — see Figure 1. In practice, given a finite size dataset, shrinking an arbitrary neighborhood radius can leave too few points inside, which tend to yield high-variance, unstable estimates; enlarging it reduces variance, but also pulls in nonlocal structure that can increase bias. This bias-variance tradeoff is the central practical obstacle in LID estimation, and it can undermine downstream applications that critically rely on accurate, stable estimations of LID. Tackling this challenge through bootstrapping-based statistical machinery, rather than simply trading variance with bias, is the main goal of this paper.

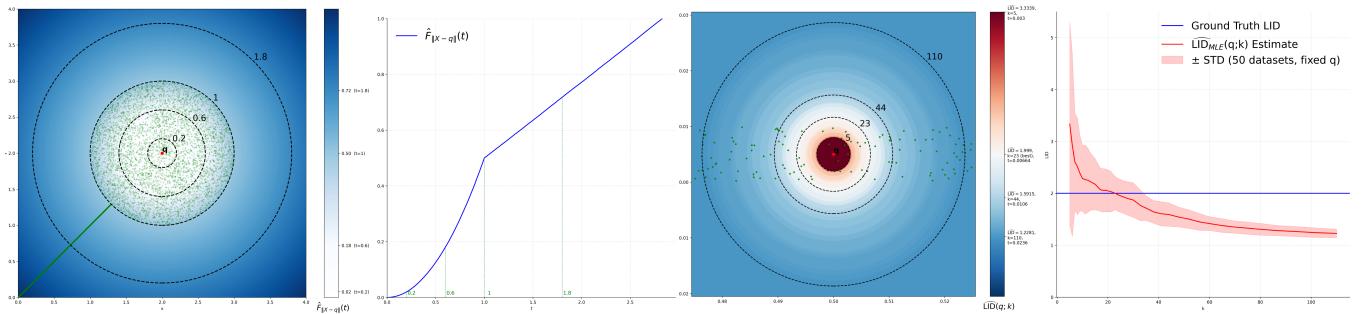


Figure 1: The leftmost figure shows the *Lollipop* dataset [44] overlaid with the cumulative distribution function (c.d.f.) of the induced empirical distance distribution from the query at $(2, 2)$, as a heatmap. The 2nd figure shows that, within close vicinity to the query, t , the c.d.f. is proportional to the square of the distance, becoming linear beyond the bounds of the 2D (circle-plate) submanifold, when the 1D (line) submanifold is reached. The 3rd figure shows a heatmap of LID estimates at the query at $(0.5, 0.005)$ using MLE [5], as a function of the k -NN hyper-parameter, overlaid with the corresponding dataset distributed uniformly on a thin ribbon-like surface. The rightmost figure displays how LID estimates vary with k , not only affected by the interplay between locality preservation and sample size, but also changing with the resolution at which it is measured in practice. Within close vicinity from the query, where neither locality or resolution is critical, the small sample size results in high variance and — for estimators that are only asymptotically unbiased (including MLE) — also in bias.

We propose to adapt *bootstrap aggregating* (a.k.a. *bagging* for short) [17] as a method-agnostic, variance-reduction wrapper for LID estimators. While bagging is a commonly used technique, e.g., in the context of decision trees [2] and ensembles more broadly, both shallow [50] and deep [21, 48], to the best of our knowledge it has not been applied to LID estimation before. In this specific setting, the standard behavior of bagging is not trivially guaranteed. To align with continuity assumptions on the underlying data density and to preserve the original distribution of distances, subsampling without replacement is required within each *bag* (i.e., ensemble member), thus causing the in-bag sample size to be reduced. Reducing the sample size increases the distance threshold required to retrieve a fixed number k of neighboring points around a query, making it so that a fixed k on a subsample corresponds to a larger effective NN radius, with potential to introduce undesirable nonlocal effects as variance decreases (e.g., see Figure 1). The problem has a close analogue in traditional EVT, where the chosen sample size determines the upper-tail threshold. When estimating the extreme value index using the k largest order statistics, the choice of k trades variance (small k) against bias (large k), and subsample-bootstrap methods show how the MSE-optimal k between subsampled and full-sample estimators can be explicitly rescaled according to the sampling rate [39, 18]. This provides critical motivation in the current study for its exploration within the locality restrictions corresponding to a lower-tail threshold for LID estimation.

We provide theoretical and empirical analyses of bagged LID estimation, focusing on how the number of bags B and the sampling rate r , together with the locality threshold (the neighborhood size k in case of NN-based LID estimators) jointly shape bias, variance, and mean-squared error (MSE). We show how the selection of these hyper-parameters can result in dramatic reduction of MSE, typically resulting from significant reduction in variance with limited or no associated compromise in bias. Our results support that this is mainly enabled by the additional degree of freedom provided by the sampling rate controlling the tradeoff between the bag size and the level of independence between bags, which often allows for wider ranges of effective locality thresholds for LID estimation, and within which the bagged estimator can achieve superior performance than the baseline equipped with its own MSE-optimal locality threshold. This provides *application-specific* insights as to why and how bagging can be effectively used to mitigate the bias-variance dilemma in LID estimation.

Additionally, we evaluate neighborhood smoothing [15] as another strong standalone variance-reduction approach and show that it is complementary to bagging: applying smoothing within each bag (pre-smoothing) and/or after aggregation (post-smoothing) yields the most substantial MSE reduction in our experiments. Our **contributions** can be summarized as follows:

- Introducing bagging for LID estimation.
- Theoretical analyses shedding further light onto the effects and interactions of the hyper-parameters governing the behavior of bagging.
- Experimental analyses of the relationship between bagging hyper-parameters as well as their potential interplay with the locality threshold of LID estimators (demonstrated through the k hyper-parameter of NN-based methods).
- Experimental results on benchmark datasets showing that bagging, as well as its combinations with smoothing, not only reduce variance but generally reduce the MSE of LID estimates compared to the baseline, in case of mutually optimal independent selection of hyper-parameters.

2 Related work

Variance reduction in LID estimation is addressed either by designing lower-variance estimators or by applying estimator-agnostic wrappers to stabilize existing methods. Next, we review approaches within these two categories.

TLE [6] is closely related to EVT-based LID estimators such as MLE [5], but it modifies the classic asymptotic distance-based likelihood function by incorporating non-central distance information to derive an extended statistic. It was shown to substantially reduce variance while maintaining comparable bias to MLE. However, TLE is tied to the EVT formulation and is not readily transferable as a generic wrapper to arbitrary LID estimators.

More general stabilization can be achieved via data pre-processing or by post-processing estimates. In [35], it has been shown that pre-processing by scale space filtering methods can contribute to LID estimation in the context of hyperspectral imaging data. These techniques work by denoising the original dataset, thus reducing variance and, accordingly, resulting in more accurate and stable LID estimates. However, the method is designed under assumptions specifically related to the type of datasets in the intended application of hyperspectral images.

A widely applicable post-processing approach is neighborhood smoothing [47], which is easily translatable to LID estimation. Given per-query LID estimates, regular *smoothing* replaces each by an average over their local neighborhood (e.g., k -NN), which can reduce variance assuming that neighboring points share similar LID. To improve alignment with this assumption, the manifold adaptive neighborhood smoothing technique presented in [15] constructs the k -NN graph of the data points based on Euclidean distance; smoothing is then performed on a neighborhood of points based on their approximated geodesic distance to the query as the shortest paths along the graph, which locally approximates the query’s submanifold. Such *geodesic smoothing* technique has been shown to reduce the variability of the non-linear least-squares estimator described in [15].

3 Background

3.1 LID

LID can be defined from a purely distributional perspective, beyond the realm of any particular data sample, as a local notion of ID at a given query location.

A theoretical, EVT-based approach to this concept that has gained increasing attention in recent years has been formulated in [27, 29]. In this theoretical framework, for a selected query location and distance metric, there exists a *distribution of distances* from the query that is *induced* from an *underlying distribution* of interest defined in the original data space. Under certain assumptions of locality and smoothness, the limiting lower tail of the cumulative distribution function (*c.d.f.*) of such a theoretical distance distribution is fully and uniquely characterized by LID as a quantifiable property at the query.

In this paper, unless stated otherwise, this is the notion of LID that will be implicitly assumed, e.g., in our experiments involving practical LID estimation. Notice, however, that the bagging techniques introduced in this paper are by no means estimator-specific, but rather broadly applicable to virtually any LID estimator regardless of their supporting LID paradigm.

3.2 Bagging

Bagging is a resampling technique introduced by Breiman [10] as a way of harnessing computational power to improve the stability of models and estimators by aggregating results across multiple resampled versions (*bags*) of the original

data. It is especially effective for models that are accurate on average but highly variable. Classic examples include bagging for decision trees and random forests [31, 11, 2], as well as a variety of modern deep learning applications [48, 21]. General theoretical results for the variance-reduction effect of bagging, including the subsampling variant adopted in the present paper, can be found in [12].

The term *bagging* is commonly referring to resampling *with replacement*, where each bag can have the same size as the original dataset and may contain duplicate samples. In our setting, however, duplicates would distort the distance distribution and violate its absolutely continuous assumption underlying most LID estimators. We therefore use the *subbagging* (*subsample aggregating*) variant, where sampling within an individual bag happens strictly without replacement and each bag thus contains a strictly smaller sample size than the whole dataset.

For this reason and for the sake of simplicity, in the remainder of this paper and unless explicitly stated otherwise, when referring to *bagging* we will assume the following formal definition of *subbagging*, which coincides with that from [12]:

Definition 1 (Subbagging). *Given n i.i.d. random vectors $D \triangleq (X_1, \dots, X_n)$ following a distribution over the ambient space that relates to a parameter θ , let the n sample estimator of θ be defined as a statistic $\hat{\theta}_n \triangleq \hat{\theta}(X_1, \dots, X_n)$. Let $m = rn < n$ be an integer for some sampling rate $r \in (0, 1)$ and create B random subsets (a.k.a. bags) of size m each, $D_{i,m} \triangleq (X_{\Pi_1^{(i)}}, \dots, X_{\Pi_m^{(i)}})$ for $i = 1, \dots, B$, by subsampling from D using random index sets, $\Pi^{(i)} \triangleq \{\Pi_1^{(i)}, \dots, \Pi_m^{(i)}\}$. Such index sets $\Pi^{(\cdot)}$ are i.i.d. (uniformly) over all $\binom{n}{m}$ possible choices of m different indices out of n .*

The bagged estimator is then defined as:

$$\hat{\theta}_{B,m} \triangleq \frac{1}{B} \sum_{i=1}^B \hat{\theta}_{m,i} \quad ; \quad \text{where} \quad \hat{\theta}_{m,i} \triangleq \hat{\theta}(X_{\Pi_1^{(i)}}, \dots, X_{\Pi_m^{(i)}}) \quad (3.1)$$

4 Bagged LID estimators

To translate Definition 1 to the specific context of LID estimation, we consider the sample set D to correspond to our full dataset of n observed points in the \mathbb{R}^{dim} ambient space, whereas the baseline LID estimator at a fixed query point $q \in \mathbb{R}^{\text{dim}}$, $\widehat{\text{LID}}(q)$, is considered to satisfy measurability assumptions and corresponds to the statistic $\hat{\theta}$, such that $\widehat{\text{LID}}_n(q) \triangleq \widehat{\text{LID}}_n(X_1, \dots, X_n; q) \equiv \hat{\theta}_n(X_1, \dots, X_n)$ is the n -sample estimator at q . We can thereby construct the bags $D_{1,m}, \dots, D_{B,m} \subset D$ and the bagged estimator $\widehat{\text{LID}}_{B,m}(q)$ according to Definition 1. Figure 2 illustrates bagged LID estimation for a single query.

Notice that most LID estimators are quantifiable at any location of the data space, albeit they are most often used only at query locations that coincide with points of the sample set ($q \in D$). After subsampling, a query point $q \in D$ will likely only be present in some bags, but the bagged estimator will still require its individual estimation within each and every bag, regardless of whether the query is present or not.

From an implementation viewpoint, the two different cases have to be taken into consideration when a distance of zero between the query location and a sample point is not allowed, such as for any LID estimator under an absolutely continuous distance distribution assumption. For the family of estimators based on the query's k -NN, one needs to ensure that the nearest neighbor of a point is never the point itself. In practice, this means that, whenever the query point q is contained in the bag, it is not counted as its own neighbor (for estimating its LID within that bag) and, as such, it does not count towards k , thus ensuring the same number of points k is always used for estimation.

4.1 Mean squared error (MSE) decomposition

The Mean-squared error (MSE) decomposition is a well-known result [45] that relates the theoretic MSE of an estimator to its bias and variance. It can be used to gain deeper insights into an estimator's error by looking at the two components individually, as $\text{E}[(\hat{\theta}_{B,m} - \theta)^2] = \text{Var}(\hat{\theta}_{B,m}) + (\text{E}[\hat{\theta}_{B,m}] - \theta)^2$. Notice that the overall bagged estimator will have at most as large MSE as the m -sample estimator deployed within each bag, i.e., $\text{E}[(\hat{\theta}_{B,m} - \theta)^2] \leq \text{E}[(\hat{\theta}_{m,i} - \theta)^2]$, which directly follows by recognizing that $\text{Var}(\hat{\theta}_{B,m}) \leq \text{Var}(\hat{\theta}_{m,i})$ and $\text{E}[\hat{\theta}_{B,m}] = \text{E}[\hat{\theta}_{m,i}]$ (see Appendix A.2 for details). However, in principle, this result alone does not provide any improvement guarantees for the bagged estimator with respect to the MSE of the n -sample estimator, which infers over the entire sample set D .

When it comes to variance, [40] shows in the context of subbagging for decision trees that as the number of bags (B) tends to infinity, the variance of the bagged estimator decreases towards a known limiting value, which can be expressed as the variance of the expectation of a single-bag estimator conditioned on the data, $\text{Var}(\text{E}(\hat{\theta}_{m,i}|D))$. In Appendix A.2, we show more broadly (for any estimator following Definition 1) that this lower-limiting variance can also be rewritten as the unconditional covariance between single-bag estimators, $\text{Cov}(\hat{\theta}_{m,i}, \hat{\theta}_{m,j})$.

In Theorem 1, we formally outline how decreasing the sampling rate (r) is expected to cap the aforementioned limiting variance of the bagged estimator. The result is a combination of the well-known Jensen-gap bound [37] and

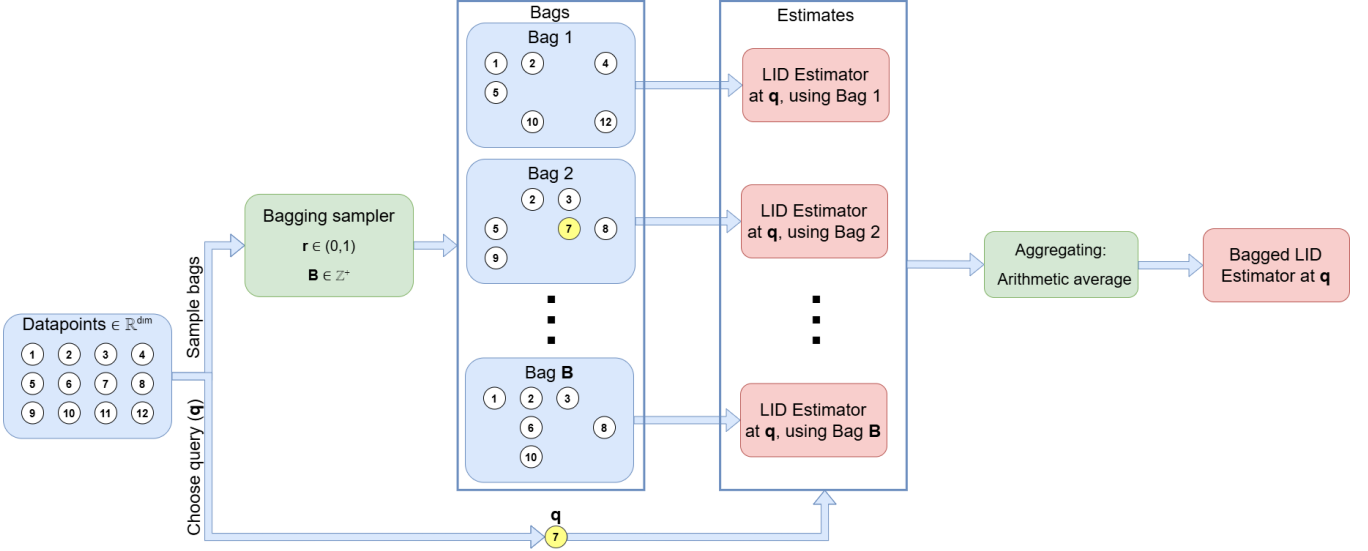


Figure 2: Flowchart illustrating bagged LID estimation on a hypothetical, toy dataset. The algorithm is displayed for a single query point (with index 7) from the dataset. Note that it suffices to sample the bags only once and reuse them for different queries. The figure makes it clear that LID estimation can be done independently for each query point and for each bag, so processing is highly parallelizable across multiple nodes. For details on estimation across a dataset of queries, see the pseudo code in Appendix A.1.

the fact that the extent of the overlap $|\Pi^{(i)} \cap \Pi^{(j)}|$ between random index sets drawn without replacement follows the Hypergeometric Distribution [33, 24].

Theorem 1. Define $\gamma(h, m) \triangleq \text{Cov}(\hat{\theta}_{m,i}, \hat{\theta}_{m,j} \mid |\Pi^{(i)} \cap \Pi^{(j)}| = h)$ for the integer domain given by $m = rn \in \mathbb{Z}^+$ and $h = 0, 1, \dots, m$, namely, the covariance of two single-bag estimators given that we know the number of dependent variables (provided that such a covariance exists and is finite for any pair of bags). Assume that there exists a twice differentiable, increasing function $\varphi : [0, 1] \rightarrow \mathbb{R}$ such that $\forall_{h,m : h \leq m} \gamma(h, m) \leq \varphi(\frac{h}{m})$, then we have:

$$\forall_{r \in [0,1]} \text{Cov}(\hat{\theta}_{m,i}, \hat{\theta}_{m,j}) \leq \varphi(r) + O\left(\frac{1}{n}\right) \quad (4.1)$$

Proof. See proof in Appendix B.2 □

In simple terms, assuming that the magnitude of the conditional covariances $\gamma(h, m)$ are roughly positively proportional to the fraction of dependent variables between the bags (h/m), Theorem 1 shows that we can set an implicit upper bound on the limiting variance of the bagged estimator, $\lim_{B \rightarrow \infty} \text{Var}(\hat{\theta}_{B,m}) = \text{Cov}(\hat{\theta}_{m,i}, \hat{\theta}_{m,j})$, by reducing r and, accordingly, $\varphi(r)$. This result suggests that we can limit variance from above by decreasing the sampling rate (r) and increasing the number of bags (B). However, recall that the resulting decrease in the bag size m can lead to more biased in-bag estimates, most noticeably, due to either fewer samples for LID estimation within a fixed local vicinity around the query or, alternatively, a less local vicinity containing a fixed sample size k (e.g., see Figure 1). Since the exact nature of this bias-variance tradeoff is dependent on the particular LID estimator and its hyper-parameters (e.g., k), as well as on the dataset in hand, experimental analyses are required to conclusively show the effects of bagging and its hyper-parameters in LID estimation.

5 Experimental methodology

5.1 Estimators

Alongside the classic MLE estimator as a standard baseline [4], we also include TLE [6] and MADA [20] to test the general applicability of bagging to different estimators without any intent of promoting a particular method. TLE, while substantially more computationally demanding, is designed to reduce variance, allowing us to test whether bagging can further enhance more sophisticated baselines already equipped with internal variance-reduction mechanisms. Table 1 summarizes the tested estimators and their essential hyper-parameters, alongside the two wrapper alternatives to mitigate variance that we experimentally investigate in this paper, namely, bagging and smoothing [15]. The goal is to compare each baseline against their own wrapped counterparts.

Table 1: LID estimators and hyper-parameters. “pre” and “post” specify whether smoothing is applied to the in-bag LID estimates (i.e. prior to aggregation) or to the bagged LID estimates, resp. All other hyper-parameters have been previously defined.

Baseline	Baseline hyper-par.	Bagging hyper-par.	Smoothing strategy
MLE [4]	k	r, B	<i>pre</i> or <i>post</i>
TLE [6]	k	r, B	<i>pre</i> or <i>post</i>
MADA [20]	k	r, B	<i>pre</i> or <i>post</i>

5.2 Datasets

As common practice in the LID literature, we use test datasets based on a foundational study of LID estimation on manifolds [26] later extended to a comprehensive benchmark framework in [14]. The data manifolds contain $n = 2500$ points with known LID, which we use as ground truth when computing the MSE of estimators for evaluation purposes. We additionally include the *Lollipop* data from [44], and a high-dimensional *Uniform* dataset. More detailed descriptions of each dataset and a summary table are provided in Appendix D.

5.3 Evaluation measures

We measure the performance of LID estimators using the empirical MSE as well as its bias-squared plus variance decomposition, for the reasons discussed in Section 4.1. Notice that in the presence of multiple ground-truth LID values across a dataset with different submanifolds, the MSE decomposition needs to be applied manifold-wise (details are provided in Appendix C).

5.4 Bagging and smoothing experiments

The first experiment evaluates the overall effectiveness of bagging as well as compares and combines it with *smoothing*, as an alternative or supplementary variance-reduction technique. We obtain smoothed LID estimates for a query by taking the arithmetic average of the estimates over its k -NN (the same neighborhood size used by the baseline estimator). This neighborhood includes the query itself only when it is present in the reference sample set (bag or full dataset). When smoothing is performed on the baseline estimates, without any bagging, we will refer to it simply as *smoothing*.

Additionally, we combine bagging and smoothing in three different ways. The simplest idea is to smooth out the aggregated bagged estimates themselves, exactly as explained above, only now for the bagged estimator. We will refer to this combination as “*post-smoothing*”.

As an alternative approach, we can instead smooth out estimates based on each bag separately, determining the query’s k -NN among only the in-bag points. This way, smoothing takes place inside the bags, before the single-bag estimates are aggregated. We refer to this combination as “*pre-smoothing*”. Finally, we can also integrate both strategies above by simultaneously applying pre-smoothing (*pre*) and post-smoothing (*post*).

This goes to show that bagging and smoothing are not necessarily competitors. Bagging actually offers new avenues for applying smoothing in different ways.

We apply bagging, smoothing, and their three combinations independently to the different baseline estimators in Table 1, *with the goal to compare each baseline to their bagged/smoothed counterparts, rather than against each other*.

For each case, we sweep the locality hyper-parameter over a 9-step geometric progression from $k = 5$ to $k = 72$. For bagged variants, we additionally sweep the sampling rate over a 9-step geometric progression from $r = 0.042$ to $r = 0.6$, evaluating all combinations of (k, r) . We are fixing the number of bags to $B = 10$, noting that increasing B can only further improve results in favor of bagging. Then, for each dataset and method variant, we individually select the hyper-parameter setting that minimizes MSE: k for baseline/smoothing, and (k, r) for all bagged variants, comparing the methods at their best observed performance.

5.5 Bagging hyper-parameters experiments

The second set of experiments focuses specifically on bagging and explores how the choice of its hyper-parameters affects performance in terms of MSE, variance, and bias. These effects are discussed using the bagged MLE estimator. The results for MADA and TLE (in Appendix E) exhibit similar trends and the main conclusions do not change:

1st test (sampling rate): We saw in Theorem 1 how decreasing r is expected to de-correlate the bags, and under certain general assumptions, reduce variance. Confirming this expected decrease in variance in the LID setting and to what extent it can overshine any potential increase in bias as a function of the sampling rate (r) are the main goals of this experiment.

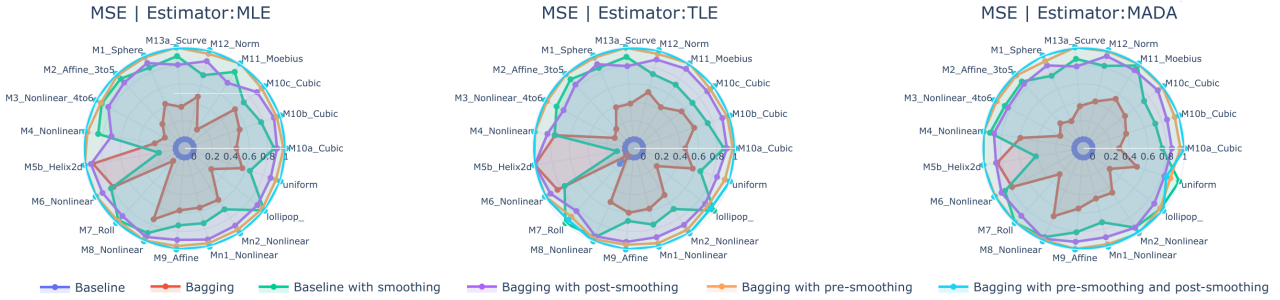


Figure 3: Comparison of the relative MSE achieved by three different LID estimators, MLE, TLE, and MADA, with and without smoothing, bagging, and three strategies for combining bagging with smoothing. The results are for 19 datasets using case-by-case optimal k and r hyper-parameters. The min-max normalized MSE values are subtracted from 1 before plotting, such that larger scores correspond to smaller relative MSEs.

For this test, we chose a fixed $k = 10$ for the baseline estimators, a relatively small value compared to the dataset size, to attain to the general importance of locality surrounding LID estimation. The effects of r may be exaggerated or reduced depending on k ; however, it is worth stressing that the general trends remain the same and the main conclusions with respect to r do not change for different, fixed values of k .

2nd test (interaction between k and r): As previously discussed, both k and r affect the radius determining the local neighborhood around the query used for estimation, which is directly proportional to k and inversely proportional to r , with the potential to affect bias through non-local effects and sample size. On the other hand, variance is generally inversely proportional to k and directly proportional to r . If both hyper-parameters are variable, then the values of k that result in more favorable bias-variance tradeoffs will depend on r and vice versa. Since the exact relationship may be complex and possibly both dataset- and estimator-dependent, the goal of this experiment is to identify major general trends allowing clear guidance on the combined choice of these hyper-parameters.

We evaluate the bagged estimator over a grid of (k, r) combinations, comparing each against the baseline with the same k . The resulting MSE differences reveal ranges of r (and ratios k/r) for which bagging improves or worsens performance.

Additional tests (number of bags): Analogous experimental setups and analyses demonstrating the (more straightforward) effects of the number of bags (B) and its interaction with r are available in Appendices A.3 and A.4.

5.6 Code and data availability

A full code that can be used to reproduce all results in our paper is available from our GitHub page at https://github.com/Campello-Lab/Bagging_for_LID, which also contains all the datasets used in our experiments. Most of these datasets were generated using the Scikit-dimension [9] public Python library, which was also the source code for the baseline LID estimators adopted in this study.

6 Results and discussion

6.1 Bagging and smoothing results

Figure 3 shows the results for the first experimental setup in Section 5.4. We use radar charts to display the *optimal* MSE values, min-max normalized across variants, separately for each dataset, in reverse.¹ Thus, scores lie in $[0, 1]$, where 1 denotes the lowest relative MSE and 0 the highest, therefore, larger covered area indicates better performance.

There is a very clear trend. First, both bagging and smoothing improve over the baseline in almost all cases when used independently, with only one exception (TLE on M7.Roll), noting that smoothing is often the stronger standalone variant in these experimental conditions. Second, it is clear that combining them yields further gains, with a common performance ordering, consistently across the baselines: baseline $<$ bagged $<$ smoothed $<$ bagged with post-smoothing $<$ bagged with pre-smoothing $<$ bagged with pre- and post-smoothing. Therefore, the main conclusion is that not only do both bagging and smoothing achieve their purpose on their own, but combining them provides further improvements.

¹Tables of the raw MSE values are reported in Appendix E.1.

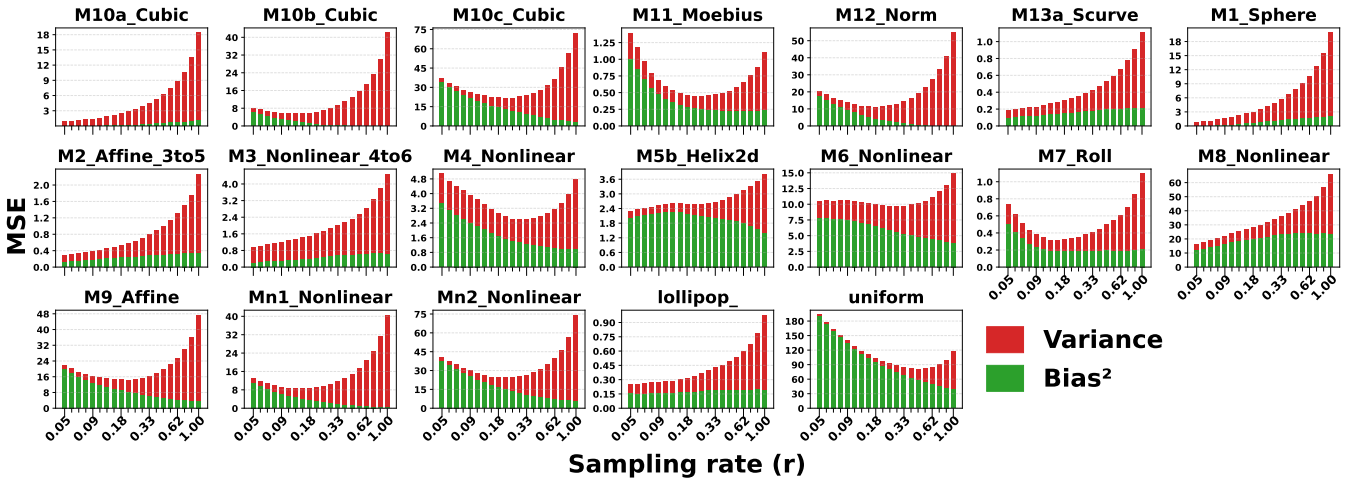


Figure 4: MSE and its decomposition for each of the 19 datasets as a function of the sampling rate r used for bagged MLE as the LID estimator. Note that the baseline MLE is equivalent to $r = 1$, displayed on the rightmost bar of the individual charts.

6.2 Sampling rate results (1st test on hyper-parameters):

Figure 4 illustrates the experimental behavior of the MSE decomposition for bagging as a function of the sampling rate r . The exact relationship is dataset-dependent, but in general, by decreasing r (right-to-left along the x-axis) we observe that: (i) bias² (green sub-bars) tends to increase or stay relatively stable in most cases; and (ii) variance (red sub-bars) shows a highly consistent, decreasing behavior. This robust effect on variance reduction supports the validity of our assumptions in Theorem 1 and confirms the bag de-correlating benefits of reducing r .

The opposing trends often yield an intermediate “sweet spot” where an optimal bias-variance tradeoff is achieved in terms of a minimal MSE, confirming our arguments in Section 4.1. However, for some datasets (M10a_Cubic, M13_Scurve, M1_Sphere, M2_Affine.3to5, M3_Nonlinear_4to6, and M8_Nonlinear), smaller r reduced both variance and bias, so the best MSE occurred at the smallest tested r , suggesting that potential non-local biases associated with decreasing r did not manifest within the given range of r values in those datasets.

Overall, the experiment mostly confirms the anticipated behavior for r , noting that results that were somewhat surprising, actually did so in a favorable way.

6.3 Interaction between k and r results (2nd test on hyper-parameters):

Figure 5 illustrates how the bagged LID estimator’s performance depends jointly on the baseline’s k -NN hyper-parameter and the sampling rate. As previously conjectured, the bias increase from the expansion of the effective local neighborhood radius, for sufficiently large k compounding with sufficiently small r , may overpower the combined variance reduction caused by both these settings, potentially resulting in a larger MSE for the bagged estimator than the baseline.

Overall, the heatmaps in Figure 5 confirm this expectation, as for most datasets, the hyper-parameter space is divided along a certain left-to-right upwards white line where the two estimators achieve similar MSEs. To the right of this line, bagging tends to win out, while to the left, the baseline tends to perform better. This suggests that there is some dataset specific constant, for which, if the ratio between the two hyper-parameters ($\frac{k}{r}$) stays under, then we can expect the bagged estimator to produce favorable results, while the results are most likely not desirable otherwise. We additionally observe that the strongest gains usually occur at the bottom-left region (small k , small r), where bagging can strongly reduce MSE by simultaneously de-correlating bag estimates while preserving reasonable locality. The experiment also clarifies how in the previous test with a variable r , fixing $k = 10$ may have caused partially unexpected results for some datasets, as non-local effects were not yet expressed.

6.4 Main takeaways

From our theoretical and experimental findings, we provide the following guidelines for selecting the hyper-parameters of bagging (B , r) with respect to the degree of locality for LID estimation (quantified by the k hyper-parameter of the family of NN-based estimators adopted in this study):

- **Number of bags (B):** It is well-known that increasing B has a strictly beneficial but diminishing effect in terms of estimator variance (see Section 4.1), and this has been confirmed in our experiments (Appendices A.3

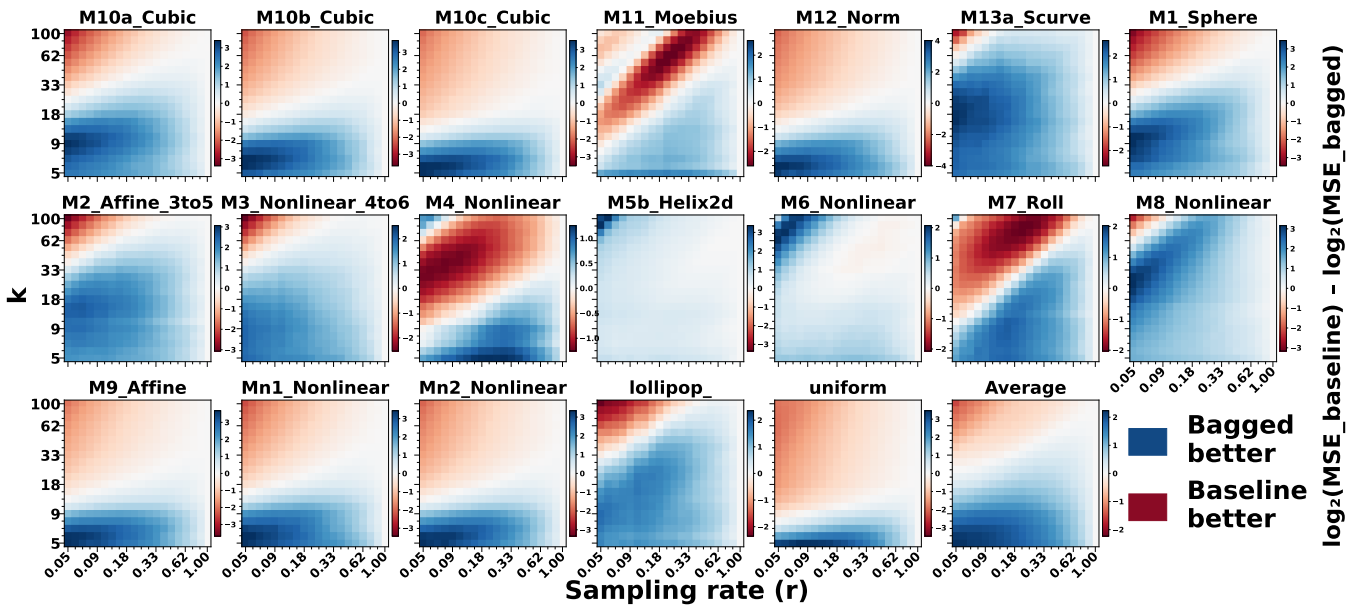


Figure 5: Heatmaps of the relative difference (log-ratio) between the MSE achieved by the baseline estimator (MLE) and the MSE of its bagged counterpart for each of the 19 datasets and cross-combinations of values for the sampling rate r (x-axis) and the k -NN neighborhood size k (y-axis). Positive values, color-coded as blue, indicate that bagging outperforms the baseline, whereas negative values, color-coded in red, indicate the opposite. The relation is symmetric around zero and the darkness of the cells are proportional to the magnitude of the corresponding absolute value for the given dataset.

and A.4). Since the resulting gains come with no counter-effect in terms of bias, this hyper-parameter is not critical. However, the runtime complexity of the bagged estimator is linearly dependent on B (see Section 7). Our experiments consistently support that increasing B beyond 10 is only recommended if one strongly favors further diminishing gains in stability over runtime.

- **Sampling rate (r) and locality (k):** As anticipated in Section 4.1 and confirmed by our experiments, the hyper-parameters k and r jointly control the bias-variance tradeoff. If the primary goal is to bind variance reduction in the bagged estimator to a positive (or at least neutral) overall impact *in terms of MSE* as compared to the baseline, our results support combining low values of both k and r . In practice, we suggest to set k roughly within $[5, 10]$ or so as a minimal local sample size for LID estimation, then choose r accordingly, roughly within $[r_{min}, 0.5]$. The low end of this range should ensure that the in-bag subsamples are still representative enough of the relevant structures in the dataset (e.g., manifolds, classes, clusters) and, as such, it is problem-dependent. Within the (MSE-orientated) rough ranges of k and r suggested above, for a fixed chosen k decreasing r is theoretically expected to decrease variance (Theorem 1), often at the expense of bias. In the context of LID, applications that can tolerate large estimation biases, e.g., requiring mostly a reliable ordering for the purpose of relative comparisons of LID values across different queries, may benefit from smaller sampling rates (closer to r_{min}), whereas in applications where systematic LID offsets can be critically detrimental, one might prefer larger, more conservative rates.

7 Complexity analysis

In this section, we summarize the time complexity of bagging for LID estimation (in a non-parallel setting). An extended analysis, including the different smoothing variants (bagging with pre/post-smoothing) is deferred to Appendix A.5.

Let $p(n)$ denote the runtime cost of computing a baseline LID estimate for a *single query* using a sample of size n . Therefore, the *total* runtime complexity for the baseline estimator (no bagging), T_{base} , is $O(np(n))$ when taken over n different query locations. Bagging with B bags of size $m = rn$, for a *single query*, evaluates the estimator on each bag and averages, resulting in $O(Bp(rn))$ time, where the sampling step for bag construction and final averaging contribute only lower-order terms ($O(Bnr)$ and $O(B)$) and can thus be omitted. As the bags do not have to be resampled per-query, the *total* runtime complexity of the bagged estimator taken over n queries, T_{bag} , is simply $O(Bnp(rn))$.

For the wide family of NN-based LID estimators, $p(n)$ is dominated by finding the k -NN of the query in the sample set of size n , where k is assumed to be either constant or $k \ll n$. Using a naive exhaustive search, $p(n)$ is $O(n)$, which translates to $T_{\text{base}} \rightarrow O(n^2)$ and $T_{\text{bag}} \rightarrow O(B r n^2)$. For large enough n , bagging may be faster as long as $r < 1/B$. Assuming a more sophisticated (indexed) search strategy, with average estimation time $p(n)$ of order $O(\log n)$ per query (amortized over all queries), then $T_{\text{base}} \rightarrow O(n \log n)$ and $T_{\text{bag}} \rightarrow O(B n \log(rn))$.

8 Limitations and future work

The objective evaluation measures we used, namely, MSE, Variance and Bias, required datasets commonly used for benchmarking, with ground-truth LID. While these datasets undoubtedly pose a challenge for estimators, due to their manifold curvatures within higher-dimensional spaces, they may not fully span the spectrum of complex behaviors found in real data. Therefore, LID bagging, smoothing, and their combinations as proposed in this paper, are yet to be fully tested in practical scenarios with potentially more complex data distributions, noise, and related challenges. Without ground-truth LID though, this will require indirect evaluation in downstream task applications, which is left for future work.

In future work, we also intend to investigate the use of the out-of-bag (OOB) samples from each bag for evaluation and (unsupervised) model selection.

9 Conclusions

We proposed bagging as a variance reduction strategy for LID estimation, alongside different strategies for its combination with neighborhood smoothing. We theoretically and experimentally explored the behavior of bagged LID estimators, with especial focus on the interplay between the sampling rate r and the locality threshold (neighborhood size k), whereby in-depth analyses of their joint effect on variance, bias, and overall MSE have been provided. Our results show that within a wide range of these hyper-parameters, clearly characterized by small values of k and small-to-moderate values of r , the bagged estimator is not only expected to reduce variance but it also tends to outperform the corresponding baseline estimator in terms of MSE. The higher level of freedom made available by these hyper-parameters in controlling the bias-variance tradeoff also allows a reduction in MSE to be systematically observed when comparing the independently optimal bagged and baseline estimators, i.e., when they are independently set to their best preferred hyper-parameter values for each dataset. These improvements have been achieved across different baseline LID estimators and with a number of bags as small as 10, which comes with little to none additional computational price. Finally, our results robustly show that significant further improvements in performance can be achieved by combining bagging with neighborhood smoothing, which systematically outperforms both standalone approaches.

9.1 Use of Generative AI

We used ChatGPT 5.4 strictly to assist with language style and conciseness.

9.2 Disclosure of Interests

The authors have no competing interests to declare that are relevant to the content of this article.

A Supplementary contributions

A.1 Bagging for LID Algorithm

Below is the general algorithm for bagged LID estimation across the whole sample set D considered as query locations, as referenced by the main paper in Section 4.

Algorithm A.1 shows that one efficient way of handling the problem of the query being in the bag or otherwise is to loop over the points of the given bag, and then its corresponding complement (also known as the *out-of-bag*). This way, we avoid the need to check for inclusion/exclusion for each query-bag combination. This is especially helpful when the estimator is based on ordered nearest neighbor (NN) distances, in which case, definite knowledge of $q \in D_{i,m}$ or $q \notin D_{i,m}$ can help us decide if the smallest distance should be considered for estimation or not, even if NN distance calculation is only approximate.

Algorithm 1 Bagged LID estimator across all queries

Input: $D \in \mathbb{R}^{n \times \dim}$, $1 \ll n \in \mathbb{Z}^+$, $\dim \in \mathbb{Z}^+$, $r \in [\frac{1}{n}, 1)$, $B \in \mathbb{Z}^+$

Require: Baseline LID estimator oracle $\widehat{LID}_n : \mathbb{R}^{n \times \dim} \times \mathbb{R}^{\dim} \rightarrow \mathbb{R}$

```

1:  $m \leftarrow \lceil n \cdot r \rceil$ 
2: for  $i = 1$  to  $B$  do
3:   Sample  $\pi^{(i)} \sim \Pi$  (uniformly over all  $\binom{n}{m}$  possible choices of  $m$  different indices out of  $n$ )
4:    $D_{i,m} \leftarrow (D[\pi_1^{(i)}], \dots, D[\pi_m^{(i)}])$ 
5: end for
6: for  $i = 1$  to  $B$  do
7:   for  $q \in D_{i,m}$  do
8:      $\widehat{LID}_{m,i}(q) \leftarrow \widehat{LID}_{m-1}(D_{i,m} \setminus \{q\}; q)$ 
9:   end for
10:  for  $q \in D \setminus D_{i,m}$  do
11:     $\widehat{LID}_{m,i}(q) \leftarrow \widehat{LID}_m(D_{i,m}; q)$ 
12:  end for
13: end for
14: for  $q \in D$  do
15:   $\widehat{LID}_{B,m}(q) \leftarrow \frac{1}{B} \sum_{i=1}^B \widehat{LID}_{m,i}(q)$ 
16: end for
17: return  $[\widehat{LID}_{B,m}(D[1]), \dots, \widehat{LID}_{B,m}(D[n])]$ 

```

A.2 Bagging theory revisited

In the following, we discuss two results that show the general effectiveness of bagging and demonstrate the roles of its hyper-parameters, namely, the number of bags, B , and the sampling rate, $r \triangleq m/n \in (0, 1)$, as supporting material to the theoretical analysis in Section 4 of the main paper:

- Theorem 2 focuses on the asymptotic variance reduction effect of increasing the number of bags, and has analogous or similar results available in the literature, usually in the general context of classifiers or decision trees, for example, in [40], which also examines properties of the subbagging alternative. However, the current formulation in the specific context of parameter estimation is particularly convenient within our scope to interpret/explain our results.
- Theorem 1 is concerned with the variance reduction property of decreasing the sampling rate, and is already presented in the main paper; however, this section of the appendix offers additional insights and explanations to help with interpreting its assumptions and its claims.

Theorem 2. Let $\hat{\theta}_{m,i}$ and $\hat{\theta}_{m,j}$ be the single bag estimators for bags i and j ($i \neq j$) of a mutual sample set D , respectively, as defined in 1. Then, the following expressions hold for the unconditional variance of the bagged estimator, $\text{Var}(\hat{\theta}_{B,m})$, defined over $(D, \Pi^{(1)}, \dots, \Pi^{(B)})$:

$$\text{Cov}(\hat{\theta}_{m,i}, \hat{\theta}_{m,j}) \leq \text{Var}(\hat{\theta}_{B,m}) = \text{Var}(\hat{\theta}_m) \left(\rho_m + \frac{1 - \rho_m}{B} \right) \leq \text{Var}(\hat{\theta}_m) \quad (\text{A.1})$$

and $\text{Var}(\hat{\theta}_{B,m}) \rightarrow \text{Cov}(\hat{\theta}_{m,i}, \hat{\theta}_{m,j})$ as $B \rightarrow \infty$

where $\rho_m \triangleq \text{Corr}(\hat{\theta}_{m,i}, \hat{\theta}_{m,j})$ and $\text{Cov}(\hat{\theta}_{m,i}, \hat{\theta}_{m,j})$ stand for the correlation and covariance of the single bag estimators, respectively.

Proof. See proof in Section B.1. □

Theorem 2 illustrates the variance profile of the bagged estimator in terms of the number of bags (B) and shows that it is limited between the covariance of the single bag estimators (as a lower-bound) and the variance of the m sample estimator $\hat{\theta}_m$ (as an upper-bound). Assuming that for some m' we have $\text{Cov}(\hat{\theta}_{m',i}, \hat{\theta}_{m',j}) < \text{Var}(\hat{\theta}_n)$, then by properly selecting the sampling rate r such that $m' = n \cdot r$ and using a sufficiently large B , improvement can be achieved in relation to the n sample estimator as the bagged estimator variance tends to the smaller $\text{Cov}(\hat{\theta}_{m',i}, \hat{\theta}_{m',j})$ limiting value.

It is worth noticing that while using a smaller subsample size m (or equivalently, a smaller sampling rate r) tends to increase the upper-bound term, $\text{Var}(\hat{\theta}_m)$, it conversely tends to decrease the lower-bound term, $\text{Cov}(\hat{\theta}_{m,i}, \hat{\theta}_{m,j})$, by increasing the level of independence between the bags. Given that the variance of the bagged estimator converges towards the latter as we increase the number of bags, this result suggests that low sampling rates associated with a large number of bags would allow for variance reduction as compared to the n sample estimator. Of course, this result does not say anything in terms of bias. However, under the assumption that the n sample estimator is unbiased (potentially asymptotically as n increases), then so is the m sample estimator and (trivially from (3.1)) the bagged estimator as well.

Recalling Theorem 1 it is clear that, asymptotically as $n \rightarrow \infty$ (i.e., as the size of the original sample set D tends to infinity), the theoretical lower limiting value for the variance of the bagged estimator as stated in Theorem 2, $\text{Cov}(\hat{\theta}_{m,i}, \hat{\theta}_{m,j})$, is bounded from above by an increasing function of r , as long as the assumptions in the theorem hold.

In simple terms, Theorem 1 says that if the estimator and data are such that the magnitude of the conditional bag covariances $\gamma(h, m)$ are roughly positively proportional to the fraction of dependent variables between the bags (h/m), then from Theorem 1 we can expect to be able to reduce the upper bound on unconditional bag covariance (lower limiting variance of the bagged estimator) by decreasing the sampling rate (r). The assumption is natural in the sense that it captures our intuition about the covariance of the dependent estimators: if a small (large) portion of variables are dependent, we expect lower (higher) covariance. If all variables are independent, i.e. $\frac{h}{m} = 0$, then the covariance is 0, while if they are all dependent, i.e. $\frac{h}{m} = 1$, then the covariance is maximized as variance. For values in between, so when $0 < \frac{h}{m} < 1$, we can intuitively expect a roughly increasing relationship in terms of $\frac{h}{m}$, and this notion is captured by the assumed upper-bound.

By knowing more about the behavior of θ and therefore $\gamma(h, m)$, we could possibly choose φ in such a way that it is a good approximation of $\gamma(h, m)$, yielding a tight upper-bound. Apart from particular choices and their usefulness (or lack thereof) for specific purposes, for the sake of explaining the overall relationship in terms of the sampling rate, this general theorem suffices.

Note that by the nature of the expression for $\text{Var}(\hat{\theta}_{B,m})$ in (A.1), increasing the number of bags (B) has diminishing returns, depending on the magnitude of ρ_m . In case of relatively large ρ_m , the $\frac{1-\rho_m}{B}$ term accounts for a decreasingly lower portion of the variance, thence B has proportionally less impact, while the increase in runtime remains linear. Notably, according to (4.1), $\rho_m \cdot \text{Var}(\hat{\theta}_m)$ could be expected to decrease when decreasing the sampling rate (r). Depending on the data and estimator, this gives reason to expect a larger improvement from increasing B , for lower values of r .

For each dataset and estimator, the exact behavior of the bounds in (A.1) and (4.1) can be different, therefore, experimental analyses are required to show the effectiveness of bagging in specific application scenarios, such as LID estimation in this paper.

A.3 Additional experimental setups

This section introduces two additional experimental setups dealing with the role of the number of bags hyper-parameter and its interaction with the sampling rate, to confirm the theoretical predictions of Theorem 2 and Theorem 1 in the context of bagged LID estimation. This serves to complete the bagging hyper-parameter selection experiments in Section 5 of the main paper, which focused on the particular role of the sampling rate and its interaction with the k nearest neighbor (k -NN) locality hyper-parameter of certain baseline estimators (e.g., MLE).

As explained in the main paper, these experiments are specifically about bagging, designed to explore how exactly the choice of its hyper-parameters affects performance in terms of MSE, variance, and bias, when applied in the context of LID estimation. We show and discuss these effects on the bagged MLE estimator; however, the results for MADA and TLE exhibit similar general trends and can be found in Section E. They have been sidelined for the sake of clarity and compactness, since the main conclusions do not change. The results of these experiments are presented and analyzed in Section 6 and serve as the experimental basis for our proposed hyper-parameter selection guidance with regards to the number of bags hyper-parameter as presented in the main paper.

3rd test (number of bags): As shown in Theorem 2, increasing the number of bags (B) is most effective when estimates from different bags are low-correlated, which in turn tends to associate with lower sampling rates, as seen in Theorem 1. Therefore, for the current experiment, we fix the sampling rate at a relatively small value, $r = 0.05$, allowing for B to range from 3 to 400 according to a 20 step geometric progression.² The progression enables us to see the effect of the hyper-parameter according to proportional increases, while exploring a wide range of values. We mainly expect to observe the diminishing returns of increasing B as predicted by Theorem 2 and discussed in Section A.2.

The results of this experiment are presented and analyzed in Section A.4.1

4th test (interaction between B and r): These experiments are meant to test the interplay between the two hyper-parameters B and r , combining observations from the 1st sampling-rate test, presented in the main paper, and the previously discussed number of bags test, to show in practice the interacting effects we had already anticipated and discussed previously in Section A.2. They are also intended to test the robustness of bagging in terms of a sustained performance across wide ranges of hyper-parameter choices and combinations.

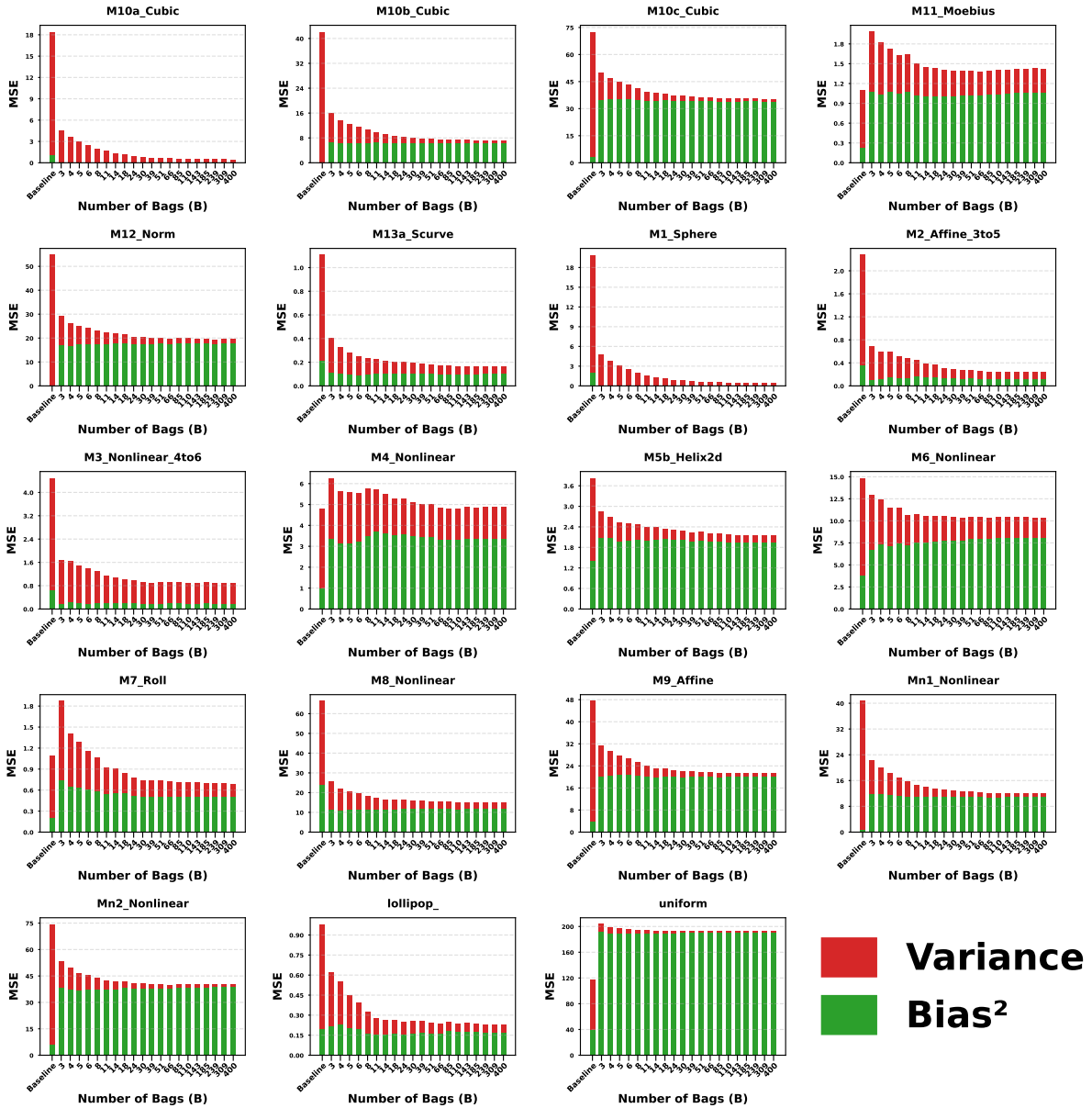
We calculate bagged estimators for every combination of hyper-parameter values, between the 20 values of sampling rates used in the previous experiments in this section, and a more comprehensive progression for the number of bags, between 1 and 100, both following roughly the same geometric rate.

The results of this experiment are presented and analyzed in Section A.4.2.

²We also include the Baseline case as the first experiment.

A.4 Supplementary result analysis

A.4.1 Number of bags (3rd test)



A.4.2 Interaction between B and r (4th test):

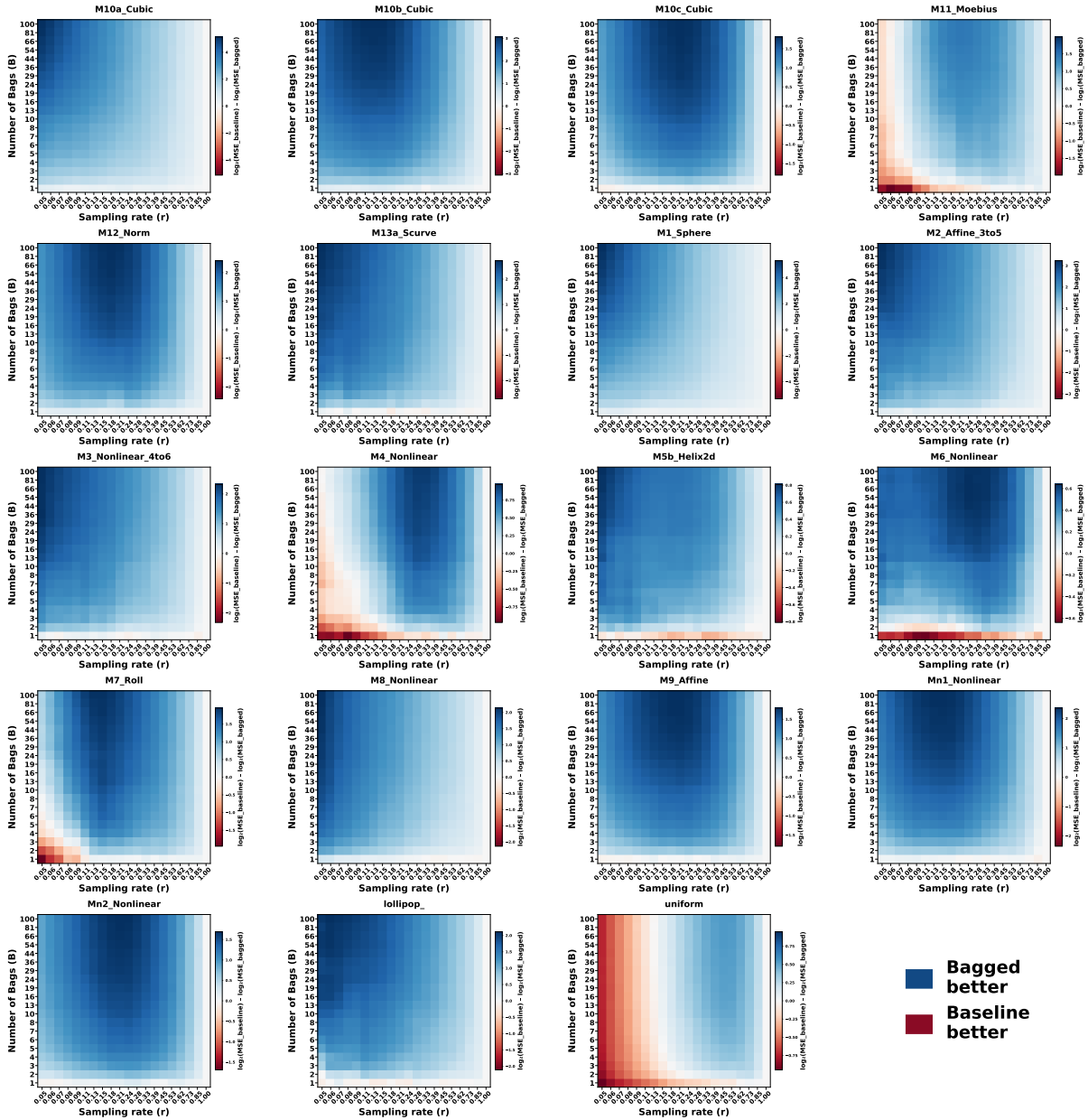


Figure 7: Heatmaps of the relative difference (log-ratio) between the MSE achieved by the baseline estimator (MLE) and the MSE of its bagged counterpart for each of the 19 datasets and cross-combinations of values for the sampling rate r (x-axis) and the number of bags B (y-axis). Positive values, color-coded as blue, indicate that bagging outperforms the baseline, whereas negative values, color-coded in red, indicate the opposite. The relation is symmetric around zero and the darkness of the cells are proportional to the magnitude of the corresponding absolute value for the given dataset. See Section A.3 for the detailed experimental setup.

Figure 7 illustrates the log-ratio between the MSE achieved by the baseline estimator (MLE) and the MSE of its bagged counterpart for each of the 19 datasets and cross-combinations of values for the sampling rate r and the number of bags B . Notice that the baseline estimator does not depend on these hyper-parameters and is only used as a basis for comparison. Also, notice that the differences in logarithmic scale reflect relative changes, as opposed to absolute differences.

White-colored cells indicate that the MSEs of the compared estimators are the same. Therefore, the rightmost column in each heatmap, which corresponds to the $r = 1$ case, is all white, since bagging with $r = 1$ is equivalent to the baseline estimator. The darkness of the blue color corresponds to the proportional difference in magnitude in favor of the bagged estimator, while the darkness of the red color indicates the opposite.

The most eye-catching result is that most heatmaps are a gradient between white and dark blue, with little to no

red to be seen, showing that bagging is very robust to these hyper-parameters, reducing MSE across wide ranges and combinations of their values. There is also a tendency to find darker blue areas towards the top left, which aligns with our expectations from Theorem 2 and Theorem 1, as we find both increasing B and decreasing r generally results in variance reduction with a positive, reinforcing interaction.

It is important to note, however, that for certain datasets the darkest blue areas, representing the optimal hyper-parameters, are not situated at the top-left corner. This may be explained by the upper range of the B hyper-parameter not being large enough to meet the requirements of the lowest sampling rates, as characterized in Theorem 2. Another possible explanation is that, with a fixed value of k in this experiment, the lowest sampling rates can result in bias due to the magnified increase in neighborhood radius around the query. This interplay between k and the sampling rate is further explored in the main paper.

A.5 Complexity analysis for the bagged LID estimator and its combinations with smoothing

Section 7 in the main paper presented a complexity analysis for the proposed bagging method for LID estimators. However, in the experiments, there have been several different combinations of bagging and smoothing tested. The current subsection of the appendix extends that analysis with more detail and provides comprehensive tables for the time complexities of the smoothing variants, in general, or assuming a k -NN estimator baseline, as well as using a naive search for finding k -NNs or an amortized search following preconstructed indices.

When using bagging to obtain LID estimates for a dataset of n data points, which are at the same time the query locations, as visualized in Figure 2, we first have to sample B bags with $n \cdot r$ points each. It takes $O(n \cdot r)$ time to generate $n \cdot r$ random indexes for each bag, therefore $O(B \cdot n \cdot r)$ time in total. Then, for each bag, a new LID estimate has to be calculated using its $n \cdot r$ points, for each of the n original query locations. This means that if we assume LID estimation is carried out individually per query, with an estimator whose runtime is $O(p(n))$, as a function $p(n)$ of the sample size n per query, then given that the bags contain $n \cdot r$ points, we get a time complexity of $O(B \cdot p(n \cdot r))$ per query, i.e., $O(B \cdot n \cdot p(n \cdot r))$ in total. Including the final averaging of each of the n LID estimates over the B bags, in $O(B \cdot n)$ time, the time complexity of the whole process can be expressed as $O(B \cdot n \cdot r) + O(B \cdot n \cdot p(n \cdot r)) + O(B \cdot n)$, and recalling that $r \in (0, 1)$, it then follows that *bagging* has a total runtime of $O(B \cdot n + B \cdot n \cdot p(n \cdot r))$. In contrast, it is clear that the time complexity of the *baseline estimator* is simply $O(n \cdot p(n))$.

For the wide family of k -NN LID estimators, finding the k nearest neighbors of each query is usually the computational bottleneck, which means the time it takes to estimate LID for a single query within a sample of size n , $O(p(n))$, is essentially determined by the time it takes to find its k -NN. Using a naive exhaustive search, we have $O(p(n)) \rightarrow O(n)$ per query assuming $k \ll n$, whereas the use of an index would allow, under the same assumption, an amortized search per query in $O(p(n)) \rightarrow O(\log n)$ time (on average, already considering the construction of the index).

For naive search, the total runtime complexity for bagging then becomes $O(B \cdot n + B \cdot r \cdot n^2) \rightarrow O(n^2)$, and the simple estimator also becomes $O(n \cdot n) \rightarrow O(n^2)$. Either can be faster or slower depending on a combination of n , B , and r . In short, for large enough n , bagging can be faster as long as $r < 1/B$.

With an index, the total runtime complexity for bagging becomes $O(B \cdot n + B \cdot n \cdot \log(n \cdot r)) \rightarrow O(n \cdot \log n)$, and the baseline estimator also becomes $O(n \cdot \log n)$. In this case, however, the baseline tends to be faster in practical terms.

Note that in our experiments, as presented in the main paper, when we applied smoothing, we obtained smoothed LID estimates for a query by taking the arithmetic average of the estimates over its k -NN (the same neighborhood size used by the baseline estimator). However, in this more general complexity analysis, we are not going to make this assumption, as smoothing can easily be applied³ using any other neighborhood sample size up to n , denoted in the following by the integer hyper-parameter $k_s \in \{1, \dots, n\}$.

As a result, the time-complexity of estimating at a single query is multiplied by the number of neighbors (k_s) we use to smooth over. Additionally, we have to take into account the time of finding the k_s -NNs of the query, which is not generally given in the case of an arbitrary estimator baseline, and is free only when assuming $k \geq k_s$ when considering k -NN estimator baselines. Additionally, for bagging with pre-smoothing, this search has to be performed per-bag, instead of the whole dataset, much like the way k_s -NN estimators are applied in bagging.

In the other usual case, when estimating at all of the sample points as query locations, the estimates to average may only be calculated once for any of the variants, as the bags can be kept fixed throughout, and smoothing can reuse the precomputed estimates around each query. This results in effectively the same runtimes as for bagging, with only an additional term for finding k_s -NNs.

The exact resulting time-complexities for the general and the k -NN baseline specific settings are listed in Tables 2, 3, and Tables 4, 5 respectively.

³Without making any claims about qualitative performance.

Table 2: Runtime complexities in general. (Naive Search)

Method	Runtime Complexity At a single query	Runtime Complexity For a dataset as queries
Baseline	$O(p(n))$	$O(np(n))$
Bagging	$O(Bp(nr))$	$O(Bnp(nr))$
Baseline with Smoothing	$O(n + k_s p(n))$	$O(n^2 + np(n))$
Bagging with post-smoothing	$O(n + Bk_s p(nr))$	$O(n^2 + Bnp(nr))$
Bagging with pre-smoothing	$O(Brn + Bk_s p(nr))$	$O(Brn^2 + Bnp(nr))$
Bagging with pre-smoothing and post-smoothing	$O(n + Bk_s nr + Bk_s^2 p(nr))$	$O(n^2 + Bn^2 r + Bnp(nr))$

Table 3: Runtime complexities in general. (Amortized search, Neighbor indices)

Method	Runtime Complexity At a single query	Runtime Complexity For a dataset as queries
Baseline	$O(p(n))$	$O(np(n))$
Bagging	$O(Bp(nr))$	$O(Bnp(nr))$
Baseline with Smoothing	$O(\log(n) + k_s p(n))$	$O(n \log(n) + np(n))$
Bagging with post-smoothing	$O(\log(n) + Bk_s p(nr))$	$O(n \log(n) + Bnp(nr))$
Bagging with pre-smoothing	$O(B \log(nr) + Bk_s p(nr))$	$O(Bn \log(nr) + Bnp(nr))$
Bagging with pre-smoothing and post-smoothing	$O(\log(n) + Bk_s \log(nr) + Bk_s^2 p(nr))$	$O(n \log(n) + Bn \log(nr) + Bnp(nr))$

Table 4: Runtime complexities for k -NN estimation methods. (Naive Search)

Method	Runtime Complexity At a single query	Runtime Complexity For a dataset as queries
Baseline	$O(n)$	$O(n^2)$
Bagging	$O(Brn)$	$O(Brn^2)$
Baseline with Smoothing	$O(n + k_s n)$	$O(n^2)$
Bagging with post-smoothing	$O(n + Brk_s n)$	$O(n^2 + Brn^2)$
Bagging with pre-smoothing	$O(Brn + Brk_s n)$	$O(Brn^2)$
Bagging with pre-smoothing and post-smoothing	$O(n + Brk_s^2 n)$	$O(n^2 + Brn^2)$

Table 5: Runtime complexities for k -NN estimation methods. (Amortized search, Neighbor indices)

Method	Runtime Complexity At a single query	Runtime Complexity For a dataset as queries
Baseline	$O(\log(n))$	$O(n \log(n))$
Bagging	$O(B \log(nr))$	$O(Bn \log(nr))$
Baseline with Smoothing	$O(k_s \log(n))$	$O(n \log(n))$
Bagging with post-smoothing	$O(\log(n) + Bk_s \log(nr))$	$O(n \log(n) + Bn \log(nr))$
Bagging with pre-smoothing	$O(B \log(nr) + Bk_s \log(nr))$	$O(Bn \log(nr))$
Bagging with pre-smoothing and post-smoothing	$O(\log(n) + Bk_s^2 \log(nr))$	$O(n \log(n) + Bn \log(nr))$

B Proofs

B.1 Proof of Theorem A.1

Proof. We start by proving the middle equality. Where first, we note the following. It follows from the assumption that X_1, \dots, X_n are i.i.d. (independent and identically distributed), and that X_1, \dots, X_n and $\Pi^{(i)}$ are independent,

that for all i , we have $\hat{\theta}_{m,i} \stackrel{d}{=} \hat{\theta}_m$.⁴

To put it more rigorously:

For any Borel set $A \subseteq \mathbb{R}^{dim \times m}$, we have that, using the Law of Total Probability:

$$\begin{aligned}
& P\left(\left(X_{\Pi_1^{(i)}}, \dots, X_{\Pi_m^{(i)}}\right) \in A\right) = \\
& = \mathbb{E}\left[P\left(\left(X_{\Pi_1^{(i)}}, \dots, X_{\Pi_m^{(i)}}\right) \in A \mid \Pi_1^{(i)}, \dots, \Pi_m^{(i)}\right)\right] \\
& = \sum_{\pi \in \text{supp}(\Pi^{(i)})} P\left(\left(X_{\pi_1}, \dots, X_{\pi_m}\right) \in A \mid \Pi^{(i)} = \pi\right) \cdot P(\Pi^{(i)} = \pi) \\
& = \sum_{\pi \in \text{supp}(\Pi^{(i)})} P\left(\left(X_{\pi_1}, \dots, X_{\pi_m}\right) \in A\right) \cdot P(\Pi^{(i)} = \pi) \\
& = \sum_{\pi \in \text{supp}(\Pi^{(i)})} P\left(\left(X_{\pi_1}, \dots, X_{\pi_m}\right) \in A\right) \cdot \frac{1}{|\text{supp}(\Pi^{(i)})|} \\
& = \sum_{\pi \in \text{supp}(\Pi^{(i)})} P\left(\left(X_1, \dots, X_m\right) \in A\right) \cdot \frac{1}{|\text{supp}(\Pi^{(i)})|} \tag{B.1} \\
& = P\left(\left(X_1, \dots, X_m\right) \in A\right) \cdot \left(\sum_{\pi \in \text{supp}(\Pi^{(i)})} \frac{1}{|\text{supp}(\Pi^{(i)})|}\right) \\
& = P\left(\left(X_1, \dots, X_m\right) \in A\right) \cdot \left(\frac{\sum_{\pi \in \text{supp}(\Pi^{(i)})} 1}{|\text{supp}(\Pi^{(i)})|}\right) \\
& = P\left(\left(X_1, \dots, X_m\right) \in A\right) \cdot \frac{\binom{n}{m}}{\binom{n}{m}} \\
& = P\left(\left(X_1, \dots, X_m\right) \in A\right).
\end{aligned}$$

Where, to get to line 4 we used the independence of X_1, \dots, X_n and $\Pi^{(i)}$ to simplify the conditional probability, then to get to line 5 we used that $\Pi^{(i)}$ is uniformly distributed over the $\binom{n}{m}$ different index permutations. And to get to line 6 we used that we have

$$(X_{\pi_1}, \dots, X_{\pi_m}) \stackrel{d}{=} (X_1, \dots, X_m),$$

for any $\pi \in \text{supp}(\Pi^{(i)})$, because for any Borel set A , we have $P\left(\left(X_{\pi_1}, \dots, X_{\pi_m}\right) \in A\right) = P\left(\left(X_1, \dots, X_m\right) \in A\right)$, for any deterministic choice of indices π by the i.i.d. assumption on X_1, \dots, X_n . After that it is simple algebraic manipulations.

Therefore, Equation B.1 shows that $(X_{\Pi_1}, \dots, X_{\Pi_m}) \stackrel{d}{=} (X_1, \dots, X_m)$, by the definition of equality in distribution, which implies that for a $\hat{\theta}$ statistic, a measurable function of the sample, $\hat{\theta}(X_{\Pi_1}, \dots, X_{\Pi_m}) \stackrel{d}{=} \hat{\theta}(X_1, \dots, X_m)$, and using the notation in Definition (3.1) this means $\hat{\theta}_{m,i} \stackrel{d}{=} \hat{\theta}_m$.

Given that $\hat{\theta}_{m,i} \stackrel{d}{=} \hat{\theta}_m$, we have $\text{Var}(\hat{\theta}_{m,i}) = \text{Var}(\hat{\theta}_m)$.

Furthermore, for any $i_1 \neq j_1, i_2 \neq j_2$, we have that $(\hat{\theta}_{m,i_1}, \hat{\theta}_{m,j_1}) \stackrel{d}{=} (\hat{\theta}_{m,i_2}, \hat{\theta}_{m,j_2})$. Which follows from the assumption that the random index sets $\Pi^{(i_1)}, \Pi^{(j_1)}$ and $\Pi^{(i_2)}, \Pi^{(j_2)}$ are independent and identically distributed respectively.

To put it more rigorously:

⁴We use the $\stackrel{d}{=}$ notation to signal equality in distribution between two random variables, that is a fairly common notation in statistics textbooks.

For any Borel sets $A_1, A_2 \subseteq \mathbb{R}^{dim \times m}$, using the Law of Total Probability we have that

$$\begin{aligned}
& P\left(\left(X_{\Pi_1^{(i_1)}}, \dots, X_{\Pi_m^{(i_1)}}\right) \in A_1, \left(X_{\Pi_1^{(j_1)}}, \dots, X_{\Pi_m^{(j_1)}}\right) \in A_2\right) = \\
& = \mathbb{E}\left[P\left(\left(X_{\Pi_1^{(i_1)}}, \dots, X_{\Pi_m^{(i_1)}}\right) \in A_1, \left(X_{\Pi_1^{(j_1)}}, \dots, X_{\Pi_m^{(j_1)}}\right) \in A_2 \mid X_1, \dots, X_n\right)\right] \\
& = \int P\left(\left(X_{\Pi_1^{(i_1)}}, \dots, X_{\Pi_m^{(i_1)}}\right) \in A_1, \left(X_{\Pi_1^{(j_1)}}, \dots, X_{\Pi_m^{(j_1)}}\right) \in A_2 \mid (X_1, \dots, X_n) = (x_1, \dots, x_n)\right) dP(X_1, \dots, X_n) \\
& = \int P\left(\left(x_{\Pi_1^{(i_1)}}, \dots, x_{\Pi_m^{(i_1)}}\right) \in A_1, \left(x_{\Pi_1^{(j_1)}}, \dots, x_{\Pi_m^{(j_1)}}\right) \in A_2\right) dP(X_1, \dots, X_n) \\
& = \int P\left(\left(x_{\Pi_1^{(i_2)}}, \dots, x_{\Pi_m^{(i_2)}}\right) \in A_1\right) P\left(\left(x_{\Pi_1^{(j_2)}}, \dots, x_{\Pi_m^{(j_2)}}\right) \in A_2\right) dP(X_1, \dots, X_n) \\
& = \int P\left(\left(x_{\Pi_1^{(i_2)}}, \dots, x_{\Pi_m^{(i_2)}}\right) \in A_1\right) P\left(\left(x_{\Pi_1^{(j_2)}}, \dots, x_{\Pi_m^{(j_2)}}\right) \in A_2\right) dP(X_1, \dots, X_n) \\
& = \int P\left(\left(x_{\Pi_1^{(i_2)}}, \dots, x_{\Pi_m^{(i_2)}}\right) \in A_1, \left(x_{\Pi_1^{(j_2)}}, \dots, x_{\Pi_m^{(j_2)}}\right) \in A_2\right) dP(X_1, \dots, X_n) \\
& = P\left(\left(X_{\Pi_1^{(i_2)}}, \dots, X_{\Pi_m^{(i_2)}}\right) \in A_1, \left(X_{\Pi_1^{(j_2)}}, \dots, X_{\Pi_m^{(j_2)}}\right) \in A_2\right).
\end{aligned} \tag{B.2}$$

Where to get to line 4 we used the independence of X_1, \dots, X_n and $\Pi^{(i_1)}, \Pi^{(j_1)}$. Then, to get to line 5 we used the independence of $\Pi^{(i_1)}$ and $\Pi^{(j_1)}$. Then, to get to line 6 we used that $\Pi^{(i_1)}$ and $\Pi^{(i_2)}$ and $\Pi^{(j_1)}$ and $\Pi^{(j_2)}$ are identically distributed. After that, the same equalities can be repeated backwards with the same reasoning, just using $\Pi^{(i_2)}, \Pi^{(j_2)}$ instead, to arrive at the desired result.

Therefore, we have shown that

$$\left(\left(X_{\Pi_1^{(i_1)}}, \dots, X_{\Pi_m^{(i_1)}}\right), \left(X_{\Pi_1^{(j_1)}}, \dots, X_{\Pi_m^{(j_1)}}\right)\right) \stackrel{d}{=} \left(\left(X_{\Pi_1^{(i_2)}}, \dots, X_{\Pi_m^{(i_2)}}\right), \left(X_{\Pi_1^{(j_2)}}, \dots, X_{\Pi_m^{(j_2)}}\right)\right) \tag{B.3}$$

which implies that for the $\hat{\theta}$ statistic, a measurable function of the sample, we have

$$\left(\hat{\theta}\left(X_{\Pi_1^{(i_1)}}, \dots, X_{\Pi_m^{(i_1)}}\right), \hat{\theta}\left(X_{\Pi_1^{(j_1)}}, \dots, X_{\Pi_m^{(j_1)}}\right)\right) \stackrel{d}{=} \left(\hat{\theta}\left(X_{\Pi_1^{(i_2)}}, \dots, X_{\Pi_m^{(i_2)}}\right), \hat{\theta}\left(X_{\Pi_1^{(j_2)}}, \dots, X_{\Pi_m^{(j_2)}}\right)\right) \tag{B.4}$$

with equivalent notation $(\hat{\theta}_{m,i_1}, \hat{\theta}_{m,j_1}) \stackrel{d}{=} (\hat{\theta}_{m,i_2}, \hat{\theta}_{m,j_2})$. Given that $(\hat{\theta}_{m,i_1}, \hat{\theta}_{m,j_1}) \stackrel{d}{=} (\hat{\theta}_{m,i_2}, \hat{\theta}_{m,j_2})$, we have $\text{cov}(\hat{\theta}_{m,i_1}, \hat{\theta}_{m,j_1}) = \text{cov}(\hat{\theta}_{m,i_2}, \hat{\theta}_{m,j_2})$.

As we have shown that the covariances $\text{cov}(\hat{\theta}_{m,i}, \hat{\theta}_{m,j})$ are always the same for $i \neq j$, we have that $\text{cov}(\hat{\theta}_{m,i}, \hat{\theta}_{m,j}) =: \gamma_m$ is a constant. We've already shown that $\text{Var}(\hat{\theta}_{m,i}) = \text{Var}(\hat{\theta}_m)$ for all i , so that the variances are constant as well. Putting these together, implies that we have

$$\rho_m := \text{corr}(\hat{\theta}_{m,i}, \hat{\theta}_{m,j}) = \frac{\text{cov}(\hat{\theta}_{m,i}, \hat{\theta}_{m,j})}{\sqrt{\text{Var}(\hat{\theta}_{m,i})\text{Var}(\hat{\theta}_{m,j})}} = \frac{\gamma_m}{\sqrt{\text{Var}(\hat{\theta}_m)\text{Var}(\hat{\theta}_m)}} = \frac{\gamma_m}{\text{Var}(\hat{\theta}_m)},$$

which provides us the $\gamma_m = \rho_m \text{Var}(\hat{\theta}_m)$ relationship.

Now we can continue with the main part of the proof, showing the middle equality.

According to definition (3.1), and the derived equalities of variances, we have

$$\begin{aligned}
& \text{Var}(\hat{\theta}_{B,m}) = \\
& = \text{Var}\left(\frac{1}{B} \sum_{i=1}^B \hat{\theta}_{m,i}\right) \\
& = \frac{1}{B^2} \sum_{i=1}^B \sum_{j=1}^B \text{cov}(\hat{\theta}_{m,i}, \hat{\theta}_{m,j}) \\
& = \frac{1}{B^2} \sum_{i=1}^B \text{cov}(\hat{\theta}_{m,i}, \hat{\theta}_{m,i}) + \frac{1}{B^2} \sum_{i=1}^B \sum_{j \neq i}^B \text{cov}(\hat{\theta}_{m,i}, \hat{\theta}_{m,j}) \\
& = \frac{1}{B^2} \sum_{i=1}^B \text{Var}(\hat{\theta}_{m,i}) + \frac{1}{B^2} \sum_{i=1}^B \sum_{j \neq i}^B \gamma_m \tag{B.5} \\
& = \frac{1}{B^2} \sum_{i=1}^B \text{Var}(\hat{\theta}_m) + \frac{1}{B^2} \sum_{i=1}^B \sum_{j \neq i}^B \rho_m \text{Var}(\hat{\theta}_m) \\
& = \frac{1}{B} \text{Var}(\hat{\theta}_m) + \frac{B^2 - B}{B^2} \rho_m \text{Var}(\hat{\theta}_m) \\
& = \text{Var}(\hat{\theta}_m) \left(\frac{1}{B} + \rho_m - \frac{\rho_m}{B} \right) \\
& = \text{Var}(\hat{\theta}_m) \left(\rho_m + \frac{1 - \rho_m}{B} \right)
\end{aligned}$$

This proves the middle equality, and from here we only need to know that the correlation is always such that $-1 \leq \rho_m \leq 1$. Therefore, for $B > 1$ we have,

$$\begin{aligned}
& \rho_m \leq 1 \\
& \rho_m + \frac{1 - \rho_m}{B} = \frac{\rho_m(B - 1) + 1}{B} \leq \frac{B - 1 + 1}{B} = 1 \\
& \rho_m + \frac{1 - \rho_m}{B} \leq 1 \tag{B.6} \\
& 0 \leq \text{Var}(\hat{\theta}_m) \\
& \text{Var}(\hat{\theta}_m) \left(\rho_m + \frac{1 - \rho_m}{B} \right) \leq \text{Var}(\hat{\theta}_m)
\end{aligned}$$

as the variance is always non-negative, and

$$\begin{aligned}
& \rho_m \leq 1 \\
& 0 \leq \frac{1 - \rho_m}{B} \\
& \rho_m \leq \rho_m + \frac{1 - \rho_m}{B} \\
& 0 \leq \text{Var}(\hat{\theta}_m) \tag{B.7} \\
& \rho_m \text{Var}(\hat{\theta}_m) \leq \text{Var}(\hat{\theta}_m) \left(\rho_m + \frac{1 - \rho_m}{B} \right) \\
& \text{cov}(\hat{\theta}_{m,i}, \hat{\theta}_{m,j}) = \gamma_m = \rho_m \text{Var}(\hat{\theta}_m) \leq \text{Var}(\hat{\theta}_m) \left(\rho_m + \frac{1 - \rho_m}{B} \right) \\
& \text{cov}(\hat{\theta}_{m,i}, \hat{\theta}_{m,j}) \leq \text{Var}(\hat{\theta}_m) \left(\rho_m + \frac{1 - \rho_m}{B} \right)
\end{aligned}$$

It's also clear that

$$\lim_{B \rightarrow \infty} \text{Var}(\hat{\theta}_m) \left(\rho_m + \frac{1 - \rho_m}{B} \right) = \rho_m \text{Var}(\hat{\theta}_m) = \gamma_m = \text{cov}(\hat{\theta}_{m,i}, \hat{\theta}_{m,j}) \tag{B.8}$$

as $\text{Var}(\hat{\theta}_m)$ and ρ_m are not functions of B . □

B.2 Proof of Theorem 1

Proof. Let's denote:

$$\gamma(m) := \text{cov}(\hat{\theta}_{m,i}, \hat{\theta}_{m,j} \mid |\Pi^{(i)} \cap \Pi^{(j)}|), \quad (\text{B.9})$$

where we have that $\gamma(m) = f_m(|\Pi^{(i)} \cap \Pi^{(j)}|)$ is a random variable that is a function of the random variable $|\Pi^{(i)} \cap \Pi^{(j)}|$, for some f_m measurable function. With this notation we may write $\gamma(h, m) = f_m(h)$ and $\gamma(H, m) = f_m(H)$ for a random variable H , where $H \stackrel{d}{=} |\Pi^{(i)} \cap \Pi^{(j)}|$ implies $\gamma(H, m) = f_m(H) \stackrel{d}{=} f_m(|\Pi^{(i)} \cap \Pi^{(j)}|) = \gamma(m)$. Meaning that for any $H \stackrel{d}{=} |\Pi^{(i)} \cap \Pi^{(j)}|$, we have that $\gamma(H, m) \stackrel{d}{=} \gamma(m)$, along the definition of $\gamma(h, m)$ in the theorem statement. ⁵

First we show,

1. $|\Pi^{(i)} \cap \Pi^{(j)}| \sim \text{Hypergeometric}(n, m, m)$,
2. $|\Pi^{(i)} \cap \Pi^{(j)}| \perp \Pi^{(i)}$,
3. $|\Pi^{(i)} \cap \Pi^{(j)}| \perp \Pi^{(j)}$,

which we will make use of in the later parts of the proof.⁶

1.

Observe that for a given index set $\pi^{(i)}$ we have that $|\pi^{(i)} \cap \Pi^{(j)}| \sim \text{Hypergeometric}(n, m, m)$ distributed. As for any $h \in \{0, 1, \dots, m\}$, we can select, without permutations, in $\binom{m}{h}$ different ways, the h elements from $\pi^{(i)}$ to be matched by $\Pi^{(j)}$. Then we can select out of the remaining $n - h$ elements those $m - h$ which are not matching in $\binom{n-m}{m-h}$ different ways, giving us that $P(|\pi^{(i)} \cap \Pi^{(j)}| = h) = \frac{\binom{m}{h} \binom{n-m}{m-h}}{\binom{n}{m}}$ for $h = 0, 1, \dots, m$, which is the probability mass function of the Hypergeometric(n, m, m) distribution. From this, we can easily deduce using the Law of Total Probability, that,

$$\begin{aligned} P(|\Pi^{(i)} \cap \Pi^{(j)}| = h) &= \\ &= \mathbb{E}\left[P(|\Pi^{(i)} \cap \Pi^{(j)}| = h \mid \Pi^{(i)})\right] \\ &= \sum_{\pi^{(i)} \in \text{supp}(\Pi^{(i)})} P(|\pi^{(i)} \cap \Pi^{(j)}| = h \mid \Pi^{(i)} = \pi^{(i)}) \cdot P(\Pi^{(i)} = \pi^{(i)}) \\ &= \sum_{\pi^{(i)} \in \text{supp}(\Pi^{(i)})} P(|\pi^{(i)} \cap \Pi^{(j)}| = h) \cdot \frac{1}{\binom{n}{m}} \\ &= \sum_{\pi^{(i)} \in \text{supp}(\Pi^{(i)})} \frac{\binom{m}{h} \binom{n-m}{m-h}}{\binom{n}{m}} \cdot \frac{1}{\binom{n}{m}} \quad (\text{B.10}) \\ &= \frac{\binom{m}{h} \binom{n-m}{m-h}}{\binom{n}{m}^2} \cdot \left(\sum_{\pi^{(i)} \in \text{supp}(\Pi^{(i)})} 1 \right) \\ &= \frac{\binom{m}{h} \binom{n-m}{m-h}}{\binom{n}{m}^2} \cdot \binom{n}{m} \\ &= \frac{\binom{m}{h} \binom{n-m}{m-h}}{\binom{n}{m}}. \end{aligned}$$

Where the argument goes similar to B.1 in the previous proof. To get to line 4 we used the independence of $\Pi^{(i)}$ and $\Pi^{(j)}$, then we use the uniform distributional assumption for $\Pi^{(i)}$, and then we substitute the probability mass function of the Hypergeometric(n, m, m) distribution, which we showed before. Completed by simple algebraic manipulations.

Equation B.10 shows that $|\Pi^{(i)} \cap \Pi^{(j)}|$ is also Hypergeometric(n, m, m) distributed, according its probability mass function.

2./3.

⁵We use the $\stackrel{d}{=}$ notation to signal equality in distribution between two random variables, that is a fairly common notation in statistics textbooks.

⁶We use the \perp notation for independence between random variables, and the \sim notation to point out the distribution of a random variable.

This also means, that because $\Pi^{(i)}$ and $\Pi^{(j)}$ are independent, we have for any $\pi^{(i)} \in \text{supp}(\Pi^{(i)})$, and for any $h \in \text{supp}(|\Pi^{(i)} \cap \Pi^{(j)}|)$,

$$\begin{aligned}
P(|\Pi^{(i)} \cap \Pi^{(j)}| = h \mid \Pi^{(i)} = \pi^{(i)}) &= \frac{P(|\pi^{(i)} \cap \Pi^{(j)}| = h \cap \Pi^{(i)} = \pi^{(i)})}{P(\Pi^{(i)} = \pi^{(i)})} \\
&= \frac{P(|\pi^{(i)} \cap \Pi^{(j)}| = h) \cdot P(\Pi^{(i)} = \pi^{(i)})}{P(\Pi^{(i)} = \pi^{(i)})} \\
&= P(|\pi^{(i)} \cap \Pi^{(j)}| = h) \\
&= \frac{\binom{m}{h} \binom{n-m}{m-h}}{\binom{n}{m}} \\
&= P(|\Pi^{(i)} \cap \Pi^{(j)}| = h)
\end{aligned} \tag{B.11}$$

and therefore we have shown that $|\Pi^{(i)} \cap \Pi^{(j)}|$ and $\Pi^{(i)}$ are independent. We can make a similar argument to show that $|\Pi^{(i)} \cap \Pi^{(j)}|$ and $\Pi^{(j)}$ are independent, as i and j are interchangeable.

Now, onto the main proof, first we show that,

$$\text{cov}(\hat{\theta}_{m,i}, \hat{\theta}_{m,j}) = \mathbb{E}[\gamma(m)]. \tag{B.12}$$

Apply the Law of Total Covariance to get

$$\begin{aligned}
\text{cov}(\hat{\theta}_{m,i}, \hat{\theta}_{m,j}) &= \mathbb{E}[\text{cov}(\hat{\theta}_{m,i}, \hat{\theta}_{m,j} \mid |\Pi^{(i)} \cap \Pi^{(j)}|)] + \text{cov}(\mathbb{E}[\hat{\theta}_{m,i} \mid |\Pi^{(i)} \cap \Pi^{(j)}|], \mathbb{E}[\hat{\theta}_{m,j} \mid |\Pi^{(i)} \cap \Pi^{(j)}|]) \\
&= \mathbb{E}[\gamma(m)] + \text{cov}(\mathbb{E}[\hat{\theta}_{m,i} \mid |\Pi^{(i)} \cap \Pi^{(j)}|], \mathbb{E}[\hat{\theta}_{m,j} \mid |\Pi^{(i)} \cap \Pi^{(j)}|])
\end{aligned} \tag{B.13}$$

As we have that $\Pi^{(i)}$ and $|\Pi^{(i)} \cap \Pi^{(j)}|$ are independent, and X_1, \dots, X_n and $(\Pi^{(i)}, \Pi^{(j)})$ are independent, X_1, \dots, X_n and $|\Pi^{(i)} \cap \Pi^{(j)}|$ are also independent, and therefore $(\Pi^{(i)}, X_1, \dots, X_n)$ and $|\Pi^{(i)} \cap \Pi^{(j)}|$ are independent, implying that for the $\hat{\theta}_{m,i}$ measurable function of $(\Pi^{(i)}, X_1, \dots, X_n)$, we have that $\hat{\theta}_{m,i}$ and $|\Pi^{(i)} \cap \Pi^{(j)}|$ are independent. A similar argument can be made to show that $\hat{\theta}_{m,j}$ and $|\Pi^{(i)} \cap \Pi^{(j)}|$ are independent. Therefore,

$$\begin{aligned}
\mathbb{E}[\hat{\theta}_{m,i} \mid |\Pi^{(i)} \cap \Pi^{(j)}|] &= \mathbb{E}[\hat{\theta}_{m,i}] \\
\mathbb{E}[\hat{\theta}_{m,j} \mid |\Pi^{(i)} \cap \Pi^{(j)}|] &= \mathbb{E}[\hat{\theta}_{m,j}] \\
\text{cov}(\mathbb{E}[\hat{\theta}_{m,i} \mid |\Pi^{(i)} \cap \Pi^{(j)}|], \mathbb{E}[\hat{\theta}_{m,j} \mid |\Pi^{(i)} \cap \Pi^{(j)}|]) &= \text{cov}(\mathbb{E}[\hat{\theta}_{m,i}], \mathbb{E}[\hat{\theta}_{m,j}]) = 0.
\end{aligned} \tag{B.14}$$

As the covariance of two constants $\mathbb{E}[\hat{\theta}_{m,i}]$ and $\mathbb{E}[\hat{\theta}_{m,j}]$ is 0. So, going back to (B.13) we have shown that

$$\text{cov}(\hat{\theta}_{m,i}, \hat{\theta}_{m,j}) = \mathbb{E}[\gamma(m)]. \tag{B.15}$$

Now we can complete the proof.

Using the assumption that $\gamma(h, m) \leq \varphi(\frac{h}{m})$, and that $\gamma(H, m) \stackrel{d}{=} \gamma(m)$ for $H \sim \text{Hypergeometric}(n, m, m)$, we have the bound

$$\mathbb{E}[\gamma(m)] = \mathbb{E}[\gamma(H, m)] \leq \mathbb{E}\left[\varphi\left(\frac{H}{m}\right)\right], \tag{B.16}$$

now, using our assumptions on the properties of φ , for the right side we can apply the generalized Jensen Bound

[37], to arrive at

$$\begin{aligned}
\text{cov}(\hat{\theta}_{m,i}, \hat{\theta}_{m,j}) &= \mathbb{E}[\gamma(m)] = \mathbb{E}\left[\varphi\left(\frac{H}{m}\right)\right] \leq \\
&\leq \varphi\left(\mathbb{E}\left[\frac{H}{m}\right]\right) + \text{Var}\left(\frac{H}{m}\right) \sup_{x \in [0,1]} \frac{\varphi''(x)}{2} = \\
&= \varphi\left(\frac{\mathbb{E}[H]}{m}\right) + \frac{\text{Var}(H)}{m^2} \sup_{x \in [0,1]} \frac{\varphi''(x)}{2} \\
&= \varphi(r) + \frac{n \cdot r \cdot \frac{n-r}{n} \cdot \frac{n-n \cdot r}{n} \cdot \frac{n-n \cdot r}{n-1}}{n^2 \cdot r^2} \sup_{x \in [0,1]} \frac{\varphi''(x)}{2} \\
&= \varphi(r) + \frac{(1-r)^2}{n-1} \sup_{x \in [0,1]} \frac{\varphi''(x)}{2} \\
&= \varphi(r) + (1-r)^2 O\left(\frac{1}{n}\right) \leq \\
&\leq \varphi(r) + O\left(\frac{1}{n}\right)
\end{aligned} \tag{B.17}$$

where in line 4 we substitute in the known theoretical mean and variance of the Hypergeometric(n, m, m) distribution [46]. \square

Variants of Theorem 1: Notice that our main assumption in Theorem 1 (there exists a $\varphi : [0, 1] \rightarrow \mathbb{R}$ such that $\forall_{h,m : h \leq m} \gamma(h, m) \leq \varphi(\frac{h}{m})$) requires the existence of a single such function for all values of h and m , and therefore all values of n as well. This allowed us to merge the $\sup_{x \in [0,1]} \frac{\varphi''(x)}{2}$ constant term into the asymptotic expression ($O(\frac{1}{n})$). In the main part of the thesis, we argued that the assumption is natural because the $\gamma(h, m)$ covariance is expected to increase with a larger $\frac{h}{m}$ ratio. While this is a reasonable idea, the assumption has to hold true for the same function for an infinite number of covariances. Whereas, given any fixed n -value, assuming the existence of a $\varphi_n : [0, 1] \rightarrow \mathbb{R}$ such that $\forall_{h,m : h \leq m, m \leq n} \gamma(h, m) \leq \varphi_n(\frac{h}{m})$ may be an easier condition to satisfy. This assumption, however, on its own, is not enough to obtain the same asymptotic relationship, as we arrive at the

$$\text{cov}(\hat{\theta}_{m,i}, \hat{\theta}_{m,j}) \leq \varphi_n(r) + \frac{(1-r)^2}{n-1} \sup_{x \in [0,1]} \frac{\varphi_n''(x)}{2}$$

inequality, following the same reasoning up until this point as in the proof of Theorem 1. Here the $\sup_{x \in [0,1]} \frac{\varphi_n''(x)}{2}$ term remains dependent on n . An avenue to obtain a similar asymptotic term can be found by additionally assuming $\sup_{n \in \mathbb{Z}^+} \sup_{x \in [0,1]} \varphi_n''(x) < \infty$, and therefore we force the $\sup_{x \in [0,1]} \frac{\varphi_n''(x)}{2} \leq \sup_{m \in \mathbb{Z}^+} \sup_{x \in [0,1]} \varphi_n''(x)$ constant upper bound, allowing us to once again merge this constant term into the asymptotic expression, and arrive at the

$$\text{cov}(\hat{\theta}_{m,i}, \hat{\theta}_{m,j}) \leq \varphi_n(r) + O\left(\frac{1}{n}\right)$$

more specific inequality, for a specific n , in terms of φ_n . Therefore, we can state the following variant of Theorem 1:

Theorem 3. Define the two-variable deterministic function $\gamma(h, m) := \text{cov}(\hat{\theta}_{m,i}, \hat{\theta}_{m,j} \mid |\Pi^{(i)} \cap \Pi^{(j)}| = h)$ for the integer domain given by $m = r \cdot n \in \mathbb{Z}^+$ and $h = 0, 1, \dots, m$, namely, the covariance of two single bag estimators given that we know the number of dependent variables, provided that such a covariance exists and is finite for any pair of bags. Assume that there exists for each n , a twice differentiable, increasing function $\varphi_n : [0, 1] \rightarrow \mathbb{R}$ such that $\forall_{h : h \leq m, m \leq n} \gamma(h, m) \leq \varphi_n(\frac{h}{m})$ and $\sup_{n \in \mathbb{Z}^+} \sup_{x \in [0,1]} \varphi_n''(x) < \infty$, then we have for every n and $m = r \cdot n \in \mathbb{Z}^+$:

$$\forall_{r \in [0,1]} \text{cov}(\hat{\theta}_{m,i}, \hat{\theta}_{m,j}) \leq \varphi_n(r) + O\left(\frac{1}{n}\right) \tag{B.18}$$

Of course, this is only required if we want to be able to retain the same order, namely $O(\frac{1}{n})$. We can even further generalize our assumptions as $\sup_{x \in [0,1]} \varphi_n''(x) = O(n^t)$ with a fixed $t \in [0, 1)$, in which case we still arrive at a vanishing asymptotic term $O(n^{t-1})$.

C Pointwise MSE decomposition for submanifolds

The following is a simple generalization of the common MSE decomposition formula, for the case where queries are allowed to have different ground truth LID.

Given an LID estimator \widehat{LID} and a union of manifolds $D = D_1 \cup D_2 \cup \dots \cup D_L$, $D_i = \{X_{i1}, \dots, X_{i|D_i|}\}$, with known, constant ground truth LIDs per manifold $LID(D_1), \dots, LID(D_L)$, we calculate the total pointwise mean squared error and its decomposition as follows,

$$\begin{aligned}
\overline{LID}(D_i) &:= \frac{1}{|D_i|} \sum_{j=1}^{|D_i|} \widehat{LID}(D_i; X_{ij}), & n &:= \sum_{i=1}^L |D_i|, \\
MSE &:= \frac{1}{n} \sum_{i=1}^L \sum_{j=1}^{|D_i|} \left(\widehat{LID}(D_i; X_{ij}) - LID(D_i) \right)^2 \\
&= \sum_{i=1}^L \frac{|D_i|}{n} \frac{1}{|D_i|} \sum_{j=1}^{|D_i|} \left(\widehat{LID}(D_i; X_{ij}) - LID(D_i) \right)^2 \\
&= \sum_{i=1}^L \frac{|D_i|}{n} MSE_{D_i} \\
&= \sum_{i=1}^L \frac{|D_i|}{n} [VAR_{D_i} + BIAS_{D_i}^2] \\
&= \sum_{i=1}^L \frac{|D_i|}{n} VAR_{D_i} + \sum_{i=1}^L \frac{|D_i|}{n} BIAS_{D_i}^2 \\
&= \underbrace{\sum_{i=1}^L \frac{|D_i|}{n} \left[\frac{1}{|D_i|} \sum_{j=1}^{|D_i|} \left(\widehat{LID}(D_i; X_{ij}) - \overline{LID}(D_i) \right)^2 \right]}_{\text{" VAR "}} + \underbrace{\sum_{i=1}^L \frac{|D_i|}{n} \left(\overline{LID}(D_i) - LID(D_i) \right)^2}_{\text{" BIAS^2 "}}.
\end{aligned} \tag{C.1}$$

where total empirical variance " VAR " and total bias squared " BIAS² " are interpreted as the respective weighted sums of the manifold-wise empirical variances VAR_{D_i} , and bias squares $BIAS_{D_i}^2$, accordingly, for the purposes of the result data in our experiments involving datasets with different LID submanifolds (*Lollipop* data D.13). Note that in the case of varying LID between manifolds, the error is influenced more by estimates of the high ground truth LID points. Therefore, we have to be careful when using evaluation by MSE if we want proportionally low errors for each manifold.

D Dataset descriptions

Table 6: Collection of all datasets used in the experiments. Here d represents the ground-truth LID (GT LID) of the datasets, dim is their representation dimension (i.e., the full dimensionality of the data space), and the last column displays references to detailed descriptions of their sampling function as well as an example visualization.

Dataset Name	d (GT LID)	dim	Ref. (Appendix)
M1_Sphere	10	11	D.1
M2_Affine_3to5	3	5	D.2
M3_Nonlinear_4to6	4	6	D.3
M4_Nonlinear	4	8	D.4
M5b_Helix2d	2	3	D.5
M6_Nonlinear	6	36	D.4
M7_Roll	2	3	D.6
M8_Nonlinear	12	72	D.4
M9_Affine	20	20	D.7
M10a_Cubic	20	11	D.8
M10b_Cubic	17	18	D.8
M10c_Cubic	24	25	D.8
M11_Moebius	2	3	D.9
M12_Norm	20	20	D.10
M13a_Scurve	2	3	D.11
Mn1_Nonlinear	18	72	D.12
Mn2_Nonlinear	24	96	D.12
Lollipop	1,2	2	D.13
Uniform	30	100	D.14

D.1 M1_Sphere

This manifold is a partial sphere surface with local intrinsic dimension d at its points, created using a transformation from a $d + 1$ dimensional parameter space, embedded in m dimensions. We sample from the parameter space using the standard normal distribution and at the end the data points come from the distribution of $\phi(X_1, \dots, X_{d+1})$ where specifically:

$$\begin{aligned}
 X_i &\stackrel{\text{iid.}}{\sim} \mathcal{N}(0, 1), \quad i = 1, \dots, d + 1. \\
 \phi : \mathbb{R}^{d+1} &\longrightarrow \mathbb{R}^m, \\
 \phi(x_1, \dots, x_{d+1}) &:= \left(\frac{x_1}{r}, \dots, \frac{x_{d+1}}{r}, \underbrace{0, \dots, 0}_{m-d-1} \right), \\
 r &= \sqrt{x_1^2 + \dots + x_{d+1}^2}.
 \end{aligned} \tag{D.1}$$

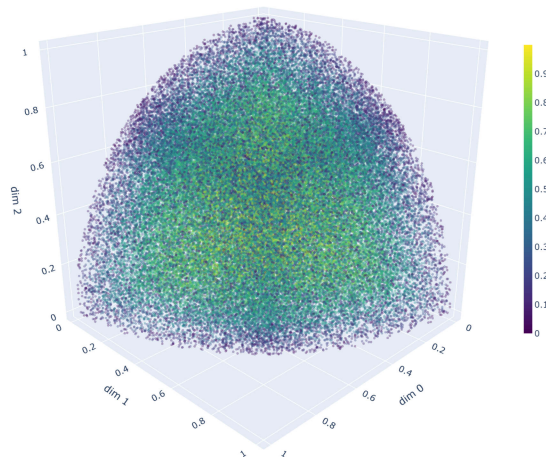


Figure 8: Example visualization of the M1_Sphere dataset, with $d = 3, m = 4$. Visualizing all 4 dimensions. The color range represents the fourth-dimensional axes.

D.2 M2_Affine_3to5

This manifold is an affine hyperplane with local intrinsic dimension 3 at its points. We sample parameters randomly according to the uniform distribution, and transform them into 5 dimensional space using the below function, so, the final data points follow the distribution of $\phi(X_1, X_2, X_3)$.

$$\begin{aligned}
 X_k &\stackrel{\text{iid.}}{\sim} \text{Unif}(0, 4), \quad k = 1, 2, 3. \\
 \phi : \mathbb{R}^3 &\longrightarrow \mathbb{R}^5, \\
 \phi(x_1, x_2, x_3) &= \begin{pmatrix} 1.2x_1 - 0.5x_2 + 3 \\ 0.5x_1 + 0.9x_2 - 1 \\ -0.5x_1 - 0.2x_2 + x_3 \\ 0.4x_1 - 0.9x_2 - 0.1x_3 \\ 1.1x_1 - 0.3x_2 + 8 \end{pmatrix}. \tag{D.2}
 \end{aligned}$$

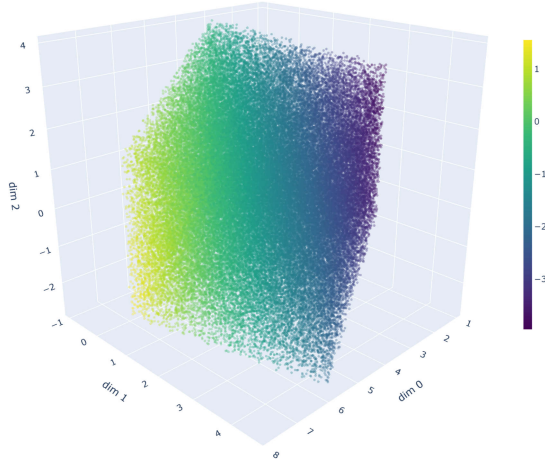


Figure 9: Example visualization of the M2_Affine_3to5 dataset, with $d = 3$. Showing 4 of the 5 dimensions. The color range represents the fourth-dimensional axes.

D.3 M3_Nonlinear_4to6

A nonlinear manifold with 4 parameters sampled from the uniform distribution. To get a feel for the shape, we can look at it in a way that the first two coordinates define a distribution on the unit disk with larger probability density near the axes because of the x_1^2 and x_2^2 multipliers, and the other coordinates in a sense pull this distribution into the other dimensions according to various quadratic structures. As data points come from the distribution of $\phi(X_0, X_1, X_2, X_3)$, where:

$$\begin{aligned}
 X_k &\stackrel{\text{iid.}}{\sim} \text{Unif}(0, 1), \quad k = 0, \dots, 3. \\
 \phi : \mathbb{R}^4 &\longrightarrow \mathbb{R}^6, \\
 \phi(x_0, x_1, x_2, x_3) &= \begin{pmatrix} x_1^2 \cos(2\pi x_0) \\ x_2^2 \sin(2\pi x_0) \\ x_1 + x_2 + (x_1 - x_3)^2 \\ x_1 - 2x_2 + (x_0 - x_3)^2 \\ -x_1 - 2x_2 + (x_2 - x_3)^2 \\ x_0^2 - x_1^2 + x_2^2 - x_3^2 \end{pmatrix}. \tag{D.3}
 \end{aligned}$$

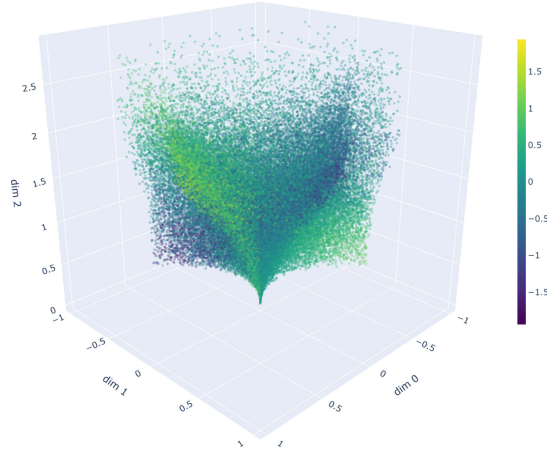


Figure 10: Example visualization of the M3_Nonlinear_4to6 dataset, with $d = 4$. Showing 4 of the 6 dimensions. The color range represents the fourth dimensional axes.

D.4 M4_Nonlinear/M6_Nonlinear/M8_Nonlinear

A highly curved nonlinear manifold. The basic shape is a hypersurface on the cartesian product of d unit disks, obeying the constraints that when thinking of each disk in terms of polar coordinates, the radius of the point according to one disk defines the angle on the next disk, and so on through the d unit disks, in a cyclic way getting back to the first disk at the end. This shape is then repeated m times along a diagonal linear subspace, or in other words is multiplied with the $(1, \dots, 1)$ m -long vector as a Kronecker product. As mathematically described, data points come from the distribution of $\phi(X_0, \dots, X_{d-1})$, where

$$X_i \stackrel{\text{iid.}}{\sim} \text{Unif}(0, 1), \quad i = 0, \dots, d-1.$$

$$\phi : \mathbb{R}^d \longrightarrow \mathbb{R}^{\text{dim}}, \quad m = \frac{\text{dim}}{2d}.$$

For $k = 0, \dots, d-1$, $\ell = 0, \dots, m-1$:

$$\phi_{2k+2d\ell}(x_0, \dots, x_{d-1}) = \begin{cases} x_{k+1} \cos(2\pi x_k), & 0 \leq k \leq d-2, \\ x_0 \cos(2\pi x_{d-1}), & k = d-1, \end{cases} \quad (\text{D.4})$$

$$\phi_{2k+1+2d\ell}(x_0, \dots, x_{d-1}) = \begin{cases} x_{k+1} \sin(2\pi x_k), & 0 \leq k \leq d-2, \\ x_0 \sin(2\pi x_{d-1}), & k = d-1. \end{cases}$$

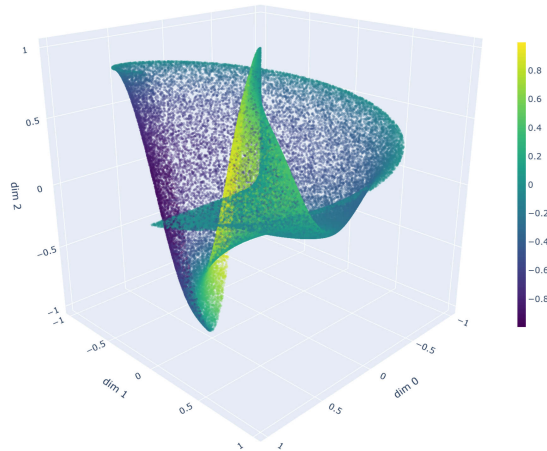


Figure 11: Example visualization of the M4_Nonlinear/M6_Nonlinear/M8_Nonlinear datasets, with $d = 4, m = 1$. Showing 4 of the 8 dimensions. The color range represents the fourth-dimensional axes.

D.5 M5b_Helix2d

A helicoid surface embedded in dim dimensions via $\text{dim} - 3$ extra, all 0 coordinates. Visually speaking, the interesting part is like a disk surface that has been cut into radially and is continually curved upwards into the 3rd dimension. Mathematically, the data points follow the distribution of $\phi(R, P)$, where:

$$\begin{aligned} R &\sim \text{Unif}(0, 10\pi), \quad P \sim \text{Unif}(0, 10\pi), \\ \phi : \mathbb{R}^2 &\longrightarrow \mathbb{R}^{\text{dim}}, \quad \text{dim} \geq 3, \\ \phi(r, p) &= \left(r \cos p, r \sin p, \frac{1}{2}p, \underbrace{0, \dots, 0}_{\text{dim}-3} \right). \end{aligned} \tag{D.5}$$

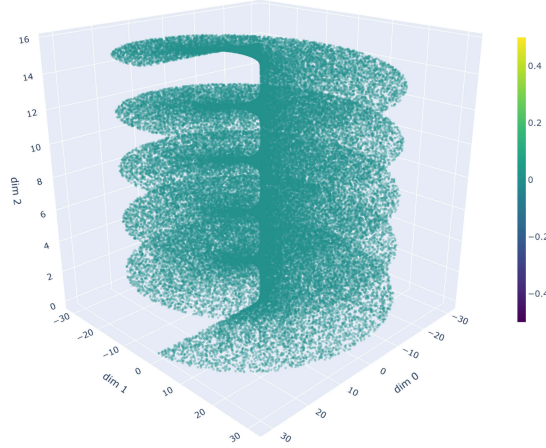


Figure 12: Example visualization of the M5b_Helix2d dataset, with $d = 2$. Showing all 3 dimensions.

D.6 M7_Roll

A loose roll surface, as if a rectangular band has been rolled up, like tape or toilet paper, but in case of this manifold, with a fairly large space in between the surface. The surface is embedded in dim dimensions via $\text{dim} - 3$ extra, all 0 coordinates. Concretely, the data points follow the distribution of $\phi(T, P)$, where:

$$\begin{aligned} T &\sim \text{Unif}(1.5\pi, 4.5\pi), \quad P \sim \text{Unif}(0, 21), \\ \phi : \mathbb{R}^2 &\longrightarrow \mathbb{R}^{\text{dim}}, \quad \text{dim} \geq 3, \\ \phi(t, p) &= \left(t \cos t, p, t \sin t, \underbrace{0, \dots, 0}_{\text{dim}-3} \right). \end{aligned} \tag{D.6}$$

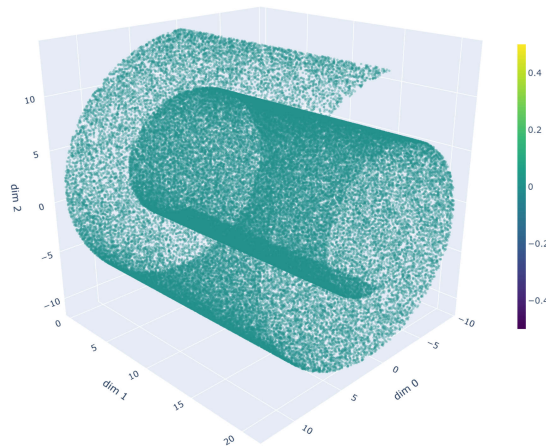


Figure 13: Example visualization of the M7_Roll dataset, with $d = 2$. Showing all 3 dimensions.

D.7 M9_Affine

A simple d dimensional hypercube embedded in dim dimensions via $\text{dim} - d$ extra, all 0 coordinates. The data points follow the distribution of $\phi(X_1, \dots, X_d)$, where

$$\begin{aligned} X_k &\stackrel{\text{iid.}}{\sim} \text{Unif}(-2.5, 2.5), \quad k = 1, \dots, d. \\ \phi : \mathbb{R}^d &\longrightarrow \mathbb{R}^{\text{dim}}, \quad \text{dim} \geq d, \\ \phi(x_1, \dots, x_d) &= (x_1, \dots, x_d, \underbrace{0, \dots, 0}_{\text{dim} - d}). \end{aligned} \tag{D.7}$$

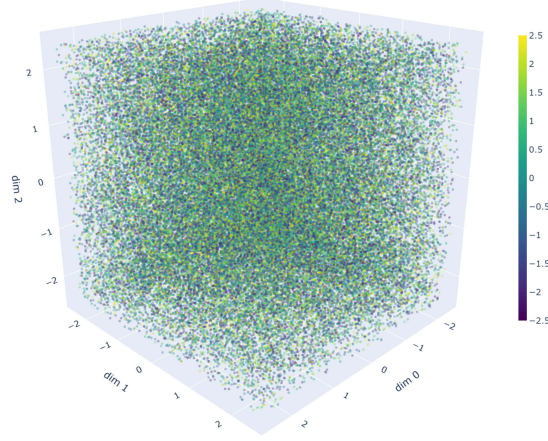


Figure 14: Example visualization of the M9_Affine dataset, with $d = 4$. Showing all 4 dimensions. The color range represents the fourth-dimensional axes.

D.8 M10a_Cubic/M10b_Cubic/M10c_Cubic

The hypersurface of a $d + 1$ dimensional hypercube, meaning that this manifold has intrinsic dimension d . The manifold is embedded in dim dimensions via $\text{dim} - d - 1$ extra, all 0 coordinates. Mathematically we can describe the points as coming from the distribution of $\psi_{I,S}(U_1, \dots, U_d)$, where (I, S) is a uniform categorical random vector over the $\{0, \dots, d\} \times \{0, 1\}$ support, and

$$\begin{aligned} U_j &\stackrel{\text{iid.}}{\sim} \text{Unif}(0, 1), \quad j = 1, \dots, d. \\ \text{Hypercube facet indices } (i, s) &\in \{0, \dots, d\} \times \{0, 1\}. \\ \psi_{i,s} : \mathbb{R}^d &\longrightarrow \mathbb{R}^{\text{dim}}, \\ \psi_{i,s}(u_1, \dots, u_d) &= (u_1, \dots, u_i, s, u_{i+1}, \dots, u_d, \underbrace{0, \dots, 0}_{\text{dim} - d - 1}). \end{aligned} \tag{D.8}$$

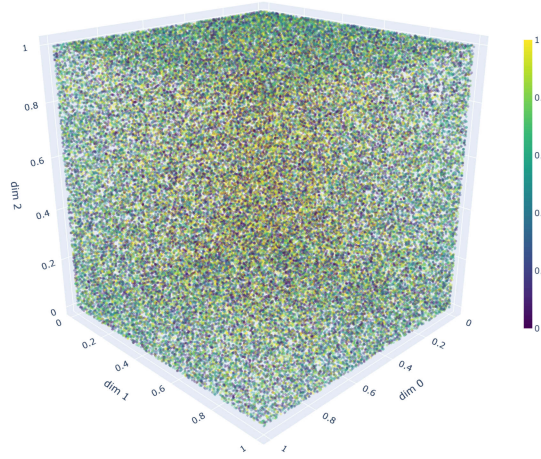


Figure 15: Example visualization of the M10_Cubic dataset, with $d = 4$. Showing all 4 dimensions. The color range represents the fourth-dimensional axes.

D.9 M11_Moebius

This manifold is a Moebius strip surface. A 2 dimensional surface, densely twisted in 3 dimensional space along a circular pattern around a central axis. Specifically, the data points follow the distribution of $\phi(\Phi, R)$ where:

$$\begin{aligned} \Phi &\sim \text{Unif}(0, 2\pi), \quad R \sim \text{Unif}(-1, 1), \\ \phi : \mathbb{R}^2 &\longrightarrow \mathbb{R}^3, \\ \phi(\varphi, r) &= \left(\left[1 + \frac{1}{2}r \cos(5\varphi)\right] \cos(\varphi), \left[1 + \frac{1}{2}r \cos(5\varphi)\right] \sin(\varphi), \frac{1}{2}r \sin(5\varphi) \right). \end{aligned} \tag{D.9}$$

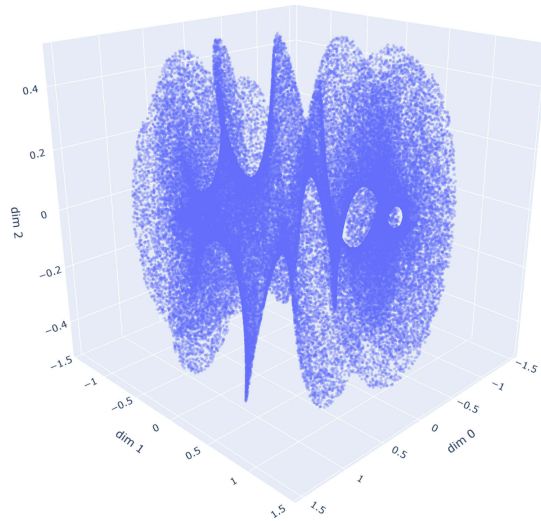


Figure 16: Example visualization of the M11_Moebius dataset, with $d = 2, \text{dim} = 3$. Showing all 3 dimensions.

D.10 M12_Norm

A d dimensional hypercube embedded in dim dimensions via $\text{dim} - d$ extra all 0 coordinates. However, the parameters are sampled from the standard normal distribution, therefore the data points follow the distribution of $\phi(X_1, \dots, X_d)$ where:

$$\begin{aligned} X_i &\stackrel{\text{iid.}}{\sim} \mathcal{N}(0, 1), \quad i = 1, \dots, d, \\ \phi : \mathbb{R}^d &\longrightarrow \mathbb{R}^{\text{dim}}, \quad \text{dim} \geq d, \\ \phi(x_1, \dots, x_d) &= (x_1, \dots, x_d, \underbrace{0, \dots, 0}_{\text{dim}-d}). \end{aligned} \tag{D.10}$$

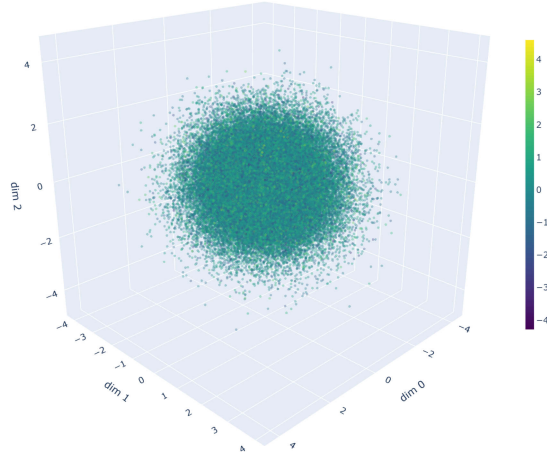


Figure 17: Example visualization of the M12_Norm dataset, with $d = 4$. Showing all 4 dimensions. The color range represents the fourth-dimensional axes.

D.11 M13a_Scurve

A rectangular band surface with intrinsic dimensionality 2 curved in an "S" shape in 3 dimensions, embedded in dim dimensions via $\text{dim} - 3$ extra all 0 coordinates. The data points follow the distribution of $\phi(T, P)$, where

$$\begin{aligned}
 T &\sim \text{Unif}(-1.5\pi, 1.5\pi), \quad P \sim \text{Unif}(0, 2), \\
 \phi : \mathbb{R}^2 &\longrightarrow \mathbb{R}^{\text{dim}}, \quad \text{dim} \geq 3, \\
 \phi(t, p) &= (\sin t, p, \text{sign}(t)(\cos t - 1), \underbrace{0, \dots, 0}_{\text{dim} - 3}).
 \end{aligned}
 \tag{D.11}$$

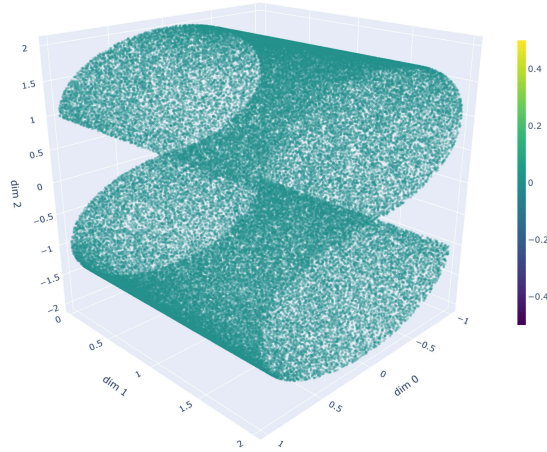


Figure 18: Example visualization of the M13a_Scurve dataset, with $d = 2, \text{dim} = 3$. Showing all 3 dimensions.

D.12 Mn1_Nonlinear/Mn2_Nonlinear

A hypersurface with gradual, multidirectional curvature, repeated twice along a diagonal linear subspace, or in other words is multiplied by $(1, 1)$ as a Kronecker product. The data points are drawn from the distribution of

$\phi(X_0, \dots, X_{d-1})$, described by

$$X_i \stackrel{\text{iid.}}{\sim} \text{Unif}(0, 1), \quad i = 0, \dots, d-1.$$

$$\phi : \mathbb{R}^d \longrightarrow \mathbb{R}^{4d}.$$

For $i = 0, \dots, d-1$ (with $j = d-1-i$) :

$$\phi_{i+1}(x) = \tan(x_i \cos x_j),$$

$$\phi_{d+i+1}(x) = \arctan(x_j \sin x_i),$$

$$\phi_{2d+i+1}(x) = \phi_{i+1}(x),$$

$$\phi_{3d+i+1}(x) = \phi_{d+i+1}(x).$$

(D.12)

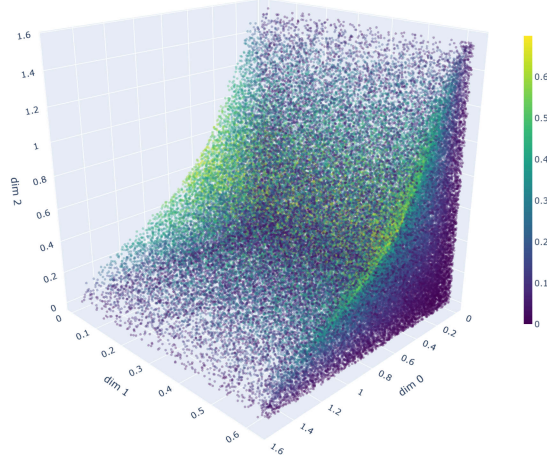


Figure 19: Example visualization of the Mn1_Nonlinear/Mn2_Nonlinear dataset, with $d = 3$, $\text{dim} = 12$. Showing 4 out of the 12 dimensions.

D.13 Lollipop

This manifold is called the "lollipop" dataset because it looks like a lollipop. It consists of two parts, a line section, or stick, which has intrinsic dimensionality 1, and at one end of it, without the two densities intersecting, there is the other part, a disk, or candy, which has intrinsic dimensionality 2. Specifically, sample points are drawn from the distribution of $\phi_Z(R, \Phi, T)$, where $Z \sim \text{Cat}\{C : 0.95, S : 0.05\}$ categorical random variable indicates the component, C the candy part with 95% probability and S the stick part with 5% probability, and we have the following component wise distributions

$$R \sim \text{Unif}(0, 1), \quad \Phi \sim \text{Unif}(0, 2\pi), \quad T \sim \text{Unif}\left(0, 2 - \frac{1}{\sqrt{2}}\right).$$

$$\phi_C : \mathbb{R}^2 \rightarrow \mathbb{R}^2, \quad \phi_S : \mathbb{R} \rightarrow \mathbb{R}^2.$$

$$\phi_C(R, \Phi) = (2 + \sqrt{R} \sin \Phi, \quad 2 + \sqrt{R} \cos \Phi),$$

$$\phi_S(T) = (T, T).$$

(D.13)

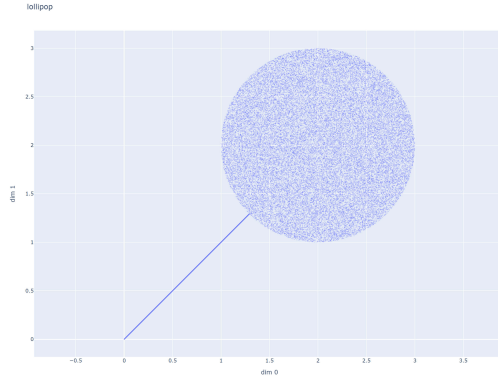


Figure 20: Example visualization of the lollipop dataset, with $d = 2$. Showing all 2 dimensions.

D.14 Uniform

Lastly we have this manifold, that we additionally included for computationally efficient testing in high ambient and local intrinsic dimensionalities. The first d coordinates are i.i.d. uniform, comprising a d dimensional hypercube, which is embedded in dim dimensions via $\text{dim} - d - 1$ exact copies of the last variable, extending the hypercube into dim dimensions along a simple linear subspace. So, sample points are drawn i.i.d. from the distribution of $\phi(V_1, \dots, V_{d-1}, T)$, where

$$V_i \stackrel{\text{iid.}}{\sim} \text{Unif}(0, 1), \quad i = 1, \dots, d - 1, \quad T \sim \text{Unif}(0, 1).$$

$$\phi : \mathbb{R}^d \longrightarrow \mathbb{R}^{\text{dim}},$$

$$\phi(v_1, \dots, v_{d-1}, t) = (v_1, \dots, v_{d-1}, \underbrace{t, \dots, t}_{\text{dim}-d+1}).$$

(D.14)

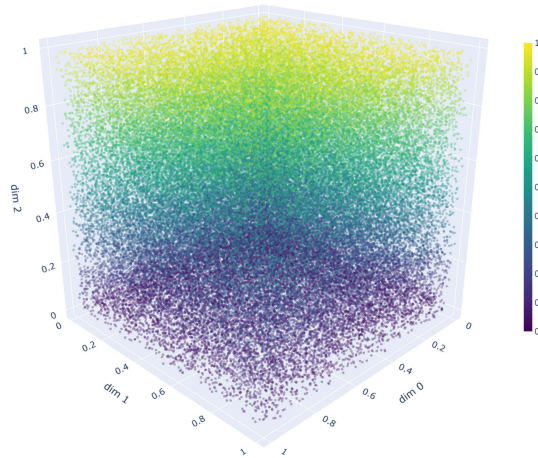


Figure 21: Example visualization of the uniform dataset, with $d = 3$, $\text{dim} = 4$. Showing all 4 dimensions.

E Supplementary results

1. Supplementary tables for the bagging and smoothing experiments E.1:
 - Table of optimal raw results (MSE) for MLE 7
 - Table of optimal raw results (MSE) for TLE 8
 - Table of optimal raw results (MSE) for MADA 9
2. Supplementary bar-chart figures for the effect of r and B experiments E.2:
 - Bar chart with B varying for TLE 22
 - Bar chart with B varying for MADA 23
 - Bar chart with r varying for TLE 24
 - Bar chart with r varying for MADA 25
3. Supplementary heatmaps for B and r interaction through comparing bagging and baseline E.3:
 - Interaction heatmap between B and r for TLE 26
 - Interaction heatmap between B and r for MADA 27
4. Supplementary heatmaps for k and r interaction through comparing bagging and baseline E.4:
 - Interaction heatmap between k and r for TLE 28
 - Interaction heatmap between k and r for MADA 29

E.1 Supplementary tables for the bagging and smoothing experiments

Table 7: Table showing the optimal results for the MLE estimator across the different bagging variants with smoothing. The shown k and r values are the ones that achieved the lowest MSE across experiments for that specific dataset and estimator variant. While the MSE is the lowest one, the Variance and Bias-squared represent the decomposition of this MSE, and therefore, not necessarily the lowest on their own. The table is colored using a per-dataset (one for each row) logarithmic color scale based on the MSE to indicate large to small values as mild red to mild blue colors across the table cells (estimator variants). The best results in a row are additionally written with a bold font. This raw data is the basis of the MLE part of the radar charts analyzed in Section 6 of the main paper.

Estimator: MLE, Optimized for: MSE

Dataset	Baseline	Simple bagging	Baseline with smoothing	Simple bagging with post-smoothing	Simple bagging with pre-smoothing	Simple bagging with pre-smoothing and post-smoothing
M10a_Cubic	k:51 MSE:3.045 Variance:1.65 Bias ² :1.395	k:14, r:0.081 MSE:1.66 Variance:1.172 Bias ² :0.488	k:19 MSE:0.4271 Variance:0.4098 Bias ² :0.01734	k:14, r:0.300 MSE:0.3347 Variance:0.2939 Bias ² :0.04085	k:10, r:0.042 MSE:0.1198 Variance:0.1152 Bias ² :0.004604	k:14, r:0.300 MSE:0.04145 Variance:0.004123 Bias²:0.002198
M10b_Cubic	k:26 MSE:16.61 Variance:8.202 Bias ² :8.405	k:10, r:0.158 MSE:8.031 Variance:6.093 Bias ² :1.938	k:14 MSE:4.048 Variance:1.779 Bias ² :2.27	k:7, r:0.081 MSE:1.652 Variance:1.647 Bias ² :0.00434	k:7, r:0.042 MSE:1.143 Variance:1.105 Bias ² :0.03834	k:7, r:0.059 MSE:0.4229 Variance:0.4227 Bias²:0.0002085
M10c_Cubic	k:19 MSE:45.13 Variance:22.32 Bias ² :22.81	k:7, r:0.081 MSE:19.19 Variance:14.71 Bias ² :4.473	k:10 MSE:13.87 Variance:7.462 Bias ² :6.411	k:7, r:0.158 MSE:5.928 Variance:3.769 Bias ² :2.159	k:7, r:0.158 MSE:3.026 Variance:2.235 Bias ² :0.7915	k:7, r:0.300 MSE:1.261 Variance:0.8185 Bias²:0.4424
M11_Moebius	k:72 MSE:0.1077 Variance:0.09647 Bias ² :0.01119	k:72, r:0.115 MSE:0.09247 Variance:0.09239 Bias ² :8.376e-05	k:72 MSE:0.01308 Variance:0.004446 Bias ² :0.008639	k:37, r:0.600 MSE:0.02813 Variance:0.0135 Bias ² :0.01462	k:72, r:0.115 MSE:0.001664 Variance:0.001035 Bias ² :0.0006287	k:72, r:0.115 MSE:0.001544 Variance:0.0009376 Bias²:0.0006066
M12_Norm	k:26 MSE:23.83 Variance:11.98 Bias ² :11.84	k:7, r:0.059 MSE:12.74 Variance:10.97 Bias ² :1.77	k:10 MSE:7.211 Variance:5.641 Bias ² :1.569	k:7, r:0.158 MSE:3.585 Variance:3.095 Bias ² :0.4903	k:7, r:0.158 MSE:1.672 Variance:1.543 Bias ² :0.1281	k:7, r:0.300 MSE:0.7032 Variance:0.6869 Bias²:0.01627
M13a_Scurve	k:72 MSE:0.06762 Variance:0.06697 Bias ² :0.0006452	k:72, r:0.214 MSE:0.04446 Variance:0.03431 Bias ² :0.01015	k:72 MSE:0.008193 Variance:0.007941 Bias ² :0.0002522	k:72, r:0.600 MSE:0.01437 Variance:0.01179 Bias ² :0.002571	k:26, r:0.059 MSE:0.002063 Variance:0.00204 Bias ² :2.305e-05	k:26, r:0.059 MSE:0.001857 Variance:0.001834 Bias²:2.287e-05
M1_Sphere	k:72 MSE:2.396 Variance:1.07 Bias ² :1.325	k:14, r:0.081 MSE:1.383 Variance:1.204 Bias ² :0.1788	k:26 MSE:0.3654 Variance:0.2095 Bias ² :0.1559	k:14, r:0.158 MSE:0.2352 Variance:0.19 Bias ² :0.0452	k:14, r:0.158 MSE:0.07912 Variance:0.07887 Bias ² :0.0002435	k:14, r:0.158 MSE:0.02414 Variance:0.02369 Bias²:0.0004429
M2_Affine_3to5	k:72 MSE:0.1758 Variance:0.1572 Bias ² :0.01857	k:37, r:0.214 MSE:0.1332 Variance:0.1095 Bias ² :0.02373	k:51 MSE:0.02284 Variance:0.0193 Bias ² :0.003536	k:37, r:0.600 MSE:0.03222 Variance:0.02941 Bias ² :0.002809	k:19, r:0.059 MSE:0.0144 Variance:0.0124 Bias ² :0.001999	k:37, r:0.600 MSE:0.01065 Variance:0.01013 Bias²:0.0005259
M3_Nonlinear_4to6	k:72 MSE:0.6424 Variance:0.6197 Bias ² :0.02265	k:72, r:0.429 MSE:0.5611 Variance:0.4952 Bias ² :0.06591	k:51 MSE:0.125 Variance:0.1166 Bias ² :0.008423	k:37, r:0.600 MSE:0.1701 Variance:0.1599 Bias ² :0.01018	k:37, r:0.600 MSE:0.1188 Variance:0.1162 Bias ² :0.002635	k:37, r:0.600 MSE:0.08245 Variance:0.07803 Bias²:0.004418
M4_Nonlinear	k:51 MSE:0.8804 Variance:0.7723 Bias ² :0.108	k:72, r:0.042 MSE:0.6842 Variance:0.6838 Bias ² :0.000397	k:37 MSE:0.1551 Variance:0.1009 Bias ² :0.05411	k:37, r:0.600 MSE:0.2795 Variance:0.1728 Bias ² :0.1067	k:72, r:0.059 MSE:0.04917 Variance:0.04137 Bias ² :0.01264	k:72, r:0.059 MSE:0.02874 Variance:0.02401 Bias²:0.004724
M5b_Helix2d	k:72 MSE:0.9155 Variance:0.1956 Bias ² :0.7199	k:72, r:0.042 MSE:0.09402 Variance:0.09399 Bias ² :3.653e-05	k:72 MSE:0.7498 Variance:0.02495 Bias ² :0.7248	k:72, r:0.042 MSE:0.07393 Variance:0.07157 Bias ² :0.002367	k:72, r:0.042 MSE:0.01259 Variance:0.0005402 Bias²:0.01205	k:72, r:0.042 MSE:0.01294 Variance:0.0005088 Bias ² :0.01243
M6_Nonlinear	k:72 MSE:3.268 Variance:2.11 Bias ² :1.158	k:72, r:0.059 MSE:0.7403 Variance:0.7389 Bias ² :0.001447	k:72 MSE:0.6402 Variance:0.3084 Bias ² :0.3317	k:72, r:0.081 MSE:0.2964 Variance:0.2872 Bias ² :0.00915	k:72, r:0.081 MSE:0.04917 Variance:0.04739 Bias ² :0.001777	k:72, r:0.081 MSE:0.02005 Variance:0.01878 Bias²:0.001274
M7_Roll	k:72 MSE:0.07171 Variance:0.07153 Bias ² :0.0001764	k:51, r:0.600 MSE:0.06615 Variance:0.06596 Bias ² :0.0001908	k:72 MSE:0.007739 Variance:0.00769 Bias ² :4.847e-05	k:51, r:0.600 MSE:0.012 Variance:0.01197 Bias ² :2.927e-05	k:51, r:0.600 MSE:0.00716 Variance:0.006642 Bias ² :0.0005175	k:51, r:0.600 MSE:0.00515 Variance:0.004605 Bias²:0.0005452
M8_Nonlinear	k:72 MSE:7.642 Variance:4.877 Bias ² :2.765	k:26, r:0.042 MSE:2.02 Variance:1.883 Bias ² :0.1366	k:72 MSE:0.7791 Variance:0.4438 Bias ² :0.3352	k:72, r:0.429 MSE:0.4266 Variance:0.4176 Bias ² :0.009027	k:19, r:0.042 MSE:0.111 Variance:0.1041 Bias ² :0.006866	k:19, r:0.042 MSE:0.03789 Variance:0.03504 Bias²:0.002853
M9_Affine	k:19 MSE:29.88 Variance:14.86 Bias ² :15.02	k:7, r:0.059 MSE:13.08 Variance:9.657 Bias ² :3.421	k:10 MSE:8.311 Variance:5.386 Bias ² :2.925	k:7, r:0.214 MSE:3.694 Variance:2.929 Bias ² :0.7654	k:7, r:0.214 MSE:1.709 Variance:1.55 Bias ² :0.159	k:7, r:0.300 MSE:0.6352 Variance:0.5453 Bias²:0.0899
Mn1_Nonlinear	k:26 MSE:21.08 Variance:9.077 Bias ² :12.01	k:7, r:0.059 MSE:9.604 Variance:8.937 Bias ² :0.6677	k:10 MSE:6.045 Variance:4.574 Bias ² :1.471	k:7, r:0.115 MSE:2.328 Variance:2.15 Bias ² :0.1779	k:7, r:0.115 MSE:1.464 Variance:1.142 Bias ² :0.3219	k:7, r:0.214 MSE:0.6844 Variance:0.6841 Bias²:0.0002162
Mn2_Nonlinear	k:19 MSE:46.58 Variance:21.23 Bias ² :25.35	k:7, r:0.081 MSE:21.25 Variance:15.05 Bias ² :6.202	k:10 MSE:15.75 Variance:5.848 Bias ² :9.901	k:5, r:0.042 MSE:6.274 Variance:6.27 Bias ² :0.004221	k:7, r:0.300 MSE:3.933 Variance:2.409 Bias ² :1.524	k:5, r:0.042 MSE:1.849 Variance:1.528 Bias²:0.3219
lollipop_	k:72 MSE:0.07194 Variance:0.07153 Bias ² :0.0004055	k:72, r:0.429 MSE:0.05584 Variance:0.04861 Bias ² :0.007233	k:72 MSE:0.01177 Variance:0.01088 Bias ² :0.0008863	k:51, r:0.600 MSE:0.01735 Variance:0.01649 Bias ² :0.000853	k:51, r:0.600 MSE:0.01329 Variance:0.0112 Bias ² :0.002095	k:51, r:0.600 MSE:0.01132 Variance:0.008999 Bias²:0.002324
uniform	k:14 MSE:108.4 Variance:38.46 Bias ² :69.93	k:5, r:0.081 MSE:50.6 Variance:34.53 Bias ² :16.07	k:7 MSE:41.53 Variance:32.09 Bias ² :9.446	k:5, r:0.214 MSE:17.08 Variance:13.67 Bias ² :3.411	k:5, r:0.214 MSE:9.665 Variance:1.018	k:5, r:0.214 MSE:5.242 Variance:3.595 Bias²:1.648

Table 8: Table showing the optimal results for the TLE estimator across the different bagging variants with smoothing. The shown k and r values are the ones that achieved the lowest MSE across experiments for that specific dataset and estimator variant. While the MSE is the lowest one, the Variance and Bias-squared represent the decomposition of this MSE, and therefore, not necessarily the lowest on their own. The table is colored using a per-dataset (one for each row) logarithmic color scale based on the MSE to indicate large to small values as mild red to mild blue colors across the table cells (estimator variants). The best results in a row are additionally written with a bold font. This raw data is the basis of the TLE part of the radar charts analyzed in Section 6 of the main paper.

Estimator: TLE, Optimized for: MSE

Dataset	Baseline	Simple bagging	Baseline with smoothing	Simple bagging with post-smoothing	Simple bagging with pre-smoothing	Simple bagging with pre-smoothing and post-smoothing
M10a_Cubic	k:51 MSE:2.817 Variance:1.332 Bias ² :1.485	k:10, r:0.059 MSE:1.555 Variance:1.45 Bias ² :0.1049	k:19 MSE:0.3865 Variance:0.3323 Bias ² :0.0542	k:14, r:0.429 MSE:0.3004 Variance:0.2826 Bias ² :0.01781	k:10, r:0.059 MSE:0.1219 Variance:0.1216 Bias ² :0.0003382	k:14, r:0.300 MSE:0.04494 Variance:0.0416 Bias²:0.003342
M10b_Cubic	k:26 MSE:17.86 Variance:6.854 Bias ² :11.01	k:7, r:0.059 MSE:7.53 Variance:6.091 Bias ² :1.439	k:10 MSE:4.815 Variance:4.153 Bias ² :0.6612	k:7, r:0.115 MSE:1.866 Variance:1.621 Bias ² :0.2457	k:7, r:0.081 MSE:0.888 Variance:0.8342 Bias ² :0.04586	k:7, r:0.115 MSE:0.3456 Variance:0.3391 Bias²:0.006504
M10c_Cubic	k:19 MSE:49.47 Variance:18.47 Bias ² :31	k:7, r:0.158 MSE:23.09 Variance:17.02 Bias ² :6.07	k:10 MSE:15.96 Variance:6.767 Bias ² :9.192	k:5, r:0.042 MSE:6.255 Variance:6.046 Bias ² :0.2085	k:7, r:0.300 MSE:4.332 Variance:2.569 Bias ² :1.763	k:5, r:0.042 MSE:1.829 Variance:1.802 Bias²:0.0274
M11_Moebius	k:51 MSE:0.0629 Variance:0.04857 Bias ² :0.01433	k:72, r:0.115 MSE:0.03707 Variance:0.03343 Bias ² :0.003645	k:51 MSE:0.01966 Variance:0.003584 Bias ² :0.01608	k:72, r:0.115 MSE:0.007439 Variance:0.007431 Bias ² :8.651e-06	k:72, r:0.115 MSE:0.003318 Variance:0.000333 Bias ² :0.002985	k:72, r:0.115 MSE:0.003311 Variance:0.0003086 Bias²:0.003003
M12_Norm	k:19 MSE:29.82 Variance:12.05 Bias ² :17.77	k:7, r:0.115 MSE:14.53 Variance:9.025 Bias ² :5.503	k:10 MSE:8.729 Variance:5.007 Bias ² :3.722	k:7, r:0.300 MSE:4.048 Variance:2.994 Bias ² :1.053	k:7, r:0.300 MSE:2.22 Variance:1.924 Bias ² :0.2952	k:7, r:0.300 MSE:0.9798 Variance:0.6695 Bias²:0.3102
M13a_Scurve	k:72 MSE:0.02966 Variance:0.02962 Bias ² :4.741e-05	k:72, r:0.214 MSE:0.01907 Variance:0.01904 Bias ² :3.223e-05	k:72 MSE:0.005174 Variance:0.004893 Bias ² :0.0002804	k:72, r:0.600 MSE:0.007913 Variance:0.007874 Bias ² :3.896e-05	k:72, r:0.158 MSE:0.002474 Variance:0.001558 Bias ² :0.0009157	k:72, r:0.158 MSE:0.002311 Variance:0.00142 Bias²:0.0008917
M1_Sphere	k:72 MSE:1.884 Variance:0.8888 Bias ² :0.9952	k:14, r:0.081 MSE:1.165 Variance:0.9346 Bias ² :0.2301	k:26 MSE:0.2953 Variance:0.1908 Bias ² :0.1044	k:14, r:0.158 MSE:0.2135 Variance:0.1766 Bias ² :0.03695	k:14, r:0.158 MSE:0.07196 Variance:0.07185 Bias ² :0.0001135	k:14, r:0.158 MSE:0.02213 Variance:0.02212 Bias²:5.993e-06
M2_Affine_3to5	k:72 MSE:0.0962 Variance:0.0827 Bias ² :0.0135	k:19, r:0.059 MSE:0.07974 Variance:0.0727 Bias ² :0.007037	k:51 MSE:0.01451 Variance:0.01145 Bias ² :0.003059	k:37, r:0.600 MSE:0.02141 Variance:0.0187 Bias ² :0.002709	k:19, r:0.059 MSE:0.008114 Variance:0.006624 Bias ² :0.00149	k:19, r:0.059 MSE:0.007194 Variance:0.005808 Bias²:0.001386
M3_Nonlinear_4to6	k:72 MSE:0.4478 Variance:0.4142 Bias ² :0.0336	k:19, r:0.081 MSE:0.3947 Variance:0.3698 Bias ² :0.02492	k:51 MSE:0.1208 Variance:0.1115 Bias ² :0.009276	k:37, r:0.600 MSE:0.1536 Variance:0.1414 Bias ² :0.01224	k:14, r:0.059 MSE:0.07543 Variance:0.07532 Bias ² :0.0001162	k:14, r:0.059 MSE:0.06555 Variance:0.0655 Bias²:4.426e-05
M4_Nonlinear	k:51 MSE:0.6478 Variance:0.5094 Bias ² :0.1383	k:72, r:0.042 MSE:0.1647 Variance:0.1349 Bias ² :0.02984	k:37 MSE:0.1614 Variance:0.07742 Bias ² :0.08399	k:72, r:0.042 MSE:0.111 Variance:0.06462 Bias ² :0.0464	k:72, r:0.059 MSE:0.02582 Variance:0.007662 Bias ² :0.01816	k:72, r:0.059 MSE:0.01868 Variance:0.00465 Bias²:0.01402
M5b_Helix2d	k:72 MSE:0.8524 Variance:0.09564 Bias ² :0.7568	k:72, r:0.042 MSE:0.01635 Variance:0.01218 Bias ² :0.004167	k:72 MSE:0.7795 Variance:0.01599 Bias ² :0.7635	k:72, r:0.042 MSE:0.008336 Variance:0.005979	k:72, r:0.042 MSE:0.00864 Variance:0.0002144 Bias ² :0.008426	k:72, r:0.042 MSE:0.008628 Variance:0.0001932 Bias²:0.008435
M6_Nonlinear	k:72 MSE:1.985 Variance:1.206 Bias ² :0.7787	k:51, r:0.059 MSE:0.3291 Variance:0.3275 Bias ² :0.001692	k:72 MSE:0.4998 Variance:0.2152 Bias ² :0.2847	k:51, r:0.059 MSE:0.1587 Variance:0.1251 Bias ² :0.03359	k:51, r:0.081 MSE:0.03552 Variance:0.03512 Bias ² :0.0003998	k:51, r:0.081 MSE:0.02237 Variance:0.00171 Bias²:0.005267
M7_Roll	k:72 MSE:0.03204 Variance:0.03078 Bias ² :0.00126	k:37, r:0.600 MSE:0.0361 Variance:0.03138 Bias ² :0.00472	k:72 MSE:0.004449 Variance:0.003242 Bias²:0.001207	k:37, r:0.600 MSE:0.01003 Variance:0.006571 Bias ² :0.003461	k:51, r:0.600 MSE:0.007404 Variance:0.003672 Bias ² :0.003731	k:51, r:0.600 MSE:0.005873 Variance:0.00231 Bias ² :0.003564
M8_Nonlinear	k:72 MSE:2.537 Variance:2.369 Bias ² :0.1686	k:51, r:0.300 MSE:1.202 Variance:1.161 Bias ² :0.04056	k:72 MSE:0.1623 Variance:0.1596 Bias ² :0.002687	k:51, r:0.600 MSE:0.1878 Variance:0.1877 Bias ² :0.0001495	k:37, r:0.300 MSE:0.1021 Variance:0.09798 Bias ² :0.004162	k:37, r:0.429 MSE:0.04088 Variance:0.04063 Bias²:0.0002501
M9_Affine	k:19 MSE:33.59 Variance:11.62 Bias ² :21.97	k:7, r:0.115 MSE:14.1 Variance:9.752 Bias ² :4.346	k:10 MSE:11.19 Variance:4.873 Bias ² :6.315	k:5, r:0.042 MSE:3.8 Variance:3.8 Bias ² :0.0003132	k:5, r:0.042 MSE:2.775 Variance:2.699 Bias ² :0.07642	k:5, r:0.042 MSE:1.115 Variance:1.024 Bias²:0.09085
Mn1_Nonlinear	k:19 MSE:24.59 Variance:10.37 Bias ² :14.23	k:7, r:0.081 MSE:10.83 Variance:7.284 Bias ² :3.541	k:10 MSE:6.56 Variance:3.457 Bias ² :3.103	k:7, r:0.214 MSE:3.18 Variance:2.169 Bias ² :1.012	k:7, r:0.300 MSE:1.566 Variance:1.426 Bias ² :0.1396	k:7, r:0.300 MSE:0.6341 Variance:0.4745 Bias²:0.1596
Mn2_Nonlinear	k:14 MSE:53.54 Variance:25.73 Bias ² :27.81	k:7, r:0.158 MSE:27.22 Variance:15.67 Bias ² :11.55	k:10 MSE:17.76 Variance:5.362 Bias ² :12.4	k:5, r:0.081 MSE:6.992 Variance:6.926 Bias ² :0.06537	k:5, r:0.059 MSE:3.675 Variance:3.478 Bias ² :0.1968	k:5, r:0.059 MSE:1.314 Variance:1.117 Bias²:0.1966
lollipop_	k:72 MSE:0.02799 Variance:0.02735 Bias ² :0.0006399	k:72, r:0.600 MSE:0.02367 Variance:0.02196 Bias ² :0.00171	k:51 MSE:0.007691 Variance:0.006603 Bias²:0.001088	k:51, r:0.600 MSE:0.01017 Variance:0.008994 Bias ² :0.001173	k:37, r:0.600 MSE:0.009419 Variance:0.006789 Bias ² :0.00263	k:37, r:0.600 MSE:0.005837 Variance:0.005837 Bias ² :0.002721
uniform	k:10 MSE:123.8 Variance:60.26 Bias ² :63.49	k:5, r:0.158 MSE:57.22 Variance:41.45 Bias ² :15.77	k:7 MSE:46.87 Variance:26.44 Bias ² :20.43	k:5, r:0.214 MSE:24.61 Variance:11.75 Bias ² :13.86	k:5, r:0.300 MSE:14.13 Variance:11.23 Bias ² :2.896	k:5, r:0.429 MSE:7.494 Variance:5.579 Bias²:1.915

Table 9: Table showing the optimal results for the MADA estimator across the different bagging variants with smoothing. The shown k and r values are the ones that achieved the lowest MSE across experiments for that specific dataset and estimator variant. While the MSE is the lowest one, the Variance and Bias-squared represent the decomposition of this MSE, and therefore, not necessarily the lowest on their own. The table is colored using a per-dataset (one for each row) logarithmic color scale based on the MSE to indicate large to small values as mild red to mild blue colors across the table cells (estimator variants). The best results in a row are additionally written with a bold font. This raw data is the basis of the MADA part of the radar charts analyzed in Section 6 of the main paper.

Estimator: MADA, Optimized for: MSE

Dataset	Baseline	Simple bagging	Baseline with smoothing	Simple bagging with post-smoothing	Simple bagging with pre-smoothing	Simple bagging with pre-smoothing and post-smoothing
M10a_Cubic	k:72 MSE:4.961 Variance:2.176 Bias ² :2.784	k:14, r:0.158 MSE:3.565 Variance:2.595 Bias ² :0.9697	k:26 MSE:1.305 Variance:0.332 Bias ² :0.9731	k:10, r:0.158 MSE:0.8069 Variance:0.5904 Bias ² :0.2165	k:10, r:0.158 MSE:0.3588 Variance:0.3323 Bias ² :0.02653	k:10, r:0.158 MSE:0.1308 Variance:0.1034 Bias²:0.02739
M10b_Cubic	k:72 MSE:25.39 Variance:4.31 Bias ² :21.08	k:10, r:0.158 MSE:17.04 Variance:10.25 Bias ² :6.786	k:14 MSE:9.873 Variance:3.563 Bias ² :6.31	k:10, r:0.429 MSE:6.985 Variance:2.199 Bias ² :4.786	k:10, r:0.429 MSE:5.09 Variance:1.434 Bias ² :3.655	k:10, r:0.600 MSE:3.979 Variance:0.5099 Bias²:3.469
M10c_Cubic	k:26 MSE:68.26 Variance:22.22 Bias ² :40.04	k:10, r:0.214 MSE:46.59 Variance:18.38 Bias ² :28.21	k:14 MSE:34.51 Variance:5.62 Bias ² :28.89	k:10, r:0.600 MSE:25.82 Variance:5.127 Bias ² :20.69	k:10, r:0.600 MSE:23.01 Variance:3.592 Bias ² :19.42	k:10, r:0.600 MSE:22.35 Variance:0.7374 Bias²:21.61
M11_Moebius	k:51 MSE:0.2415 Variance:0.2411 Bias ² :0.0003475	k:26, r:0.042 MSE:0.1142 Variance:0.07317 Bias ² :0.041	k:51 MSE:0.01254 Variance:0.01253 Bias ² :5.467e-06	k:72, r:0.158 MSE:0.02672 Variance:0.02497 Bias ² :0.001756	k:37, r:0.081 MSE:0.007707 Variance:0.002296 Bias ² :0.005411	k:37, r:0.600 MSE:0.006267 Variance:0.006077 Bias²:0.0001895
M12_Norm	k:26 MSE:40.99 Variance:22.71 Bias ² :18.28	k:10, r:0.214 MSE:28.09 Variance:15.53 Bias ² :12.56	k:14 MSE:16.04 Variance:4.265 Bias ² :11.77	k:10, r:0.600 MSE:12.71 Variance:4.266 Bias ² :8.445	k:10, r:0.600 MSE:11.1 Variance:2.857 Bias ² :8.24	k:10, r:0.600 MSE:10.66 Variance:0.6344 Bias²:10.02
M13a_Scurve	k:72 MSE:0.1395 Variance:0.1333 Bias ² :0.006197	k:72, r:0.300 MSE:0.09008 Variance:0.06925 Bias ² :0.02084	k:72 MSE:0.0194 Variance:0.01545 Bias ² :0.003946	k:72, r:0.600 MSE:0.03065 Variance:0.02122 Bias ² :0.009428	k:72, r:0.042 MSE:0.002147 Variance:0.0006217 Bias ² :0.001525	k:72, r:0.042 MSE:0.002058 Variance:0.0005653 Bias²:0.001493
M1_Sphere	k:72 MSE:4.026 Variance:2.243 Bias ² :1.783	k:14, r:0.115 MSE:3.156 Variance:2.46 Bias ² :0.6963	k:26 MSE:1.067 Variance:0.397 Bias ² :0.6701	k:10, r:0.115 MSE:0.5887 Variance:0.4991 Bias ² :0.08956	k:14, r:0.429 MSE:0.3923 Variance:0.3024 Bias ² :0.0899	k:10, r:0.115 MSE:0.1279 Variance:0.1269 Bias²:0.0009649
M2_Affine_3to5	k:72 MSE:0.3221 Variance:0.2822 Bias ² :0.03995	k:26, r:0.081 MSE:0.2413 Variance:0.1491 Bias ² :0.0922	k:72 MSE:0.05739 Variance:0.02198 Bias ² :0.03541	k:26, r:0.600 MSE:0.06743 Variance:0.05302 Bias ² :0.01441	k:14, r:0.115 MSE:0.03078 Variance:0.03057 Bias ² :0.000213	k:26, r:0.429 MSE:0.02308 Variance:0.01687 Bias²:0.006214
M3_Nonlinear_4to6	k:72 MSE:1.055 Variance:0.9946 Bias ² :0.06037	k:72, r:0.429 MSE:0.8864 Variance:0.7285 Bias ² :0.1579	k:72 MSE:0.2633 Variance:0.1682 Bias ² :0.09512	k:26, r:0.600 MSE:0.2976 Variance:0.2695 Bias ² :0.02801	k:10, r:0.042 MSE:0.1698 Variance:0.1666 Bias ² :0.003196	k:26, r:0.600 MSE:0.1433 Variance:0.1262 Bias²:0.01715
M4_Nonlinear	k:51 MSE:1.697 Variance:1.593 Bias ² :0.1032	k:72, r:0.042 MSE:0.7087 Variance:0.5364 Bias ² :0.1723	k:37 MSE:0.1522 Variance:0.1514 Bias ² :0.0007827	k:19, r:0.600 MSE:0.2236 Variance:0.2226 Bias ² :0.001049	k:72, r:0.059 MSE:0.03716 Variance:0.03208 Bias ² :0.00508	k:72, r:0.059 MSE:0.03092 Variance:0.01907 Bias²:0.01185
M5b_Helix2d	k:51 MSE:1.412 Variance:0.6586 Bias ² :0.753	k:72, r:0.042 MSE:0.2309 Variance:0.1644 Bias ² :0.06652	k:37 MSE:0.8228 Variance:0.1848 Bias ² :0.638	k:72, r:0.042 MSE:0.2123 Variance:0.121 Bias ² :0.09133	k:51, r:0.042 MSE:0.01974 Variance:0.01974 Bias ² :1.085e-06	k:51, r:0.042 MSE:0.0185 Variance:0.01843 Bias²:6.881e-05
M6_Nonlinear	k:72 MSE:4.653 Variance:3.117 Bias ² :1.535	k:72, r:0.081 MSE:1.084 Variance:1.08 Bias ² :0.003708	k:51 MSE:0.6754 Variance:0.4274 Bias ² :0.2481	k:72, r:0.115 MSE:0.4812 Variance:0.4808 Bias ² :0.0004362	k:72, r:0.115 MSE:0.1186 Variance:0.108 Bias ² :0.01063	k:72, r:0.158 MSE:0.07127 Variance:0.0693 Bias²:0.001973
M7_Roll	k:72 MSE:0.1814 Variance:0.1813 Bias ² :0.0001567	k:72, r:0.042 MSE:0.1334 Variance:0.1247 Bias ² :0.008742	k:72 MSE:0.01139 Variance:0.01095 Bias ² :0.0004379	k:37, r:0.600 MSE:0.02865 Variance:0.02192 Bias ² :0.00673	k:72, r:0.042 MSE:0.01124 Variance:0.007735 Bias ² :0.003509	k:37, r:0.600 MSE:0.01048 Variance:0.006722 Bias²:0.00376
M8_Nonlinear	k:72 MSE:8.241 Variance:6.708 Bias ² :1.533	k:72, r:0.214 MSE:2.503 Variance:2.138 Bias ² :0.3657	k:72 MSE:0.4908 Variance:0.3561 Bias ² :0.1347	k:72, r:0.600 MSE:0.3294 Variance:0.3269 Bias ² :0.002454	k:72, r:0.600 MSE:0.2341 Variance:0.2336 Bias ² :0.0005661	k:26, r:0.158 MSE:0.08596 Variance:0.07711 Bias²:0.008849
M9_Affine	k:26 MSE:47.61 Variance:19.41 Bias ² :28.2	k:10, r:0.214 MSE:29.96 Variance:13.92 Bias ² :16.04	k:10 MSE:21.78 Variance:10.13 Bias ² :11.64	k:10, r:0.600 MSE:18.47 Variance:3.336 Bias ² :15.14	k:10, r:0.600 MSE:16.02 Variance:2.326 Bias ² :13.69	k:10, r:0.600 MSE:15.82 Variance:0.5142 Bias²:15.3
Mn1_Nonlinear	k:72 MSE:34.13 Variance:4.719 Bias ² :29.41	k:10, r:0.214 MSE:22.2 Variance:12.6 Bias ² :9.606	k:14 MSE:15.29 Variance:3.016 Bias ² :12.28	k:10, r:0.600 MSE:10.95 Variance:3.59 Bias ² :7.365	k:10, r:0.600 MSE:8.935 Variance:2.071 Bias ² :6.864	k:10, r:0.600 MSE:8.213 Variance:0.4546 Bias²:7.759
Mn2_Nonlinear	k:26 MSE:74.47 Variance:26.16 Bias ² :48.31	k:10, r:0.214 MSE:52.13 Variance:18.64 Bias ² :33.49	k:10 MSE:30.8 Variance:11.64 Bias ² :19.15	k:10, r:0.600 MSE:30.74 Variance:4.375 Bias ² :26.36	k:10, r:0.600 MSE:27.3 Variance:3.032 Bias²:24.26	k:10, r:0.600 MSE:27.8 Variance:0.6357 Bias ² :27.17
lollipop_	k:72 MSE:0.1562 Variance:0.1524 Bias ² :0.003792	k:37, r:0.300 MSE:0.1197 Variance:0.1053 Bias ² :0.01442	k:51 MSE:0.02197 Variance:0.01814 Bias ² :0.003834	k:37, r:0.600 MSE:0.03437 Variance:0.02503 Bias ² :0.009338	k:37, r:0.600 MSE:0.0229 Variance:0.01721 Bias ² :0.005697	k:26, r:0.600 MSE:0.01694 Variance:0.01343 Bias²:0.003511
uniform	k:26 MSE:175.7 Variance:29.7 Bias ² :146	k:10, r:0.429 MSE:134.4 Variance:33.78 Bias ² :100.6	k:10 MSE:95.42 Variance:14.34 Bias²:81.07	k:10, r:0.600 MSE:109.1 Variance:5.519 Bias ² :103.5	k:10, r:0.600 MSE:103.6 Variance:3.725 Bias ² :99.91	k:10, r:0.600 MSE:107.4 Variance:1.034 Bias ² :106.4

E.2 Supplementary bar-chart figures for the effect of r and B experiments

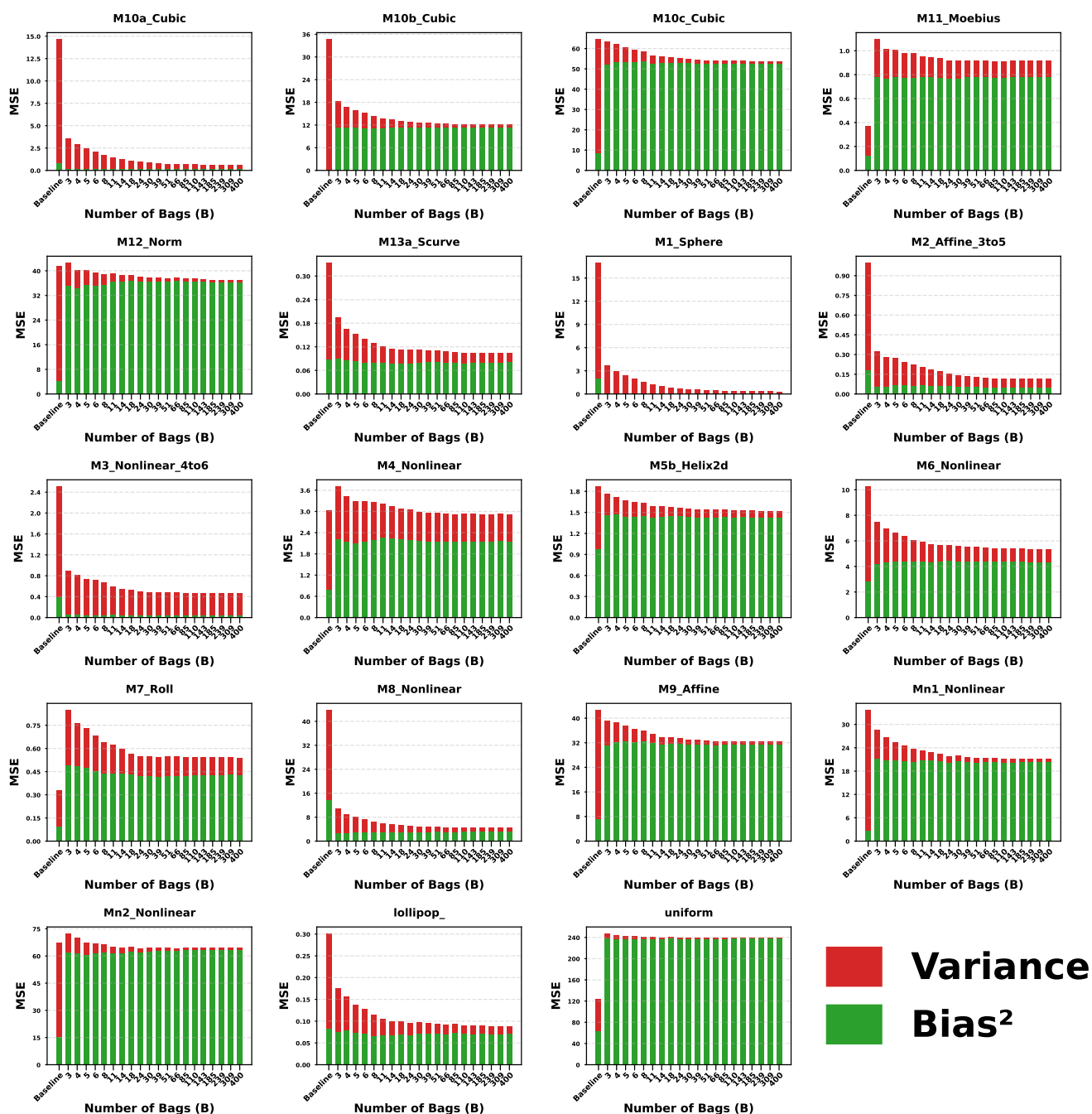


Figure 22: 19 separate bar charts, one for each data manifold. On the x-axis is a range of B (number of bags) hyper-parameters, set for the simple bagged estimator used to estimate LID, except for the first bar from the left, which represents the baseline estimator. The baseline estimator selected is the TLE. On the y-axis are the raw values of the MSE achieved by the given estimator. The bars are vertically split into variance and bias² parts to illustrate the mean squared error decomposition, signaled by green and red colors. See Section A.3 for the detailed experimental setup and Section A.4.1 for the in-depth explanation of these results (originally illustrated with the MLE version of this plot).

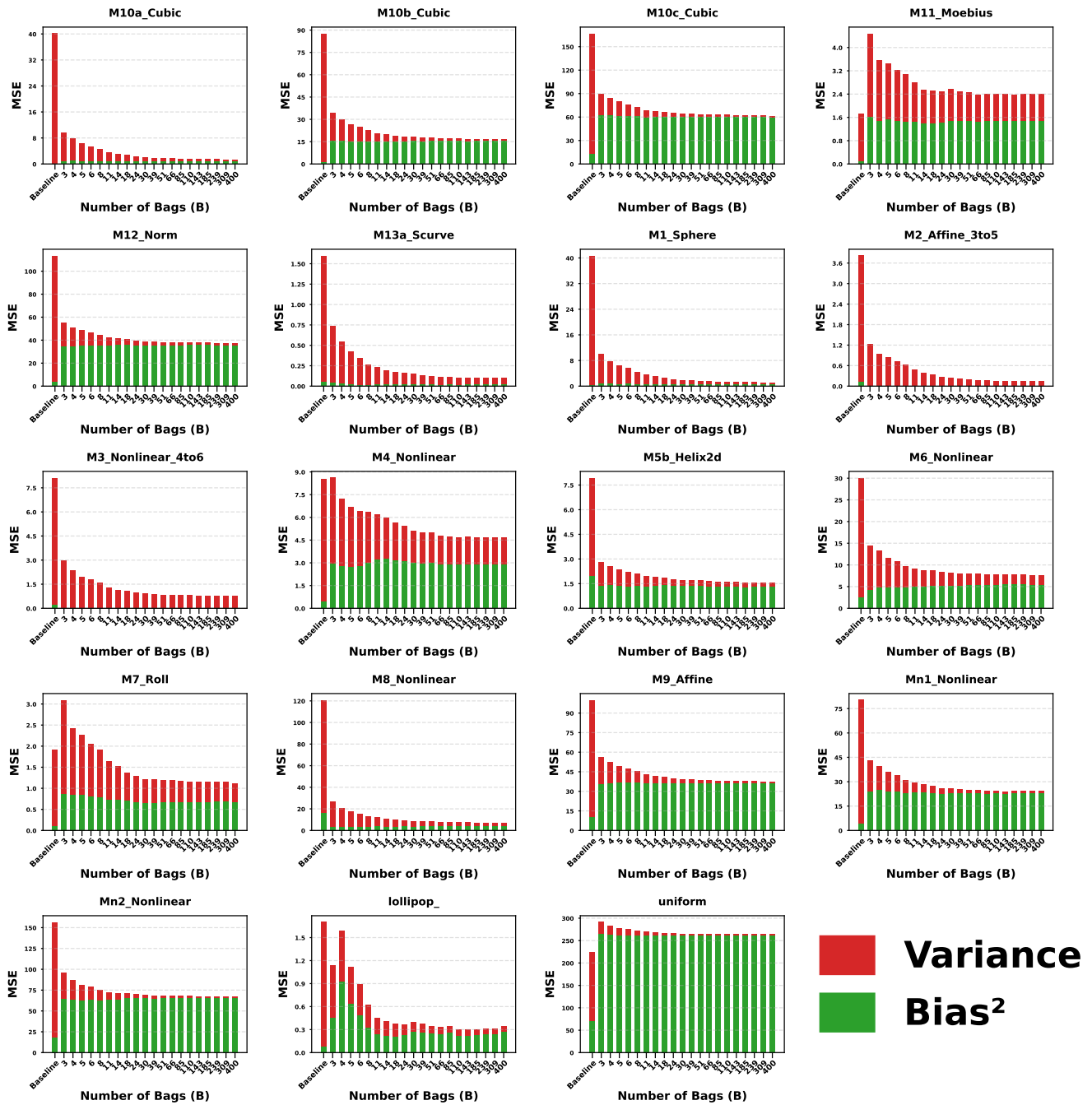


Figure 23: 19 separate bar charts, one for each data manifold. On the x-axis is a range of B (number of bags) hyper-parameters, set for the simple bagged estimator used to estimate LID, except for the first bar from the left, which represents the baseline estimator. The baseline estimator selected is the MADA. On the y-axis are the raw values of the MSE achieved by the given estimator. The bars are vertically split into variance and bias² parts to illustrate the mean squared error decomposition, signaled by green and red colors. See Section A.3 for the detailed experimental setup and Section A.4.1 for the in-depth explanation of these results (originally illustrated with the MLE version of this plot).

Supplementary bar-charts with varying r for TLE and MADA

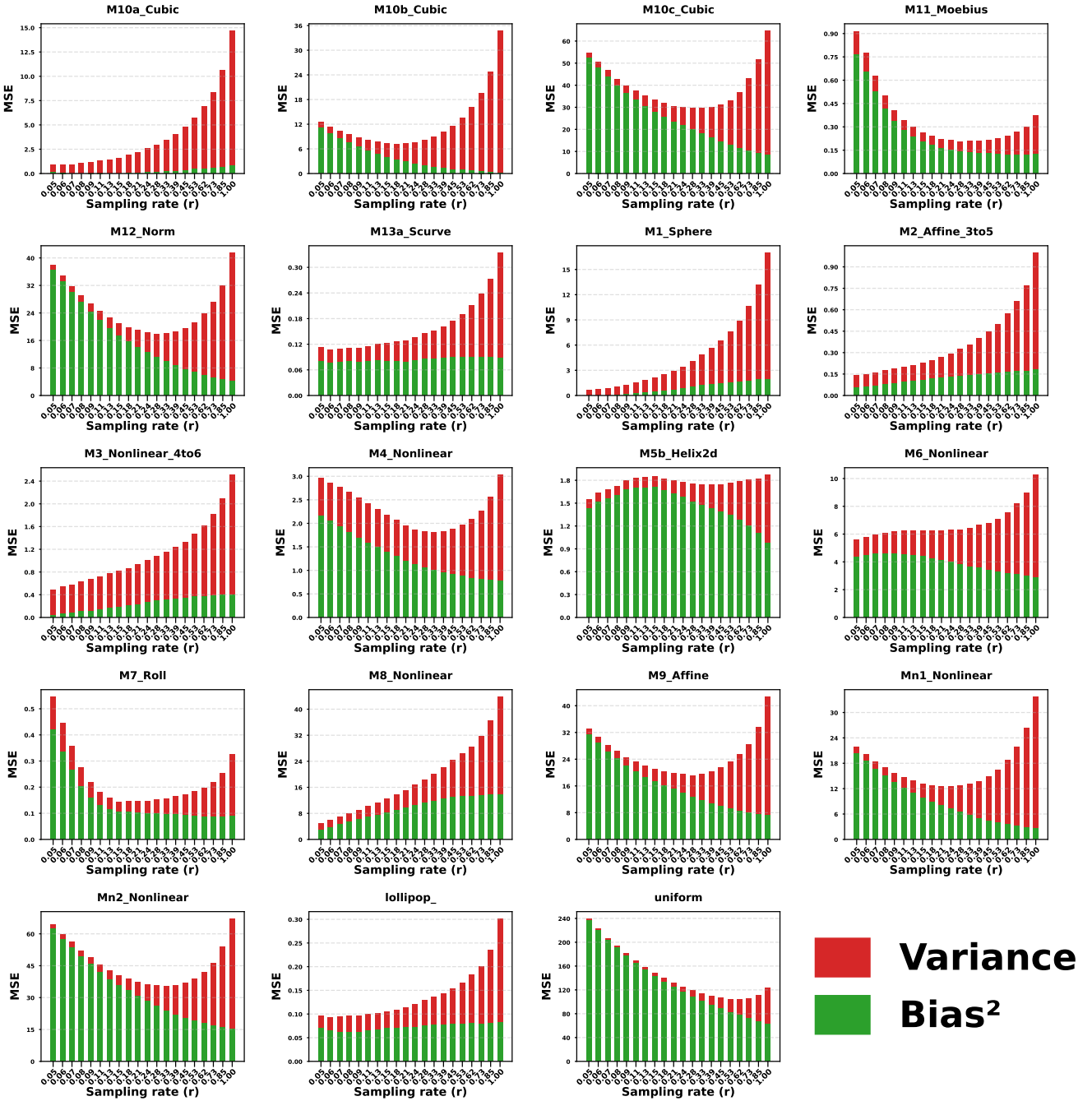


Figure 24: 19 separate bar charts, one for each data manifold. On the x-axis is a range of r (sampling rate) hyper-parameters, set for the simple bagged estimator used to estimate LID, including the last bar from the left, which represents the baseline estimator but is equivalent with the $r = 1$ case. The baseline estimator selected is the TLE. On the y-axis are the raw values of the MSE achieved by the given estimator. The bars are vertically split into variance and bias² parts to illustrate the mean squared error decomposition, signaled by green and red colors. See Section 5 of the main paper for the detailed experimental setup and Section 6 for the in-depth explanation of results (originally illustrated with the MLE version of this plot).

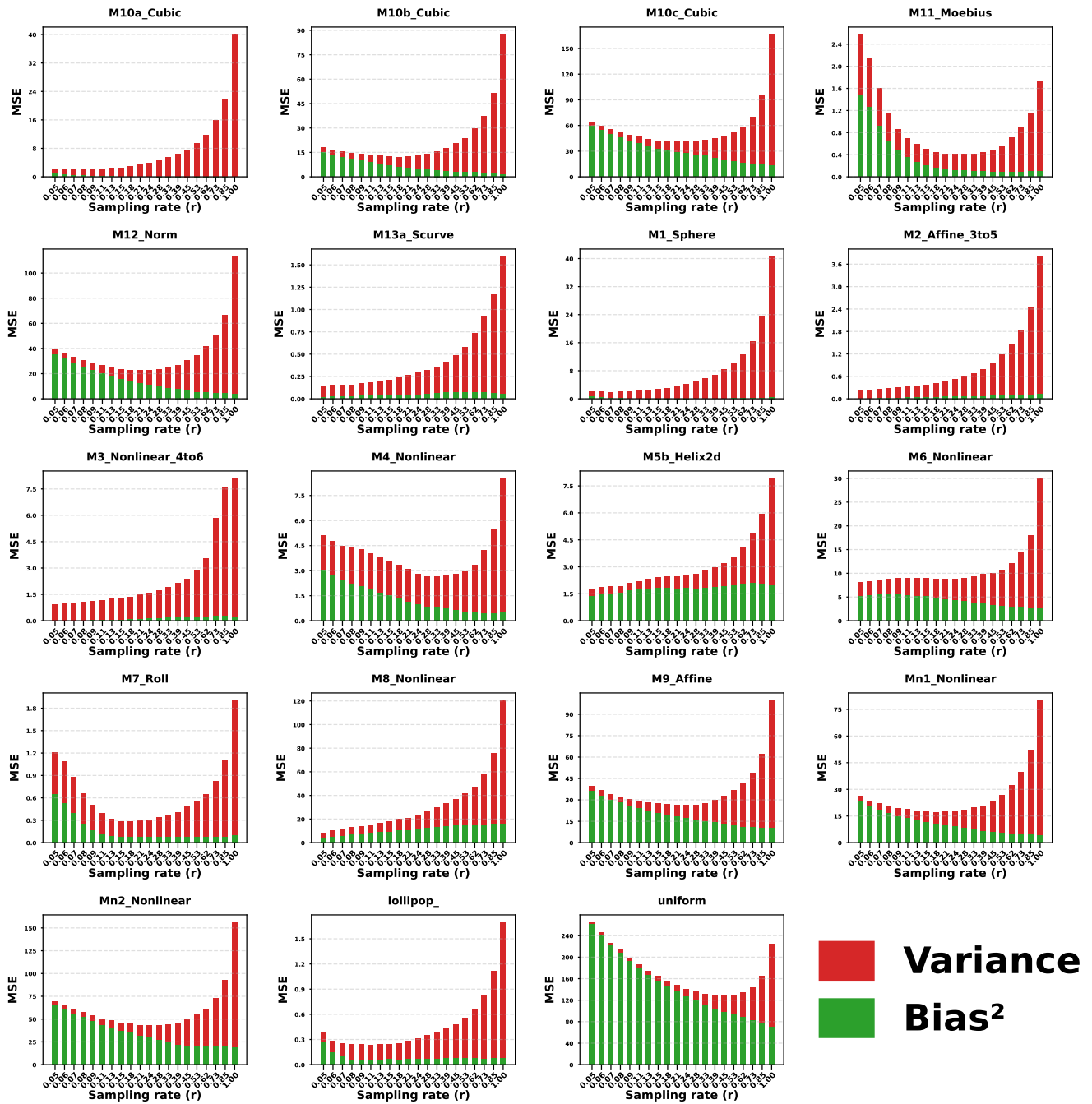


Figure 25: 19 separate bar charts, one for each data manifold. On the x-axis is a range of r (sampling rate) hyper-parameters, set for the simple bagged estimator used to estimate LID, including the last bar from the left, which represents the baseline estimator but is equivalent with the $r = 1$ case. The baseline estimator selected is the MADA. On the y-axis are the raw values of the MSE achieved by the given estimator. The bars are vertically split into variance and bias² parts to illustrate the mean squared error decomposition, signaled by green and red colors. See Section 5 of the main paper for the detailed experimental setup and Section 6 for the in-depth explanation of results (originally illustrated with the MLE version of this plot).

E.3 Supplementary heatmaps for B and r interaction through comparing bagging and baseline

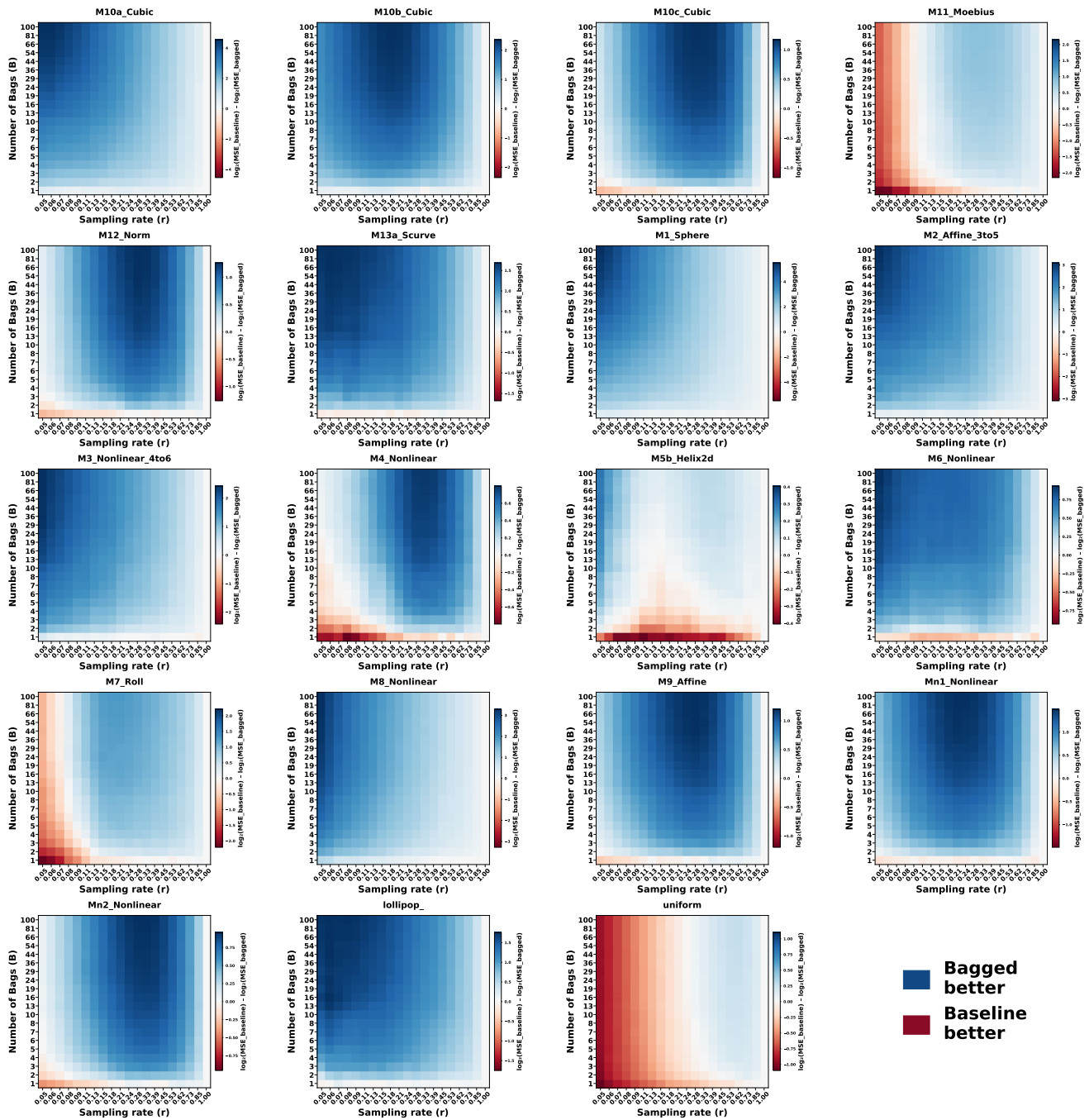


Figure 26: 19 separate heat maps, one for each data manifold. On the x-axis is a range of r (sampling rate) hyper-parameters, while on the y-axis is a range of B (number of bags) hyper-parameters. At each coordinate, the combination of the two hyper-parameters is set for the simple bagged estimator used to estimate LID. The baseline estimator selected is the TLE. The squares on the grid are colored based on the logarithm of the ratio between the MSE achieved by the baseline estimator and the MSE of the simple bagged estimator using that specific hyper-parameter combination. See Section A.3 for the detailed experimental setup and Section A.4.2 for the in-depth explanation of results (originally illustrated with the MLE version of this plot).

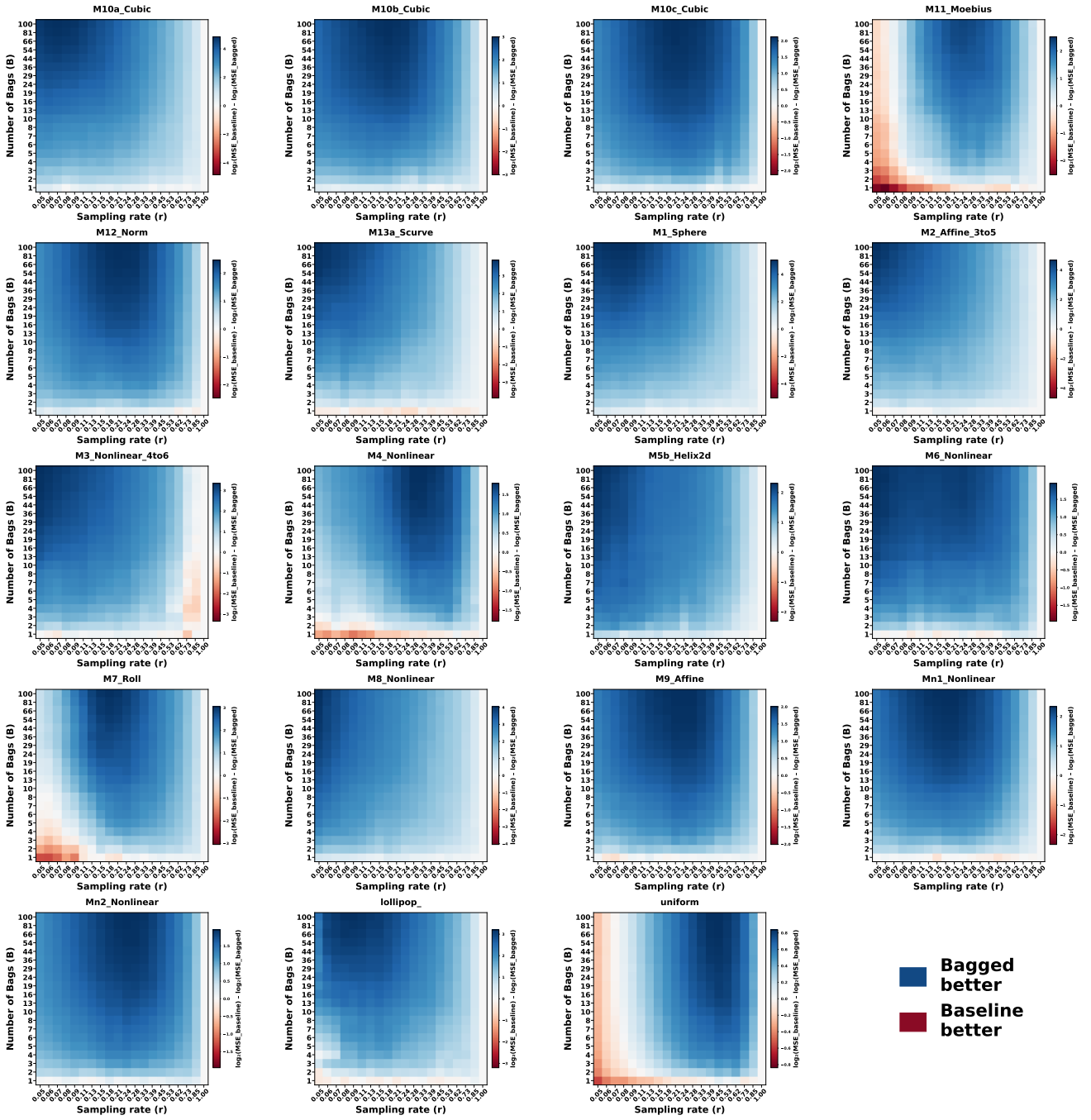


Figure 27: 19 separate heat maps, one for each data manifold. On the x-axis is a range of r (sampling rate) hyper-parameters, while on the y-axis is a range of B (number of bags) hyper-parameters. At each coordinate, the combination of the two hyper-parameters is set for the simple bagged estimator used to estimate LID. The baseline estimator selected is the MADA. The squares on the grid are colored based on the logarithm of the ratio between the MSE achieved by the baseline estimator and the MSE of the simple bagged estimator using that specific hyper-parameter combination. See Section A.3 for the detailed experimental setup and Section A.4.2 for the in-depth explanation of results (originally illustrated with the MLE version of this plot).

E.4 Supplementary heatmaps for k and r interaction through comparing bagging and baseline

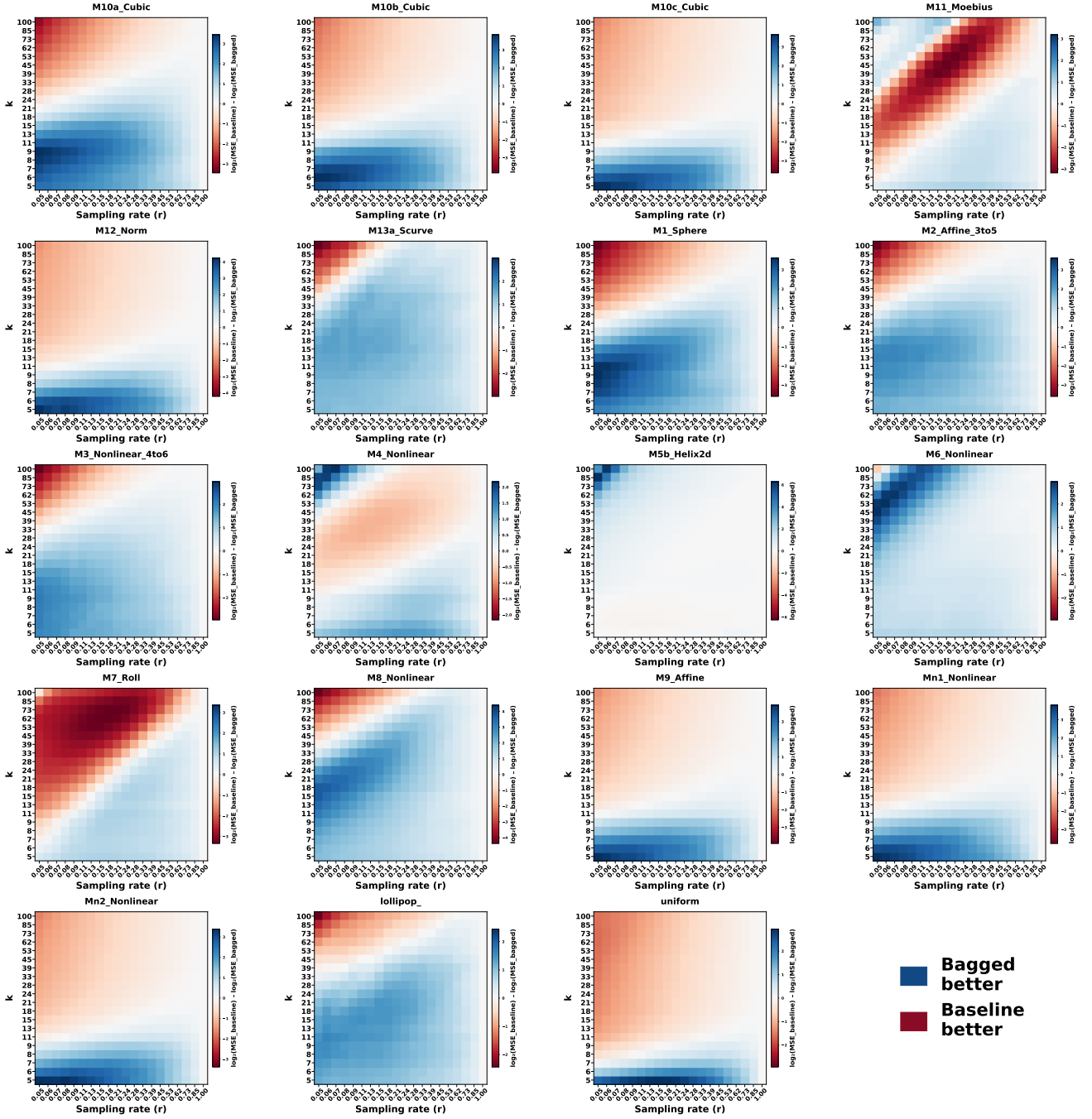


Figure 28: 19 separate heat maps, one for each data manifold. On the x-axis is a range of r (sampling rate) hyper-parameters, while on the y-axis is a range of k -NN hyper-parameters. At each coordinate, the combination of the two hyper-parameters is set for the simple bagged estimator used to estimate LID. The baseline estimator selected is the TLE. The squares on the grid are colored based on the logarithm of the ratio between the MSE achieved by the baseline estimator and the MSE of the simple bagged estimator using that specific hyper-parameter combination. See Section 5 of the main paper for the detailed experimental setup and Section 6 for the in-depth explanation of results (originally illustrated with the MLE version of this plot).

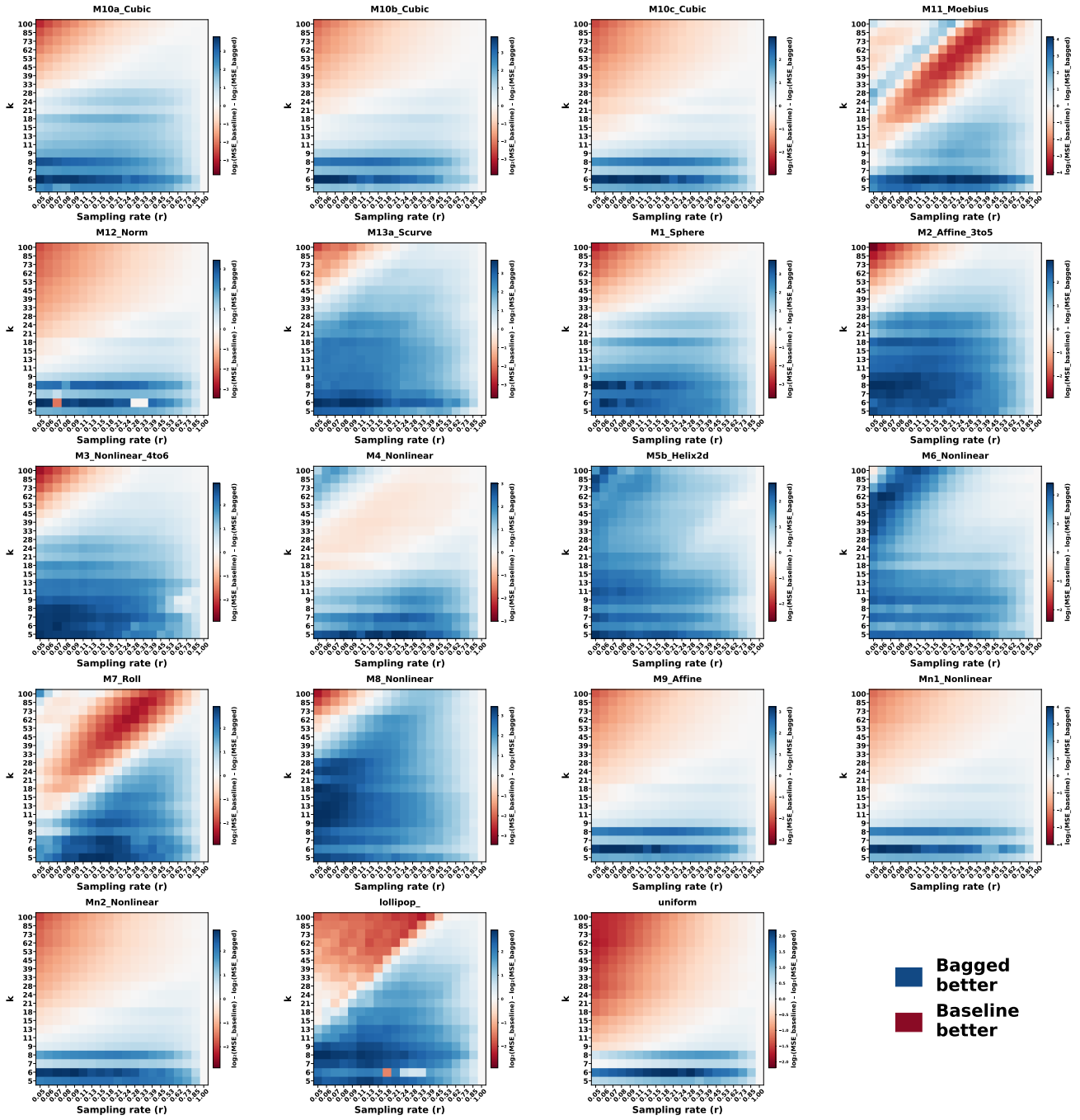


Figure 29: 19 separate heat maps, one for each data manifold. On the x-axis is a range of r (sampling rate) hyper-parameters, while on the y-axis is a range of k -NN hyper-parameters. At each coordinate, the combination of the two hyper-parameters is set for the simple bagged estimator used to estimate LID. The baseline estimator selected is the MADA. The squares on the grid are colored based on the logarithm of the ratio between the MSE achieved by the baseline estimator and the MSE of the simple bagged estimator using that specific hyper-parameter combination. See Section 5 of the main paper for the detailed experimental setup and Section 6 for the in-depth explanation of results (originally illustrated with the MLE version of this plot).

References

- [1] Allegra, M., Facco, E., Denti, F., Laio, A., Mira, A.: Data segmentation based on the local intrinsic dimension. *Sci. Rep.* **10**, 16449 (2020)
- [2] Altman, N., Krzywinski, M.: Ensemble methods: bagging and random forests. *Nat. Methods* **14**, 933–934 (2017)
- [3] Amsaleg, L., Bailey, J., Barbe, A., Erfani, S., Furon, T., Houle, M., Radovanović, M., Vinh, N.: High intrinsic dimensionality facilitates adversarial attack: Theoretical evidence. *IEEE Trans. Inf. Forensics Security* **16** (2020)

- [4] Amsaleg, L., Chelly, O., Furon, T., Girard, S., Houle, M., Kawarabayashi, K.i.: Estimating local intrinsic dimensionality (2015), doi:10.1145/2783258.2783405
- [5] Amsaleg, L., Chelly, O., Furon, T., Girard, S., Houle, M.E., Kawarabayashi, K.I., Nett, M.: Extreme-value-theoretic estimation of local intrinsic dimensionality. *Data Min. Knowl. Discov.* **32**, 1768–1805 (2018)
- [6] Amsaleg, L., Chelly, O., Houle, M.E., Kawarabayashi, K.i., Radovanović, M., Treeratanajaru, W.: Intrinsic dimensionality estimation within tight localities: A theoretical and experimental analysis (2022), arXiv:2209.14475
- [7] Anderberg, A., Bailey, J., Campello, R.J.G.B., Houle, M.E., Marques, H.O., Radovanović, M., Zimek, A.: Dimensionality-aware outlier detection: Theoretical and experimental analysis (2024), arXiv:2401.05453
- [8] Aumüller, M., Ceccarello, M.: The role of local dimensionality measures in benchmarking nearest neighbor search. *Inf. Syst.* **101**, 101807 (2021)
- [9] Bac, J., Mirkes, E.M., Gorban, A.N., Tyukin, I., Zinovyev, A.: Scikit-dimension: A python package for intrinsic dimension estimation. *Entropy* **23**, 1368 (2021)
- [10] Breiman, L.: Bagging predictors. *Mach. Learn.* **24**, 123–140 (1996)
- [11] Breiman, L.: Random forests. *Mach. Learn.* **45**, 5–32 (2001)
- [12] Bühlmann, P., Yu, B.: Analyzing bagging. *Ann. Statist.* **30** (2002)
- [13] Camastra, F., Vinciarelli, A.: Estimating the intrinsic dimension of data with a fractal-based method. *IEEE TPAMI* **24**, 1404–1407 (2002)
- [14] Campadelli, P., Casiraghi, E., Ceruti, C., Rozza, A.: Intrinsic dimension estimation: Relevant techniques and a benchmark framework. *Mathematical Problems in Engineering* **2015**, 1–21 (2015)
- [15] Carter, K.M., Hero, A.O.: Variance reduction with neighborhood smoothing for local intrinsic dimension estimation. In: *Proc. IEEE ICASSP*. pp. 3917–3920 (2008)
- [16] Casanova, G., Englmeier, E., Houle, M.E., Kröger, P., Nett, M., Schubert, E., Zimek, A.: Dimensional testing for reverse k-nearest neighbor search. *Proc. VLDB Endow.* **10**, 769–780 (2017)
- [17] Chernick, M.R., LaBudde, R.A.: *An Introduction to Bootstrap Methods with Applications to R*. Wiley (2011)
- [18] Danielsson, J., de Haan, L., Peng, L., de Vries, C.: Using a bootstrap method to choose the sample fraction in tail index estimation. *J. Multiv. Anal.* **76**, 226–48 (2001)
- [19] Facco, E., d’Errico, M., Rodriguez, A., Laio, A.: Estimating the intrinsic dimension of datasets by a minimal neighborhood information. *Sci. Rep.* **7**, 12140 (2017)
- [20] Farahmand, A.m., Szepesvári, C., Audibert, J.Y.: Manifold-adaptive dimension estimation. In: *ACM Int. Conf. Proceeding Series*. pp. 265–272 (2007)
- [21] Gencay, R., Qi, M.: Pricing and hedging derivative securities with neural networks: Bayesian regularization, early stopping, and bagging. *IEEE TNN* **12**, 726–34 (2001)
- [22] Gorbett, M., Shirazi, H., Ray, I.: Local intrinsic dimensionality of IoT networks for unsupervised intrusion detection. In: *Data and Applications Security and Privacy XXXVI*. pp. 143–161 (2022)
- [23] Grassberger, P., Procaccia, I.: Measuring the strangeness of strange attractors. *Physica D* **9**, 189–208 (1983)
- [24] Grinstead, C.M., Snell, J.L.: *Introduction to Probability*. American Mathematical Society (2003)
- [25] Gupta, A., Krauthgamer, R., Lee, J.R.: Bounded geometries, fractals, and low-distortion embeddings. In: *Proc. IEEE FOCS*. pp. 534–543 (2003)
- [26] Hein, M., Audibert, J.Y.: Intrinsic dimensionality estimation of submanifolds in R. In: *Proc. ICML*. pp. 289–296 (2005)
- [27] Houle, M.: Dimensionality, discriminability, density and distance distributions. In: *Proc. IEEE ICDMW*. pp. 468–473 (2013)
- [28] Houle, M., Kashima, H., Nett, M.: Generalized expansion dimension. In: *Proc. IEEE ICDMW*. pp. 587–594 (2012)

- [29] Houle, M.E.: Local intrinsic dimensionality I: An extreme-value-theoretic foundation for similarity applications. In: *Similarity Search and Applications*. pp. 64–79 (2017)
- [30] Huang, H., Campello, R.J.G.B., Erfani, S.M., Ma, X., Houle, M.E., Bailey, J.: *Ldreg: Local dimensionality regularized self-supervised learning* (2024), arXiv:2401.10474
- [31] James, G., Witten, D., Hastie, T., Tibshirani, R., Taylor, J.: *An Introduction to Statistical Learning: with Applications in Python*. Springer (2023)
- [32] Johnsson, K., Sonesson, C., Fontes, M.: Low bias local intrinsic dimension estimation from expected simplex skewness. *IEEE TPAMI* **37**, 196–202 (2015)
- [33] Kalinka, A.T.: The probability of drawing intersections: extending the hypergeometric distribution (2014), arXiv:1305.0717
- [34] Kamkari, H., Ross, B.L., Hosseinzadeh, R., Cresswell, J.C., Loaiza-Ganem, G.: A geometric view of data complexity: Efficient local intrinsic dimension estimation with diffusion models (2024), arXiv:2406.03537
- [35] Karantzas, K.: Intrinsic dimensionality estimation and dimensionality reduction through scale space filtering. In: *ICDSP*. pp. 1–6 (2009)
- [36] Larrañaga, P., Lozano, J.: *Estimation of Distribution Algorithms: A New Tool for Evolutionary Computation*. Springer (2002)
- [37] Liao, J.G., Berg, A.: Sharpening jensen’s inequality (2017), arXiv:1707.08644
- [38] Ma, X., Li, B., Wang, Y., Erfani, S.M., Wijewickrema, S., Schoenebeck, G., Song, D., Houle, M.E., Bailey, J.: Characterizing adversarial subspaces using local intrinsic dimensionality (2018), arXiv:1801.02613
- [39] Pictet, O., Dacorogna, M., Muller, U.: Hill, bootstrap and jackknife estimators for heavy tails. In: *A Practical Guide to Heavy Tails* (1996)
- [40] Revelas, C., Boldea, O., Werker, B.J.M.: When does subbagging work? (2024), arXiv:2404.01832
- [41] Rozza, A., Lombardi, G., Ceruti, C., Casiraghi, E., Campadelli, P.: Novel high intrinsic dimensionality estimators. *Mach. Learn.* **89**, 37–65 (2012)
- [42] Ruhl, M.: Finding nearest neighbors in growth-restricted metrics. In: *STOC* (2002)
- [43] Savić, M., Kurbalija, V., Radovanović, M.: Local intrinsic dimensionality measures for graphs, with applications to graph embeddings. *Inf. Syst.* **119**, 102272 (2023)
- [44] Tempczyk, P., et al.: *LIDL: Local intrinsic dimension estimation using approximate likelihood* (2022), arXiv:2206.14882
- [45] Wackerly, D.D., Mendenhall, W., Scheaffer, R.L.: *Mathematical Statistics with Applications*. Thomson Brooks/Cole (2008)
- [46] Wikipedia contributors: Hypergeometric distribution. https://en.wikipedia.org/wiki/Hypergeometric_distribution (2025), accessed 2025-08-04
- [47] Wikipedia contributors: Smoothing. <https://en.wikipedia.org/wiki/Smoothing> (2025), accessed 2025-07-28
- [48] Zhang, Z., Chen, B., Sun, J., Luo, Y.: A bagging dynamic deep learning network for diagnosing COVID-19. *Sci. Rep.* **11**, 16280 (2021)
- [49] Zhou, S., Tordesillas, A., Pouragha, M., Bailey, J., Bondell, H.: On local intrinsic dimensionality of deformation in complex materials. *Sci. Rep.* **11**, 10216 (2021)
- [50] Zimek, A., Gaudet, M., Campello, R.J.G.B., Sander, J.: Subsampling for efficient and effective unsupervised outlier detection ensembles. In: *Proc. ACM SIGKDD Int. Conf. Knowl. Discov. Data Min.* pp. 428–436 (2013)